ROYAL SOCIETY
OF CHEMISTRY

Check for updates

Versatile MXenes as electrochemical sensors for heavy metal ions and phenolic moiety-containing industrial chemicals: recent development and prospects

G. Manasa [ID] and Chandra Sekhar Rout [ID] *

MXenes and their hybrid materials, with good physicochemical traits, have exhibited excellent performance across numerous applications. MXenes with pre-eminent features, namely, facile surface modifications, functionalization, larger-specific surface area, and conductivity, transcend the limitations of sensor devices. MXene nanomaterials are ideal candidates for use as modifying agents in electrochemical (EC) sensor fabrication. Hence, in this review article, we provide insights into the potential of MXene-based materials for EC sensors compared to conventional materials. At first, we discuss the fundamentals of EC sensors, followed by an introduction to the physicochemical properties of MXene as an efficient working electrode modifying agent that acts as a direct transducing material. The review discusses the notable characteristics and fundamental working principles of EC sensor devices and the significance of surface modification during the fabrication of MXene-based sensors. The article emphasizes advanced sensors and outlines prospects in the field for target analytes of interest: heavy metal ions (HMIs) and phenolic moieties containing toxic molecules. A comprehensive summary of recent developments in MXene-based EC sensors for the molecules mentioned above is critically reviewed, encompassing sensor device fabrication approaches, enhanced properties, results, and discussion. The effect of different secondary organic and inorganic compounds, including carbonaceous materials, polymers, and metallic nanoparticles, on the sensing performance of MXenes is analyzed through EC techniques. Finally, we conclude by outlining the opportunities and obstacles associated with MXene-based EC methods, addressing implications for future directions for progressive research in this field. We believe this review will provide valuable information for those exploring nanomaterials to develop EC sensors.

Centre for Nano and Material Sciences, Jain (Deemed-to-be University), Jain Global Campus, Kanakapura Road, Bangalore – 562112, Karnataka, India.
E-mail: r.chandrasekhar@jainuniversity.ac.in, csrout@gmail.com

Dr Manasa G. is a post-doctoral researcher at the CNMS, Jain University. She was awarded her doctoral degree in chemistry from Bangalore University. Her research inclination is towards the synthesis of MXenes and its composites, fabrication of electro-chemical sensors, and their application concerning trace analysis of emerging pollutants. Such detections will allow the management of the pollutants and regulate them.

G. Manasa

Chandra Sekhar Rout is a full Professor at the Centre for Nano & Material Sciences (CNMS), Jain University. Before joining CNMS, he was a DST - Ramanujan Fellow at IIT Bhubaneswar, India (2013-2017). He obtained his PhD from JNCASR, Bangalore (2008), followed by postdoctoral research at NUS, Purdue University, and UNIST. His research is focused on the applications of 2D layered materials in different devices.

Chandra Sekhar Rout

He has authored more than 200 research papers and 06 books. His h-index is 54 with total citations > 12 500. He was ranked among the top 2% of scientists by the Stanford study in 2020–2022.

1. Introduction

Electrochemical (EC) analysis is a technique used for measuring and characterizing the chemical and electrical properties of the analyte, as well as the electrode surface itself. Here, the electrode surface plays a crucial role in electrochemical processes, and characterizing it is essential for understanding and optimizing the performance of the electrochemical system. In contrast to other methodologies, electrochemical sensing technologies are often given preference for target analyte determination, especially in continuous real-time, on-site analysis, and point-of-care applications.[1–3] They offer high sensitivity and selectivity for accomplishing lower detection limits, fast response time, and simple readouts due to their compatibility with integrated circuit technology. The target analyte is detected through oxidation–reduction reactions at the interface of the specifically designed working electrode.[4] Although not every analyte can elicit redox reaction mechanisms, external mediators are required to induce an EC signal proportional to the analyte concentration.[5] They fundamentally convert chemical concentrations into quantitative electric signals. Recently, the developed EC sensors have made outstanding achievements in medicine, environment, and health monitoring.[6–9] This broad application of EC sensors is attributed to their cost-effectiveness, a wide window of voltage and current, and the trace theoretical detection limits conceived from faradaic currents. Other credentials include its long-term stability and satisfactory biocompatibility. The scenario of age-related diseases is expected to soar in the coming decades due to aging societies worldwide. Thus, there is a pressing need for strategies to impede an emerging global epidemic. The most efficient method to address the issue is the change of diet and lifestyle in combination with the possibility of continuously monitoring the health characteristic index (glucose, BP, and cholesterol) at a healthy level employing real-time EC sensors.[10–12] At the same time, the environment is continuously contaminated by the people as a consequence of modern developments. Thus, the impact on future generations will hinge on the present procedures for detection, laying down regulations, and controlling the contamination.[13]

Therefore, from the perspective of growing interest in 2D materials other than graphene, and MXene-materials comprising a vast family of novel and exciting 2D materials, it was deemed suitable to provide an investigative report on the recent developments and the current state of affairs in MXene research, constituting their structure, properties, and potential application in EC sensor devices.[14] Unlike the exploding research on MXene-supercapacitors, only a few researchers have addressed the potential of MXenes for EC sensing of various analytes. The characteristics of MXenes include sufficient surface terminal functional groups, high hydrophilicity, and surface conductivity with robust mechanical strength. The literature unveils numerous articles regarding the different applications of MXenes.[15,16] However, we categorized crucial characteristics to comprehend the underlying chemistry, procedures, and phenomena in MXenes. We have attempted to cover the fundamentals of MXene 2D materials in this review,

from their types and properties to application aspects. We aim to draw attention to the enhancing effects of the material on EC sensing. The advancement of MXene-based sensors toward commercial viability depends on this school of thought.

Therefore, the review is organized into several sections. In Section 1, we introduce the readers to the featured principles of EC transduction and their wide applications. In Section 2, we provide a brief introduction to electrochemical sensors and their methodologies, serving as a beginner's guide. Section 3 is devoted to the essential attributes of 2D materials with a special focus on MXenes and their properties. Section 4 describes the different approaches adopted to fining-tune MXenes for EC performances. Section 5 briefly describes the methods of electrode substrate modification and the fabrication of an EC sensor. Section 6 reviews MXene-based sensors for heavy metal ions (HMIs) and phenolic moiety-containing molecules as reported in the literature concerning their fundamental design, structure, properties, experimental results, and strengths and weaknesses. Section 7 is dedicated to the broader perspective of the EC field, outlining the opportunities and obstacles of MXene-based EC methods and considering implications on future directions for progressive research in this field. We believe that this review will provide valuable information to those exploring nanomaterials to develop EC sensors. Fig. 1 summarizes the content of this review article.

2. Basic working principle of electrochemical sensors

The domain of sensors has evolved unprecedently attributed to the integration of advanced materials. EC sensors detect modulations in faradaic current (voltammetry) or the interfacial impedance in the case of electrochemical impedance spectroscopy (EIS).[17] Voltammetric sensors detect the change in current as a function of applied potential to the working electrode, while few electrochemical sensors rely on potentiometric detection (detect the change in surface potential) or impedance spectroscopy (modulation of impedance as a function of applied frequency).[18] Voltammetric sensors rely on various techniques, including cyclic voltammetry (CV), linear sweep voltammetry (LSV), staircase voltammetry (SCV), pulse voltammetry {normal pulse voltammetry (NPV) and differential pulse voltammetry (DPV)}, stripping voltammetry {anodic stripping voltammetry (ASV), cathodic stripping voltammetry (CSV) and adsorptive stripping voltammetry (AdSV)}, amperometry (AMP), square wave adsorptive stripping voltammetry (SWASV) and rotating disk voltammetry, among others. DPV, SWV, and stripping techniques are much more sensitive than CV as their sampling method minimizes the non-faradaic (charging) current. In a foresight, during differential pulse voltammetric examinations, the potential is scanned with a series of pulses, and the current is measured at two points for each pulse. The initial measurement is taken shortly before the application of the pulse, while the second is at the end of each pulse. These sampling points enable the decay of non-faradaic current,
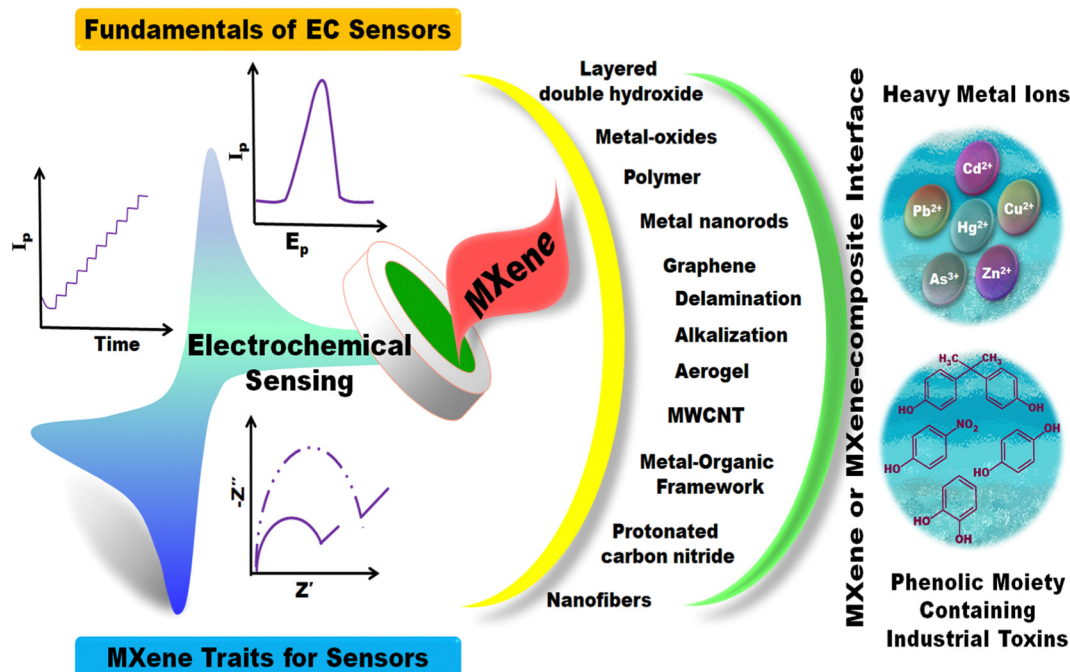
Fig. 1 Summarized illustration of the content of this review article.

favoring greater sensitivity of the technique than CV (sensitive to residual current).

To conduct EC measurements, the primary requirement is an electrochemical cell in which the redox reaction occurs, apart from an EC analyzer equipped with appropriate circuitry and software (Fig. 2). Another principal component is

the three-electrode configuration constituted by reference, working, and auxiliary electrodes (RE, WE, and AE, respectively). Among them, the WE (carbon paste electrode, glassy carbon electrode (GCE), diamond electrode, gold (Au) electrode, platinum (Pt) electrode, and screen-printed electrode (SPE)) is the core of this configuration as the redox reactions take place
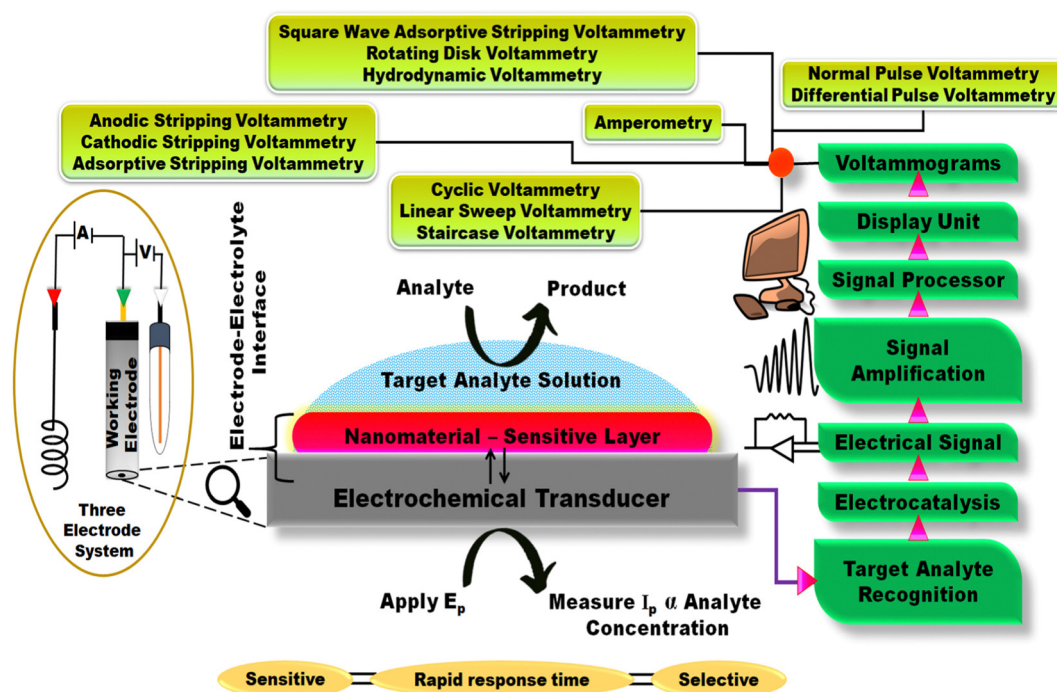

Fig. 2 Working principle and methods involved in electrochemical sensors.

at this electrode. The current is generated as a result of the reaction flow through the WE and AE (Pt electrode), while the potential of the WE is controlled in relation to the RE (saturated calomel, Ag/AgCl), which has a constant and reproducible potential.[19,20] More importantly, since the reactions are detected only in proximity to the WE surface, the electrode plays a significant role in the overall performance of the sensor. This EC sensor comprises an EC transducing element denoted as an EC transducer and a recognition layer. The detection ability of the sensor is based on the characteristics of the electrode material, dimensions, and the recognition layer (surface modification).[21] This recognition layer is modified in compliance with the requirements as it is pivotal for interacting with the analyte of concern to yield an EC signal. The recognition layer might contain either nanomaterials or biological components, or both.[22,23]

Thus, the work function of a chemical sensor is to detect the target analyte qualitatively and quantitatively, followed by transferring the detected signal into useful analytical information. Conventionally, sensitivity (limit of detection – LOD), linear sensitivity, accuracy, selectivity, and response time are the standards for quantitative assessments of chemical sensors. Here, sensitivity implies the ratio of the detected analyte's concentration to the detected signal's intensity before saturation of the signal, while the linear sensitivity is a measure of the reliability of the sensing mechanism and saturation concentration. The LOD is associated with the sensitivity and noise ratio. It is computed through theoretical assessment of the target analyte concentration at which the signal-to-noise ratio (SNR) is three. Besides, selectivity denotes the specificity (selectivity) of the sensor towards the target analyte, even in the presence of other co-existing molecules. Among these, the LOD estimation is crucial in fabricating a sensor. Therefore, to magnify the LOD, the sensor's sensitivity must be enhanced, and the primary method to do so is to surface modify the electrode substrate with various types of nanomaterials that impart excellent physicochemical properties to the electrode.

2.1. The necessity of working electrode surface modification

Developing an EC sensor is a novel strategy that contrasts with conventional analytical techniques. The introduction of nanomaterials in fabricating sensors emerges as an efficient analytical tool for determining numerous analytes.[24–27] The EC method for analysis depends on the nanomaterials (modifying agents) used, their physicochemical traits, and optimization upon modification of the sensing substrate. Indisputably, EC measurements are based upon charge transfer at the heterogeneous electrode–electrolyte interface; thus, appropriate electrode surface modification results in improved electrocatalytic properties, sensitivity, reproducibility, and system stability. Such modifications reduce the electrode surface's passivation and the so-called 'chemical noise' caused by impurities discharge and charging currents. To resolve this issue, modifications of the bare WE are widely investigated.[28–31] This modification process accelerates the electrode kinetics and enhances the selectivity and sensitivity of determination. A survey of the

literature revealed that EC sensors were increasingly built using 2D materials that included graphene-based materials, transition metal dichalcogenides (TMDCs), black phosphorous (BP), hexagonal boron nitride (h-BN), metal-oxides (MO), metal–organic frameworks (MOFs), 2D carbides and nitrides of transition metals (MXenes).[18,24,28,32–36] Their unique physicochemical properties are to be exploited and employed in fabricating EC sensors for enhanced selectivity and sensitivity. Modern EC sensors utilize various features to determine the physical, chemical, and biological aspects of day-to-day life. An ideal sensor exhibits high sensitivity with a lower LOD and a comprehensive linear response, low hysteresis and fabrication cost, and is miniaturized and compact for portability. EC sensors measure the EC reactions and determine them as a consequence of electrode–analyte interactions.

3. 2D materials and MXenes for electrochemical sensors

Carbon nanostructures are pioneering materials. The classification of materials is based on their nanoscopic dimensions:[37] (i) If all three dimensions (x,y,z) of the material are nano-sized (no dimension is more significant than 100 nm), it is considered a 0D material, more frequently termed as a nanoparticle/quantum dot (quantum dots, nanospheres, and nanoclusters). (ii) If the two dimensions (x,y) of a material are nanosized, while the other dimension is significantly larger (outside nanoscale), then it is denoted as a 1D material or nanowire/nanotube (nanofibers, nanorods, and carbon nanotubes). (iii) Furthermore, if only one dimension (x) is nano-sized, while the other two are outside the nanoscale, then it is considered a 2D material resembling a large but fragile sheet (nanolayers, nanofilms, and nanocoatings with nanometer thickness). (iv) The material not confined to the nanoscale in any direction is designated as a 3D material (3 arbitrary dimensions above 100 nm). Here, the nanomaterial comprises multiple arrangements of nanosize crystals in various orientations, including dispersions of nanoparticles, bundles of nanotubes/nanowires, and multi-nanolayered structures in which 0D, 1D, and 2D structural elements are in intimate contact with one another, forming interfaces. Ever since the exfoliation of graphene, the tremendous application of its characteristics has driven rapid advancements in the field of 2D materials. It has paved the way for other layered materials and structures. The traits of these materials are a function of chemical bonds, shape, and dimensionality. Carbon has four valence electrons in the ground state, two each in 2s and 2p subshells. Bond formation occurs with other carbon atoms via sp hybrid orbitals when one of the 2s electrons migrates to an unfilled 2p orbital. Likewise, there are different types of sp hybrid orbitals, namely, sp, sp^2, and sp^3, and carbon atoms possessing those hybrid orbitals establish bonds with other carbon atoms in their vicinity. Hence, the upcoming section is focused on carbon atoms containing sp^2 bonds. On the other hand, apart from graphene, different 2D materials have received much interest among researchers due to their exceptional physicochemical characteristics. 2D materials,

composed of atomically thin sheets with weak interlayer bonding, are isolated from bulk phases of layered materials, forming a finite library for discovering new materials.[38] By selecting constituent elements and substrates, novel 2D materials can be synthesized, providing access to a broader range of properties. Of particular interest are 2D MXenes, attributed to their unique properties. Hence, in this review, we investigate the progress made in the synthesis and sensing applications of MXenes, followed by challenges and perspectives.

3.1. Advantages of 2D materials and MXenes for electrochemical sensing

Comprehensively, 2D materials exhibit a larger surface-to-volume ratio than 0D, 1D, or 3D analogs and ensure good sensitivity at trace concentrations of the target analyte. Their distinct features arise from the crystalline nature of a single or a few layers of atoms and the rare blend of ceramic and metallic properties. Due to their good chemical, electrical, thermal, structural, and mechanical properties, 2D materials are widely explored for EC sensing. Typically, 2D materials are categorized based on their structure such as graphene, TMDC (MoS_2, $MoSe_2$, WS_2, and WSe_2), hexagonal boron nitride (h-BN), black phosphorous (BP), MOs, layered (LDHs), graphitic carbon nitride (g-C_3N_4), metal nitrides/carbides (MXenes), perovskite-oxides, transition metal-halides/oxides and others.[39] The fundamental phenomenon of these materials continues to be researched, and the development of effective device architectures is now pushing 2D materials toward innovative technological applications. Currently, the paradigms that comprehend research and development of EC sensors enable the investigation of new materials, manufacturing methods, and strategies to improve the sensitivity and detection limits. 2D materials have been proven to enhance the performance of EC sensors.[28,40,41] They are often utilized to modify the transducer surface, aiming to enhance charge transfer, facilitate preparation procedure, ensure compatibility with biological molecules, achieve good reproducibility, and provide large specific surfaces. 2D layered materials are characterized by atomically thin crystalline solids without dangling bonds, thus rendering good intralayer charge transport.[42]

Material science and engineering is a branch of science considered to manipulate and maneuver atoms/molecules with a diameter up to the nanometer range. Based on this conception, the development of hybrid nanomaterials with different properties from primitive nanomaterials has caught the attention of researchers. Due to their application in nano- and atomic-scale devices, 2D materials are significant. Several studies have been conducted on the growth of free-standing 2D materials.[43] Thin sheets of 2D materials can be grown over various substrates to meet device applications.[44] The potential application of 2D materials such as h-BN, MOs, metal halides, and MXenes may help address various limitations in different devices. This is because nearly all the atoms on the surface of these materials are exposed after exfoliation; consequently, the surface area of 2D materials is noticeably enhanced.[45]

Graphene, a single layer of carbon atoms hexagonally bound in a honeycomb lattice, is an eminent member of the primitive 2D layered material class, possessing excellent properties extensively described in the literature.[42–45] The integration of graphene-based materials into the EC transducer offers merits that include an improved charge transfer rate, conductivity, and an increased surface-to-volume ratio of the transducer.[42,46,47] Additionally, graphene's capability to functionalize with functional groups and heteroatoms is integral to its superior properties. Furthermore, the chemical and electronic properties of graphene-based materials are influenced by the content of oxygen functional groups. Due to the presence of oxygen-containing groups and hydrophilicity, graphene oxide (GO) and reduced graphene oxide (rGO) enable broad possibilities for functionalization. Additionally, the intercalation of inorganic hosts (clays, graphite, dichalcogenides, and others) has also garnered attention due to their distinct physical and chemical conditions.[42] The de-intercalation of these compounds under specific conditions or reactions in the interlayer space led to the formation of extensively applied exfoliated graphite and 2D materials. Not long ago, were MXene materials extracted from A-elements for layered ternary carbides (Ti_3AlC_2 and other MAX phases) with numerous exorbitant properties, mainly electrochemical properties, surpassing those of graphene.[48] 2D titanium carbide (Ti_3C_2) MXene was the first material to be identified among several others from the MXene family; it has demonstrated conductivity, surface area, facile tuneable structures, and film forming ability. Another striking property is its greater intercalation capacity compared to other 2D materials. Other MXenes, like Ti_3CN, Mo_2C, Mo_2TiC_2, and Hf_3C_2, have also been prepared and investigated for their physical and chemical characteristics.[49]

Since in this review, we will discuss the potential of MXene nanomaterial as electrode modifiers, here are a few attributes we would like to discuss regarding the advantages of MXenes over graphene, the most commonly employed 2D material for EC sensing. Of course, the applications of graphene nanosheets are irreplaceable; however, we aim to comprehend the primary advantages of emerging new material MXenes. The most significant advantage of MXene over graphene lies in the surface chemistry of the former. It is rich in several surface terminal groups, which are a by-product of synthesis processes. Due to the nature of each of the surface terminations and inherent transition metals, the MXene surface can be functionalized with a multitude of molecules. In contrast, graphene mainly comprises oxygen and hydrogen-terminated functionalities, limiting its functionalization possibilities. Furthermore, compared to other 2D materials, MXene has an obvious merit of high electrical conductivity, essential for accelerating the rate of heterogeneous charge transfer. Generally, MXenes comprise more than one element ($Ti_3C_2T_x$ with titanium and carbide), unlike graphene, which includes only one element (C). Hence, a heterogenous catalytic process benefits from the presence of multiple elements due to their different affinities for the target molecules. Furthermore, since the MXene core is metallic and, upon surface functionalization, it retains its conductivity, unlike graphene, whose conductivity is disturbed upon surface

treatment. This feature of MXene makes it unique among other 2D nanomaterials such as TMDs, boron nitrides, phosphorene, and others.[50] MXene could be dispersed in common solvents (DMF, ethanol, water, and others) with high stability for a few days. Additionally, its dispersion stability is improved by functionalization.[51] In contract, in its pristine form, graphene tends to agglomerate and achieving a stable dispersion is a tedious task. Although the functionalization of graphene can yield stable dispersions in a few solvents, it may compromise electrical conductivity. Therefore, MXenes offer stable dispersion while retaining their electrical conductivity, which is crucial for applications wherein the physical coating is essential, as in the case of GCE modification. This kind of well-dispersed, stable nanomaterials will form a homogenous film over the electrode surface, facilitating a larger surface area and equal access to target analytes to approach the surface of the working electrode.

The emergence of novel 2D materials besides graphene has depicted promising applications across diverse technologies. The redox properties of metal-oxide nanomaterials are crucial in engineering electrochemical sensor platforms, as they exhibit interesting physiochemical properties attributed to their size, stability, and high specific surface area. Moreover, hybridizing metal oxides with other materials enhances electrical conductivity, electron transfer kinetics, and stability during electrocatalytic reactions.[52–54] These principal factors ensure greater sensitivity of the sensor materials in detecting the target analyte molecules. Yet among all the other 2D materials, MXenes stand out with their thickness (can possess a single unit thickness of M–X–M trilayer or several units thick), rich surface chemistry, high aspect ratio, electroconductivity, tuneability (of the thickness of single unit of M_2X), making them an ideal candidate for sensor construction.[55] MXenes enable the tailoring of their properties for numerous applications, including supercapacitors, water purification, catalysis, fuel cells, gas sensing, EC biosensing, and many others.[56–59] Because MXene, a promising layered structure, possesses atomically thin structures, high ion intercalation nature, electronic and quantum confinement effects, high surface area and charge transfer enhanced sensitivity and selectivity, and robust, nontoxic nature, they suffice as one among the transducer materials.

The literature survey showed us that titanium carbide has been the most explored MXene compared to other members due to its remarkable ability to delaminate multi-layered Ti_3C_2 into few-layered nanosheets, which significantly enhances the EC performance of Ti_3C_2; second, the facile etching process results in numerous active sites, and third, Ti_3C_2 not only possesses all the merits of the MXene family but also features facile preparation and structural stability compared to other types of MXenes.[60] Significantly, given these merits, Ti_3C_2 is popularly employed for EC sensor fabrication. To cite a few applications, Ti_3C_2/MXene immobilized with an enzyme was applied for phenol detection, sensing of H_2O_2 and small molecules was achieved using MXene decorated with Pt nanoparticles, and a mediator-free biosensor comprised a TiO_2/ Ti_3C_2 MXene nanocomposite encapsulating hemoglobin.[61–63]

The literature survey unveiled a few reviews about the MXene-based EC sensors. However, their central attention was different, or they emerged a couple of years before. For instance, Kailasa, Wang, and Shazad have discussed, through their review, MXene-based sensors for the detection of small molecules (dopamine and uric acid) pesticides like (carbendazim and methamidophos), bromate ions, nitrite, naphthalene, dyes, neurotransmitters, small molecules, pharmaceuticals, cancer markers, and others.[64–66] Ho and team have provided a gist of MXene-sensors categorized under physical, chemical, and biological sensors.[55] Rhouati and researchers have reviewed the MXene-based biosensors (enzymatic and affinity) for environmental pollutants such as pesticides and nitrates.[66] There are several reports on MXene for biosensing, and many discuss the role of MXene in biomedical applications.[67–72] While not all MXene-based sensing reviews have prioritized EC technology, they heed a range of technologies including magnetic resonance imaging, computed tomography photoacoustics, biosensors, optical biosensors, adsorption strategies, etc.[73–76] The other reports are dated to have been published a few years ago.

Therefore, there is a necessity for an updated review of MXene-based EC sensing applications. Through this review and in the upcoming sections, we pragmatically discuss the chemistries and properties of MXenes for sensing. We also prioritize the utilization of MXenes either standalone or as a composite (to render a magnified sensing signal) for target analyte detection. Furthermore, we identified a research gap in the existing literature, indicating that MXene-EC sensors for HMIs and phenolic moiety-containing toxin detection are unexplored review topics. Successively, we focused on bridging this gap by discussing the state-of-the-art MXene-based EC sensors for HMIs and other miscellaneous toxic molecules.

3.2. Chemistries and properties of MXenes for electrochemical sensing

It is noteworthy that MXenes are a relatively new and emerging family of 2D materials that pave the way for excellent research. As a predecessor of MXenes, MAX phases are conventionally a series of layered compounds in which 'M' is a transition metal, while 'A' is an element of group 13–15 in the periodic table, and X is nitrogen and/or carbon. Hence, the structure and composition of MXenes rely on the MAX phases.[77]

MXenes are obtained by selectively chemically etching the element 'A' in MAX phases. Unlike graphite, which allows exfoliation, M–A metallic and M–X covalent bonds in the MAX phase are relatively strong. Thus, to break bonds to make MXenes, strong etchants like hydrofluoric acid (HF), ammonium hydrogen bi-fluoride, lithium fluoride-hydrochloric acid mixtures, and other novel etchants are used.[78] A reaction with these etchants will break the M–A bonds and selectively remove A-element layers, eventually resulting in multi-layered MXene with a generic formula $M_{n+1}X_nT_x$ (n = 1, 2, or 3). T_x are surface-termination functionalities, while the suffix "ene" in the MXene is because MXene properties are analogous to 2D graphene material with morphological, mechanical, and electrical properties.[79] Generally, MXenes have more than one 'M'
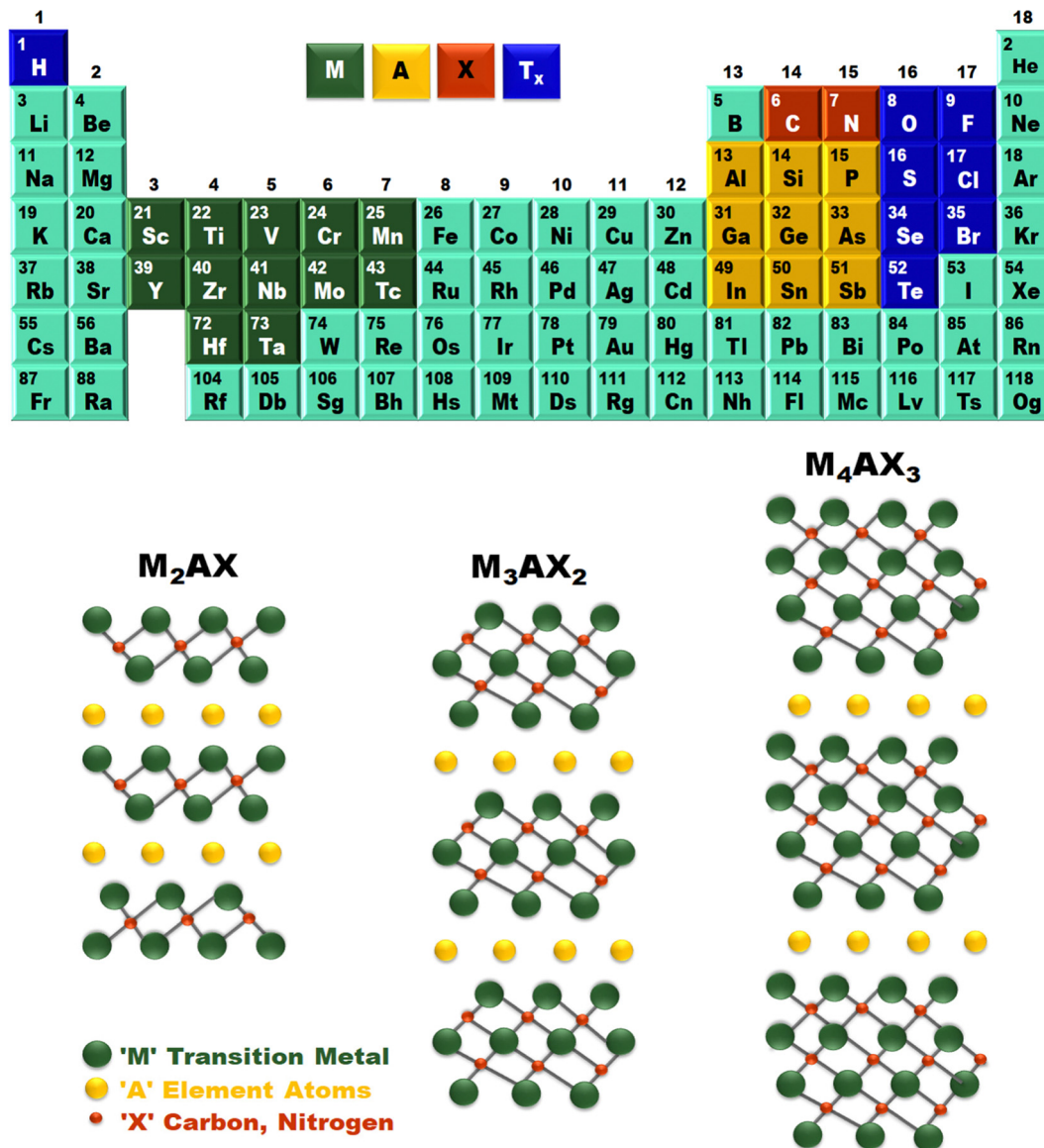
Fig. 3 MXene precursors: crystal structure of M_2AX, M_3AX_2, and M_4AX_3 phases.

element and two structural forms, namely, solid solutions and ordered phases. Fig. 3 summarizes different MXene precursors and the crystal structure of the M_2AX, M_3AX_2, and M_4AX_3 phases. The former depicts an arbitrary arrangement of two different transition metals that is witnessed in the 'M' layers, while the latter is composed of single or double layers of a single transition metal sandwiched between the layers of a second transition metal of a 2D carbonitride structure. However, if in the MAX phases, the value of 'n' is in the range of 1 to 3, then the resulting MXenes are obtainable in three possible lattice structures, namely, M_2X, M_3X_4, and M_4X_4 (3, 5/7 atomic layers). In M_2X, ABABAB (hexagonal close packing sequence) is the order observed in transition metal atoms, whereas ABCABC (face-centered cubic sequence) is witnessed in M_3X_2 and M_4X_3.[80] As a consequence of their ceramic trait, MXenes display a monolayer (few-layer/multilayers) structure,

and good chemical, and mechanical stability. Hence, among the two structural forms, it is established from the DTF examinations that ordered MXenes forms are energetically more stable than their solid-solution counterparts for a few compositions of transition metals.[81]

Typically, MXenes exhibit accordion-like several layered structures.[82,83] MXenes with various structures are also synthesized (scroll-like, flower-like, nanoribbons, *etc.*). On the other hand, MXene terminations are generally mixed with random distribution, which hinges on the transition metal elements, synthesis conditions, and post-synthesis treatments (Fig. 4). These terminal functional groups induce hydrophilic MXenes, allowing them to be prepared and utilized as colloidal or film-form in their pristine form or combined with polymer matrices to result in nanocomposites. The free-standing films formed using delaminated MXenes give rise to films with good conductivity.
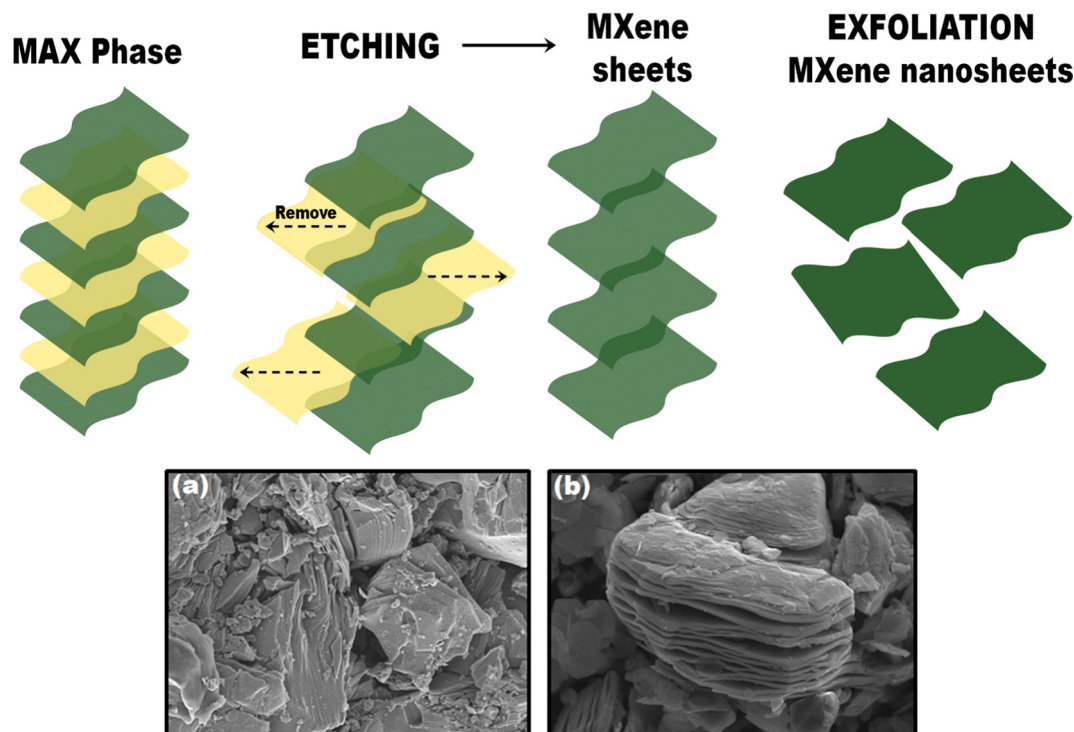
Fig. 4 Synthesis of multilayer or monolayer MXenes through etching. FESEM images of (a) MAX phase and (b) MXene after etching.

Likewise, there are notable review articles on MXenes and their synthesis schemes; the reviews provide a wealth of information on the MXene and its properties for EC sensors.[57]

The versatility of MXene compositions and the capability to tailor the material for specific sensing needs make them eminent nanomaterials in fabricating sensors. Although several reviews involving MXenes for EC sensors have been published, they have prioritized material preparation. Currently, the literature unveils several carbides-MXenes for sensing with considerable potential for exploring nitride and carbonitride-MXenes.

3.3. Advantages of MXenes for electrochemical sensors

The feasibility of using various techniques for recognizing the analyte of interest and transduction of signals has empowered EC sensing devices to adapt to the matrix environment and nature of the target species. The WE engineering with various nanomaterials is pivotal for designing a robust sensing system. This is because the conventional transducers exhibit low surface area and require high overpotentials besides the sluggish electron transfer kinetics and mass transport limitations. To overcome this, diverse materials including combinations of metals, metal-oxides, polymers or carbonaceous nanomaterials in composites and hybrids are explored. 2D materials, despite their elementary application as energy materials (supercapacitors and batteries), are receiving unparalleled attention from the sensing research community.

The primary cause for their expanding role in sensor science is directly associated with their chemical characteristics and surface versatility. As discussed in the previous section,

regardless of its excellent conductivity, integrating graphene with electrode systems is challenging due to restacking of sheets and low hydrophilicity. Fig. 5 illustrates the properties of MXenes for sensor application. MXene nanomaterials, on the other hand, with ample surface moieties (–F, –O, and –OH) to anchor other functional materials, proffer relatively high hydrophilicity. MXenes exhibit high conductivity (850–2410 S cm^{-1}), excellent surface characteristics, and metal-like traits, making them a modified agent of choice when fabricating an EC sensor. They are classified based on the nature of the output signal, and among them, EC sensors have gained recognition. In contrast, the application of MXenes in gas, biosensors, fluorescent sensors, and chemiluminescence is gradually increasing. MXenes, with their compositional counterparts, modest synthesis recipe and tuneable surface properties are highly favorable for sensor applications. MXenes and $Ti_3C_2T_x$ simultaneously act as charge transfer facilitators with catalytic traits during EC reduction or oxidation reactions. Therefore, in this section, we have discussed the EC sensors that employ MXenes and their composites/hybrids as direct or indirect redox transducers and as an electrocatalyst.

4. Important electronic properties of MXenes for sensors

The excellent electronic features of MXenes ($Ti_3C_2T_x$) are attributable to the availability of narrow band gaps and excellent conductivity, bringing about rapid electron transfer. The MXene structure is composed of three sections: (i) an intralayer
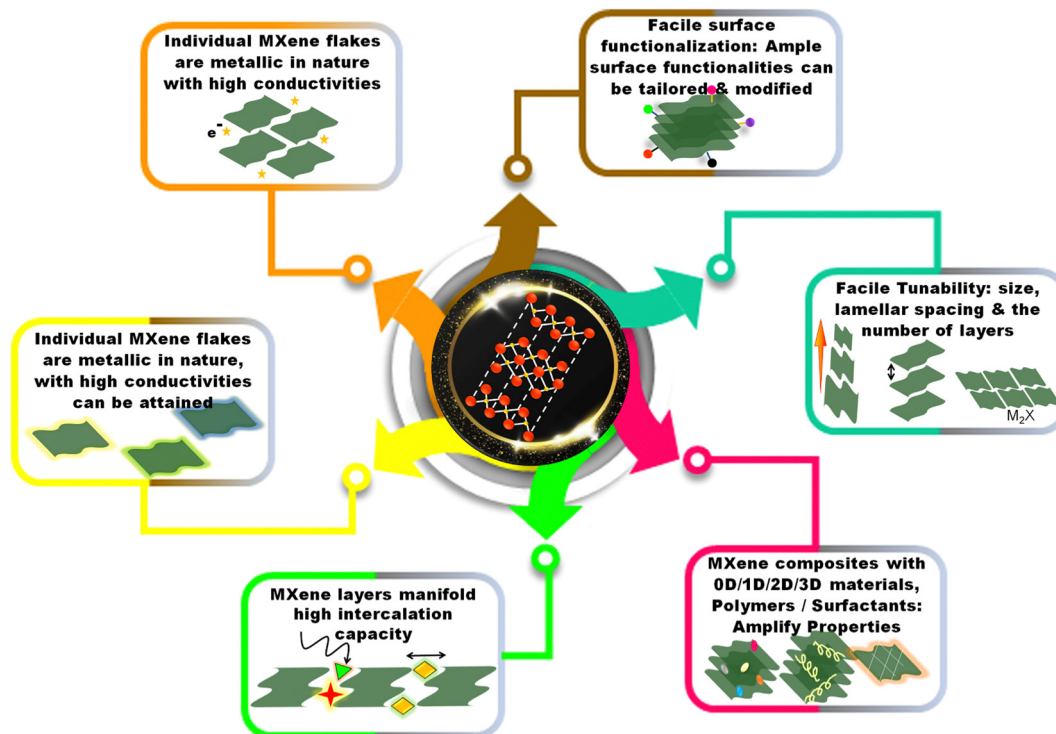
Fig. 5 Important and favorable properties of MXenes for electrochemical sensors.

skeleton layer, wherein Ti and carbide atoms are alternately stacked through ionic bonds; (ii) an interlayer region, where the layers interact *via* hydrogen bonds between –F and –O atoms bound to the surface and *via* van der Waals forces, (iii) surface terminal moieties are randomly distributed on the MXene surface.[57]

Individual MXene flakes are metallic, and the electrical behavior of MXene films is determined by the type of conductivity among layers. Typically, high conductivities can be achieved if the contact between large MXene flakes with few defect concentrations is good. MXenes have displayed excellent structural traits which could make them a potential group of 2D materials for sensors, such as[84] (i) MXenes possess planar structures, good hydrophilicity, chemical, and structural stability in aqueous solutions, (ii) a significant number of –O and –OH moieties on the surface of MXene, establish strong correlation with numerous analytes, (iii) metal sites exposed at the terminals of MXene facilitate strong redox activity, (iv) good electrical conductivity of MXenes enables efficient electron transfer, and (v) with their large surface area they boost the catalytic activity.

4.1. Factors affecting the properties of MXenes

EC sensors are employed to convert the chemical properties of an analyte into electrical signals. Hence, MXenes are gaining prominence in the fabrication of sensor devices, as their properties demonstrate enhancement effects. Through this section, we have highlighted that during MXene synthesis, various etching and delamination processes result in the surface functionalization of MXenes with different functional groups. We have described

the structure of MXenes, and after that, we shall discuss the exfoliation process of MXene from MAX and the properties derived through this approach.

Eliminating the 'A' element from the MAX phase generated a variety of MXenes, which when intercalated, MXenes undergo exfoliation/ delamination upon interaction. The fundamental bonds in the structure of MXenes are responsible for their unique traits, whereas M–X bonds include a combination of covalent and ionic interactions. Besides, the nature of the M–A bond is entirely metallic, unlike other 3D layered materials. Furthermore, post delamination, the delaminated single-layer 2D materials often display different properties compared to their bulk counterparts, which is attributed to significant enhancement in the surface-area-to-volume ratio of the 2D flakes that dramatically affect the physical and chemical properties of the material.[78–80,85]

(i) Insights on the effect of etching. Currently, over 150 variants of MAX phases have been identified, and different MXenes with excellent characteristics have been prepared. As aforementioned, the $Ti_3C_2T_x$ type of MXene is the most widely explored 2D MXene.[86] Conventionally, the synthesis of MXene transpires in three stages, involving the formulation of the Ti_3AlC_2 precursor MAX phase, Al layer etching, intercalation, and exfoliation. MXenes are prepared by etching the 'A' element layer, which imparts good electrical properties.[87] Although the most commonly used etchants are HF and LiF/HCl, numerous parameters influence MXene's chemical and physical properties.[88,89] For instance, the etchant's moiety, concentration, duration of etching, the surfactant employed, stirring, sonication time, and etching temperature manifest

variations in the resulting MXene architecture.[90] Consequently, the optimization of the synthesis procedure is crucial. Hence, through this subsection, we briefly describe the effect of the synthesis procedure on the structure, defects, and surface terminations in the resulting MXene-based materials.

Etchant. Ever since the introduction of nanolayered MXenes through a wet etching procedure with HF to achieve multi-layered flakes of $Ti_3C_2T_x$, progressions in MXene synthesis and MXene-nanocomposite synthesis resulted in numerous elemental compositions and surface-functionalities. The most appropriate combination involved the use of the etchant LiF/HCl with the minimally intensive delamination method (MILD) instead of sonication to synthesize large MXene flakes with minimal defects.[87,91] Hence, the optimized etching process is cardinal to access individuals to a few layers of Ti_3C_2-MXene nanoflakes. The water molecules and surface functional groups influence the MXene crystal structure.[86] Therefore, rationally tuning the etching agent will result in regulation of the water content in the solvent, which will assist in controlling the lattice constant and thereby tuning the crystalline structure. Unlike TMDs and graphite (which possess weak van der Waals interactions among layers), MAX phases are bound by stronger van der Waals, and their exfoliation is intricate.[92,93] Hence, wet-chemical etching in the presence of HF or HF-containing solutions led to the displacement of the strong M–A bonds by weaker –F, –O, and –OH bonds, generating much more stable and closely packed $M_{n+1}X_nT_x$ layers.[94] Thus, etching and exfoliation procedures generate functionalities on the MXene surface, with plenty of –F, –O, and –OH containing functional moieties, leading to enhanced hydrophilicity.[95] Peng *et al.* demonstrated that O-functionalized MXenes exhibited mechanical flexibility attributed to the charge transport between the internal Ti–C bonds and the surface Ti–O. However, when functionalized with –OH groups, it demonstrated a stronger interlayer coupling than MXenes terminated by –O or –F attributed to the hydrogen bonds. Therefore, the –OH functionalized surface might possess a greater effect on MXene characteristics and tailoring the –OH functionalization surface is an efficient and feasible strategy to modify the properties of materials.[96]

Furthermore, the various synthesis methods include etching in halogen, molten states, non-aqueous etchants, a mixture of fluorides, and different acids.[97] However, to avoid the utilization of hazardous HF, a modified etching assay with a combination of lithium fluoride (LiF) and HCl is currently employed as a substitute.[98,99] This mild reagent imparted hydrophilic characteristics with good mechanical stability as an outcome of Li intercalation. Interestingly, fluoride termination-free MXenes have been reported for application in biomedicine fields.[100,101] This goal of producing MXenes without hazardous acids is a blossoming research field. For further specifics concerning synthetic routes followed to make MXenes, we recommend our readers to other reviews in the literature.[102–104] Nonetheless, with the advancements in MXenes, various methods such as hydrothermal, thermal reduction, chemical vapor deposition (CVD), spray drying, and electrochemical techniques are effectively used to generate 2D MXenes devoid of hazardous etchants. The various types of MXenes that are synthesized based on the MAX phase can be referred to in detail from other reports in the literature.[86]

It is relevant to note that Lipatov and co-workers have substantiated that the metal layers in the MXene structure are an important factor in impacting the electronic characteristics of MXene.[105] While Anasori *et al.* have verified the existence of a subtle balance between the etchant's activity and temperature, it must be sustained; the electronic functionality, from metallic to semiconductor-like, could be regulated by modifying the outer transition M-layer of a 2D carbide.[106] MXenes, constituted by early transition metal carbonitrides and carbides, not only possess conductivity comparable to copper but also harbor the traits of nitride/carbide. Density functional theory investigations have aided in understanding the MXene's electronic density of state and energy band structure. It has been revealed that the pristine MXene single layer is foreseen to be a metal layer possessing high electron density close to the Fermi level.[107,108]

(ii) Intercalation/delamination and intercalation[82]. These are indispensable steps to inflate the interlayer spacing of multilayer MXene flakes to produce a few or individual 2D MXene sheets. The delamination process involves the isolation of individual layers of MXene by adding salts and organic solvents (tetrabutylammonium hydroxide, NH_4, HF_4, *etc.*) during preparation resulting in delaminated MXene layers. Additionally, exfoliation increases the contact angle between the interface and the electrolyte, resulting in better EC sensing. Hence, many compounds are utilized to achieve intercalation (cetyltrimethylammonium bromide (CTAB), dimethyl sulfoxide (DMSO), metal cations/hydroxides, alkylamines, *etc.*) that significantly tailor MXene functionality. The intercalation of these guest molecules magnifies the *c*-lattice parameters and weakens the van der Waals forces and hydrogen bonds between 2D MXene layers; consequently, the multilayered MXene flakes get delaminated. These delaminated MXene layers demonstrate a larger specific surface area than multilayer MXene stacks.

Conventionally, the MXene structure is composed of weak hydrogen bonds. van der Waals's interaction between the Ti_3C_2 layers results in restacking and aggregation, causing great difficulty in research works and limited EC activity. Hence, it is crucial to synthesize MXene-based nanocomposites to magnify the EC performance purposefully. After extensive research, the introduction of interlayer spacers is established as an effective strategy. Some carbon materials, including alkaline cations, fullerenes, carbon nanotubes (CNTs), and graphene nanosheets, have been employed as anti-pile layers and intercalators to mitigate the stacking issues of Ti_3C_2-MXene to some extent and improvise the stability and reusability. This process also magnifies the EC response towards the target analyte.[109] Typically, MWCNTs form a uniform network over the MXene sheets' surface, impeding oxidation, and they are intercalated between the sheets to amplify the electrical conductivity and provide increased active sites.[110] For example, Zhen *et al.* described that MWCNTs have hollow structures, good electronic

transport capacity, and larger specific surface area, enabling their use as spacers in the synthesis of Ti_3C_2-MWCNTs nanocomposites to improve the EC performance of individual Ti_3C_2. This incorporation into the hierarchical Ti_3C_2 ensured large open spaces and exposed active sites. While on the other hand, alkaline cations (K^+, Na^+, Mg^+, and Li^+) have demonstrated spontaneous and feasible intercalation between Ti_3C_2 sheets. This alkaline cation intercalation modified the MXene characteristics by enlarging the interlayer spacing and improving structural stability that greatly favored good practical applicability.[111–113] Also, Shankar et al. described the MXene/graphite composite paste with greater adrenaline quantification sensitivity.[114] Also, Karaman et al. recorded an amplified signal for fatty acids utilizing $Cd_{0.5}Zn_{0.5}S/D$-$Ti_3C_2T_x$-MXene composites.[115]

(iii) Surface termination groups. The surface functional groups of MXenes affect their ion transport and electronic features that are directly linked to their conductivity and heterogenous charge transport process occurring on the surface.[95] Experimentally, MXene's surface termination depends on the synthetic conditions, like etching, delamination conditions, nature of the 'M' element, post-synthetic procedures, and storage.[116] Furthermore, theoretical investigations recommend that MXenes should have numerous specific properties in addition to good electronic conductivity, chemical stability, and hydrophilic surface traits.[117,118] To impart unique conductive, electrical, and EC capabilities, surface functional groups are specifically tailored to the features of MXenes.[78] For instance, the surface termination with oxygen tends to foster the highest capacity in contrast to H or/and OH-terminated MXenes.[119] Besides, other investigations have led to the expansion of the surface terminations with methoxy groups P and Si.[120] These surface functional groups alter the surface electronic structure, creating a synergistic effect with the catalyst. It is also documented that MXenes with terminations furnish lower electron transfer resistance for proficient charge migration during the electrocatalytic process.[121] Furthermore, attributed to the higher electronegativity contributed by N than C, nitride or carbonitride MXenes with M–N bonds are stronger than those with M–C bonds. Hence, M–N MXenes possess distinct electronic features compared to M–C MXenes.[122]

(iv) Defects. Furthermore, the synthesis process affects the vacancies and defects in the MXene anatomy. It influences the electroconductivity due to the surface termination and defects.[123,124] Foreseeably, higher concentrations of HF introduce more defects into the MXene flakes. The greater the defects, the lower the electroconductivity MXenes possess due to the destruction of the ordered structure. Hence, these defects are regulated by doping various atoms. Furthermore, the defects of charge imbalance are generated via the exchange of ions with different electronic densities. Because of the commonly used HF-etching solution, the surface of MXenes generally contains –O, –F, and –OH functional groups. So, if the surface terminations are modified, there is a possibility that small molecule adsorption can lead to the amplification of electrical conductivity of MXenes.[125,126]

(v) Hybrids or heterostructures. Through this review, we have come across several excellent characteristics of MXene; to recap, the prominent ones include high hydrophilicity, metal-like electronic conductivity, and greater specific surface area with abundant terminal groups. Appropriate surface modification and functionalization are essential for optimum use, as they will primarily magnify the chemical stability. Typically, surface modification and functionalization are accomplished through covalent (molecule attachment) and non-covalent interactions (electrostatic and physical adsorption). Considering the ease of the process, the latter is widely applied. To exemplify, positively charged molecules quickly form composites with MXene as its surface is abundant with –OH and –F ions.

Although MXene portrays interesting features and combinatorial flexibility, it also possesses some hereditary demerits, such as restacking after delamination and modest air stability. MXene's stability is crucial for different applications and long-term stability. Hence, hybridization has the potential to enhance the MXene's stability. To circumvent these constraints, researchers have attempted the synthesis of MXene nanocomposites, including carbonaceous materials, conducting polymers, MOFs, MOs, TMDCs, and others.[127] This process also amplifies the MXene sensing performance as it is inferred from the literature that atoms or molecules with different structures selectively interact with the surface of MXenes through electrostatic attractions or physical adsorption.[123]

Nanoparticles of various morphologies are termed secondary nanoparticles that can be bonded to the MXene flaky surface, resulting in a mixed-dimensional heterostructure. The nanoparticle size can be <100 nm, technically called a nanoparticle with zero dimensionality. Typically, the bonding of 0D nanoparticles onto the MXene's surface is achieved using salts like $SbCl_3/AgNO_3$. Attributed to their electrostatic attractions in an aqueous environment, the cations of each of these salts are absorbed by the MXene layers. At the same time, 0D nanoparticles, such as Ag nanoparticles, are formed via a reduction reaction.[128] These secondary nanoparticles can be rod or tubular-shaped structures (1D nanoparticles) such as carbon nanotubes. The sheet-like structures are denoted as 2D nanoparticles like MXene or graphene. An example of a 2D–2D heterostructure is the hybridization of MXene with rGO. The aforementioned electrostatic attraction strategy is also employed to modify the MXene with secondary 1D and 2D nanoparticles to form various heterostructures. Likewise, the secondary nanoparticles are functionalized utilizing a modifier like a silane coupling agent to endow the material with the positive charge of the MXene surface. These mixed-dimensional MXene structures have broad applications in sensor fabrication technology.[129] Considering the excellent properties of MXenes, there are several reports on the preparation and application of 0D, 1D, 2D, and 3D MXenes.[130,131] 0D MXene $Ti_3C_2T_x$ quantum dots are employed for ultra-fast and narrow laser fiber production, while 1D MXene fibers, 2D Ti_3C_2 MXene nanosheets, and 2D MXene architecture are used for efficient sensing applications. Their accessible greater specific surface area that leads to interactions, selective binding,

and the capability of transducing these interactions into recognizable analytical signals make them an ideal sensing material. Similarly, to enhance the conductive network of MXenes, Au NPs were tagged to design a composite heterostructure and serve as signal amplifiers and reusable sensing platforms.[132,133] Such tagging of Ag or Au onto the MXene surface influences the EC capacity of MXenes.[134] Furthermore, a hybrid MXene/carbonnanohorn/beta-cyclodextrin/metal–organic framework composite was fabricated through electrostatic self-assembly accompanied by surface charge interaction, and also a blend of metal alloy loaded MXene with $CuCl_2$ nanowires on a metallic–nonmetallic electrode was designed for the enzyme-free EC sensor that demonstrated excellent sensitivity for the target analyte.[135,136]

Furthermore, a thorough blending with different types of dispersion leads to a positive zeta potential and negative surface charges on MXene flakes, resulting in flocculation and, consequently, the formation of hybrids.[137] The literature reveals the utilization of metal-oxides, graphene, CNTs, silicon carbide nanowires, polymers, and others for chemically modifying MXenes, imparting a positive surface charge.[138,139] The MXene surface can be patterned through electrostatic interactions between chitosan/polyaniline/polypyrrole, forming a nanocomposite *via* negatively charged $Ti_3C_2T_x$ MXene and the positively charged polymer.[140] Another important parameter is electrochemical impedance spectroscopy (EIS) of pristine MXene and hybridized MXene, wherein the hybridized MXene depicts the lowest R_{ct} value over the pristine one.

5. Methods of electrode surface modification

A prerequisite for fabricating the sensor is homogeneously dispersing the nanomaterial in an appropriate solvent. It must be noted that the synthesis route and the type of terminal functional groups on MXenes affect their dispersibility. Hence, solvents like N-methyl-2-pyrrolidone (NMP), ethanol, DMSO, and dimethylformamide (DMF) are suitable carriers of MXene nanosheets. Dispersing MXenes in non-aqueous polar solvents minimizes their interaction with dissolved oxygen and/or water, extending their shelf life and stability.[141] It is crucial to mention that a modified electrode can be constructed *via* electropolymerization, covalent bond formation, and surface adsorption.[142] In brief, during electropolymerization, the pre-treated WE was immersed into an electrochemical cell system with a definite concentration of monomer and electrolyte. During electrolyzation, the electrically active monomer undergoes transformation into ions and free radicals, initiating polymerization to form a stable, uniform polymer film. Covalent bond formation is the attachment of modifying agents onto the sensing substrate *via* covalent adsorption. The adsorption method of surface modification of the WE can be performed *via* chemical adsorption (mutual adsorption between the solution and the solid material interface), self-assembled monolayers (SAMs synthesized through chemical and physical interactions among the film-forming molecules' functional moieties, or *via* spontaneous adsorption),

and coating (dip, spin and dispense coatings). Fig. 6(a) illustrates the admirable characteristics of modified EC sensors.

Several methods are utilized to deposit nanomaterials as thin films, mono/multilayers, onto the electrode substrate. Typically, experimental parameters, including choice of solvent, particle volume, and concentration, affect the deposition process, which is tuned to achieve a film with the desired thickness and morphology. On occasions when continuous conductive films that are thin are required, direct coating methods demonstrate facile routes with pleasing versatility. These methods include but are not limited to drop cast coating, dip coating, spray coating, spin coating, *etc.* Herein, we briefly describe the methods of electrode surface modification as illustrated in Fig. 6(b).

(i) Drop cast coating[143]

The most popularly used method of electrode surface modification is drop cast coating. A drop of liquid composed of particles or nanomaterials of interest is first deposited on the electrode surface and is left to dry (evaporation of solvent) without spreading. It is the most straightforward film-forming technique as it does not involve specific equipment. However, the film thickness and properties hinge on nanomaterial concentration and volume of dispersion cast. Additionally, this method requires solvents other than water for dispersion.

(ii) Dip coating[144]

The dip-coating process has the following steps: dipping, immersion, deposition, draining, and evaporation of the solvent. This method allows the layer-by-layer assembly process through electrostatic interactions. For example, dipping the substrate in a poly(diallyldimethylammonium chloride) and MXene/MXene-composite dispersion has facilitated the construction of bendable, stretchable, and conductive films for wearable sensors.

(iii) Spray coating[145]

The literature reveals that delaminated MXene aqueous dispersions are generally employed for an ethanol-based colloidal solution, whereas non-aqueous MXene dispersions are limited. The sprayed delaminated MXene nanosheet films, known for their excellent mechanical and electrical properties, are utilized as electrical contacts for thin film transistors (gate, source, and drain), bottom electrodes for triboelectric nanogenerators, *etc.*[146,147]

(iv) Spin coating[148]

The spin-coating methodology, also known as the solution processing method, leads to the production of thin and homogenous films from dispersions. In this method, the substrate is spun at high RPM, and a known concentration and volume of material is introduced into the center. Spin-coated films possess better flake alignment (without wrinkles) than films fabricated by other methods. This is attributed to the centrifugal force applied on the liquid layer that forces the suspended nanosheets to comply and align parallel (in the direction of outward centrifugal force). In brief, the dispersion wets the substrate's surface, and then the liquid layer spreads over the substrate on rotation, resulting in a thin layered film.
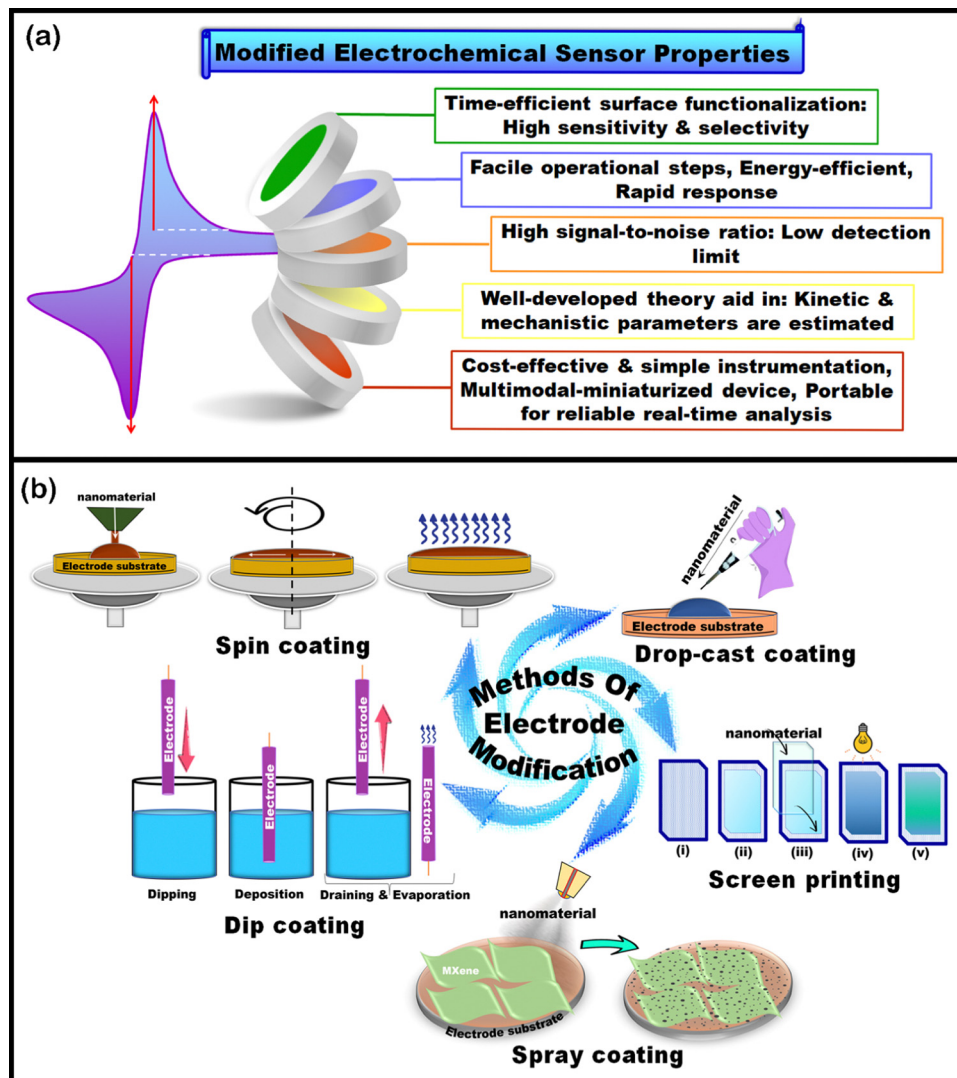
Fig. 6 (a) Graphical representation of modified electrochemical sensor properties. (b) Illustrations of methods of electrode modification.

(v) Screen printing[149]

Screen printing is employed for depositing 1 to 100 μm thick films. It can be carried out in a flatbed automated mode, wherein the screen, with a narrow gap on the substrate, is filled with the flooded ink. Subsequently, a squeegee is traversed across the screen to expel the thrust out of the ink and transfer it to the electrode substrate. The construction of screens is straightforward and serves as a rapid prototyping method.

6. Recent developments in 2D MXenes for electrochemical sensing of HMIs and phenolic moiety-containing toxic molecules

Several traditional techniques, such as inductively coupled plasma mass spectroscopy, inductively coupled plasma atomic emission spectroscopy, atomic adsorption spectroscopy, GC,

GC–MS, HPLC, and many others, are available for the quantification of HMI and enlisted phenolic moiety-containing molecules with good accuracy and sensitivity. However, they have several drawbacks, such as[150] (i) prolonged sample preparations, (ii) bulky instruments that do not favor on-site analysis and require professional personnel to operate, (iii) inability to detect multi-metal elemental analysis simultaneously, making them not cost-effective for wide application. Hence, EC sensors have garnered attention and found broad applications owing to their advantages, attributable to their straightforwardness, reasonable sensitivity, and cost-effectiveness.

The advancements in EC sensors fundamentally rely on the charge transfer phenomenon among the various nanomaterials deposited onto the WE surface. While the key features of the nanomaterials include electrical conductivity, specific surface area, electrocatalysis, electrochemically enhanced signal-to-noise strength, and mass transport, their activities play a pivotal role in regulating efficient sensing results. The forthcoming subsections of the article describe the MXenes and

their hybrids for EC sensing of HMIs and toxic phenolic molecules in various environmental matrices. HMIs are non-degradable and persistent in the environment, which is hazardous to the ecosystem.[150] Meanwhile, phenolic groups containing molecules continuously infiltrate the ecosystem through industries and sewage draining, which are toxic in terms of teratogenic, carcinogenic, and mutagenic features that pose severe health complications. Several anthropogenic activities have contributed to their accumulation. These emerging contaminants are widely used, and their associated risks to humans and the environment have been well-documented.[151] Fig. 7(a) and (b) depict the adverse effects of HMIs and toxicities of phenolic moiety-containing industrial chemicals on humans.[152–156] Through this review, we have attempted to outline the status of MXene EC methods for determining emerging contaminants, focusing on HMIs and phenolic moiety-containing industrial chemicals, since EC sensors are field-ready, cost-effective, and enable rapid analysis.

6.1. MXene EC sensors for HMIs

Although trace HMIs are fundamental for living organisms for a healthy life, their excessive environmental levels are detrimental. Several inorganic species are the major ecological contaminants frequently detected in water bodies. HMIs, also known as trace elements such as Pb^{2+}, Hg^{2+}, Cd^{2+}, As^{3+}, Zn^{2+}, and Cu^{2+}, are significant contaminants released by anthropogenic activities in domestic, chemical, and other technological applications.[157,158] Acute or chronic poisoning can occur
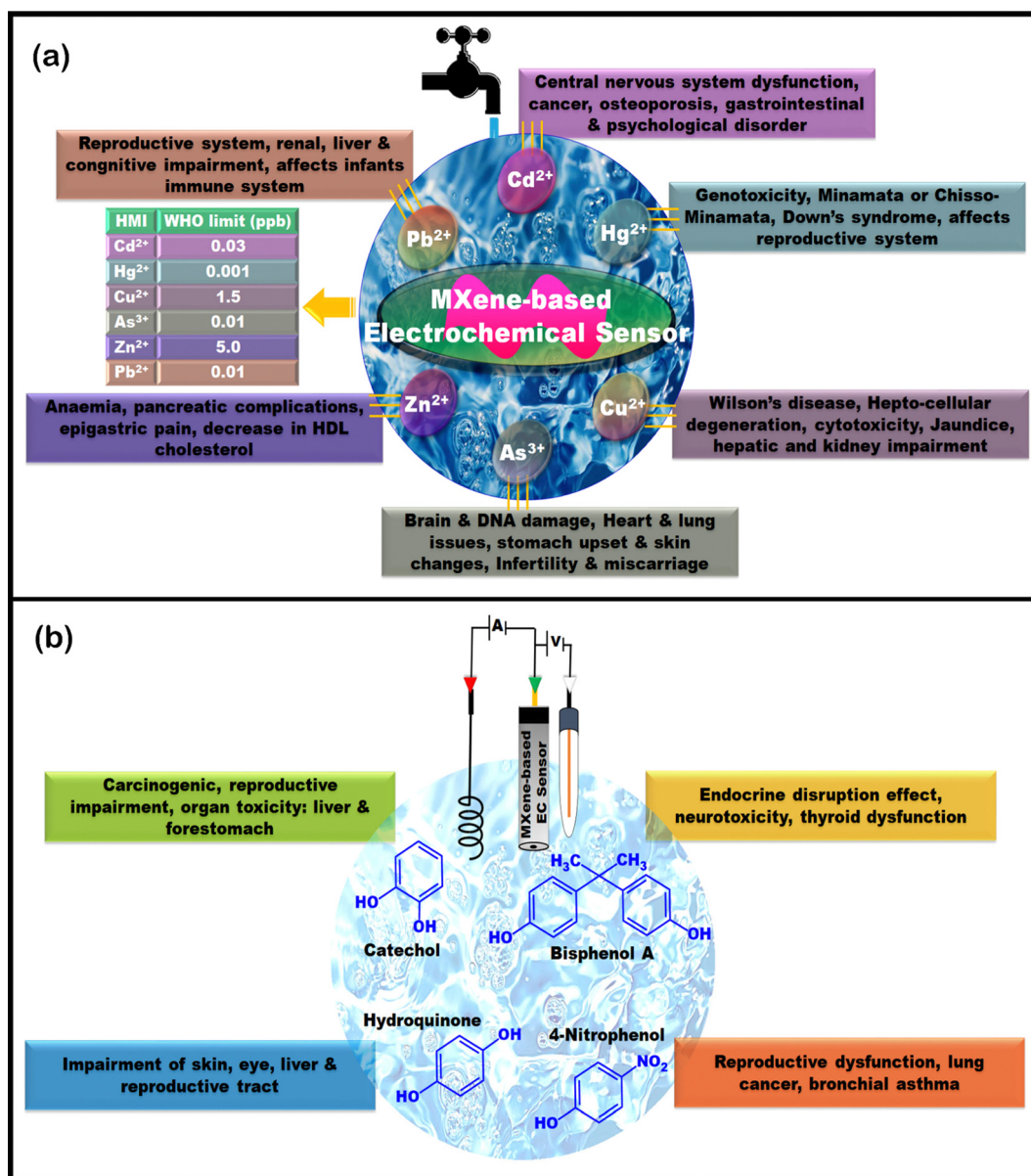

Fig. 7 (a) Adverse effects of HMIs on humans and their limits set by WHO in drinking water. (b) Toxicities of phenolic moiety containing industrial chemicals on humans.

following exposure to these elements through air, water, and food as they disrupt cellular events. Although various technologies have been developed for the de-pollution and monitoring of HMIs from different environmental media, they have inevitable setbacks.[159–161] Hence, there is a demand for facile and quick detection of these analytes from ecological systems. The literature depicts several reports on HMI detection using inorganic material-modified WEs, micro-, macro-, and nano-particle-based biosensors to detect HMI, functionalized layered double hydroxides, and several others.[142,162,163] Hence, the literature lacks a review MXene-based sensors for HMIs. MXene-based sensors are excellent candidates for sensing HMIs, as their multi-layered structure generally comprises elements that possess high-affinity properties to HMIs. As noted from the literature, MXene-based EC sensors for HMIs commonly employ the SWASV technique. This technique is readily amendable for the determination of HMIs. It typically involves two steps: (a) EC deposition or accumulation of HMIs at a steady potential, pre-concentrating the analyte on the electrode surface and (b) stripping or dissolving the deposited analyte from the electrode surface.

Mercury, released from industries, enters living organisms, causing grievous and detrimental effects on human health and the environment.[164] Hence, monitoring the excessive accumulation of Hg^{2+} is beneficial in mitigating the associated risk. Cheng and researchers synthesized a PANI-Ti_3C_2 composite to develop an EC sensor for Hg^{2+}.[165] The composite was prepared by initially dispersing Ti_3C_2 in an HCl solution, followed by sonication, into which pure aniline was introduced. Later, ammonium persulphate dissolved in HCl was added dropwise into the abovementioned solution while stirring in an ice bath for 6 h. The product was then washed, freeze-dried, and used to fabricate an EC sensor. PANI-Ti_3C_2/GCE showed good sensitivity towards Hg^{2+} with a LOD of 0.017 µg L^{-1}, and the recovery % from natural water samples was acceptable in the 97.2% to 100.6% range.

Arsenic is present in water (groundwater, drinking water, and surface water) in the forms of As^{3+} and As^{5+}. World Health Organization recommends that the concentration of As^{3+} must not be more than 10.0 µg L^{-1} in drinking water and 50.0 µg L^{-1} in surface water. Therefore, more recently, Xiao and researchers have synthesized an iron–metal–organic framework/$Ti_3C_2T_x$-based MXene composite (Fe-MOF/MXene) via a facile solvothermal procedure for the determination of arsenic species for the first time.[166] MOFs are suitable electrode materials due to their tunable properties, large specific surface, stability, and active transition metal redox centers. It has been suggested that the Fe-MOF exhibits good adsorption features for As^{3+} owing to the coordination interaction between them. On the other hand, MXenes possess numerous active sites capable of intense bonding with the organic ligands of MOFs and a few inorganic compounds. In this context, they have been employed as adsorbents for arsenic removal by forming As–O bonding between the OH groups on the MXene surface and arsenic species. Furthermore, MXenes display ion insertion capability, making them an ideal material for fabricating high-performance

EC sensors. Fe-MOF/MXene was prepared by first dissolving $FeCl_3 \cdot 5H_2O$ in DMF under vigorous stirring, and then adding 2-NH_2-BDC and stripped MXenes. This mixture was transferred into a Teflon-lined autoclave to set the hydrothermal reaction and obtain the desired product. To check the optimum ratio, various mass ratios of $FeCl_3 \cdot 5H_2O$/MXenes were also prepared, which were designated as Fe-MOF/MXene-2 (2 : 1), Fe-MOF/MXene-1.5 (1.5 : 1), and Fe-MOF/MXene-1 (1 : 1). Next, the sensor was constructed on a precleaned GCE platform. 4 mg of Fe-MOF/MXene powder dispersed in DI water via sonication was drop-cast coated onto the GCE and dried to obtain Fe-MOF/MXene/GCE as illustrated in Fig. 8(a) and the SEM image of Fe-MOF/MXene is shown in Fig. 8(b). Similarly, the comparative electrodes were prepared. At the beginning of this section, we have described the two-step SWASV process for analyte detection. To substantiate the case of arsenic detection, during the preconcentration step, As^{3+} in solution was adsorbed on the Fe-MOF/MXene/GCE surface via coordination with –OH groups from Fe-MOF and MXene and then transformed into zero valence As(0) through reduction. The proposed Fe-MOF/MXene/GCE with a mass ratio of 1.5 delivered a strong stripping current with a well-defined peak shape and peak signal. This was attributed to the synergistic effect of MXene and Fe-MOF for As^{3+}, which facilitated the adsorption and bonding of As^{3+}. XPS investigations were conducted to determine the interaction mechanism of Fe-MOF/MXene and As^{3+}. Since it is conceptually interesting, we briefly describe the XPS analysis results herein. The successful formation of the Fe-MOF was ascertained by the presence of satellite signals at 720.0 and 730.0 eV. In summary, no evident transformation of Fe^{3+}/Fe^{2+} was witnessed for the As adsorbed Fe-MOF/MXene, implying that Fe species acted as adsorption sites rather than oxidation agents. Next, the oxidative stripping signal of arsenic was captured through a positive potential scan. The LOD estimated using SWASV (Fig. 8(c)) was down to 0.58 ng L^{-1}. Furthermore, the selectivity examination was performed more vigilantly with Cu^{2+} because its stripping potential is close to that of As^{3+}, and the results indicated that Cu^{2+} did not interfere significantly. A 100-fold excess of other ions, such as Pb^{2+}, Mn^{2+}, Cd^{2+}, Hg^{2+}, Fe^{3+}, Cl^-, and NO_3^-, was tested, and the results showed no apparent peak response variation for arsenic. This selective trait of the sensor favored its performance in natural water systems (taps, rivers, and lakes) with acceptable recoveries in the range of 97.4% to 98.4%. The sensor also exhibited good reproducibility and repeatability with an RSD of 3.9% and 2.19%, respectively. However, this report lacks a long-term stability study of the proposed sensor. Finally, yet importantly, the Fe-MOF/MXene composite preserved the original octahedral structure in the Fe-MOF. Due to the synergistic effect of the Fe-MOF, MXene promoted arsenic deposition and drastically amplified the detection response of As^{3+} at Fe-MOF/MXene/GCE.

Chen and team synthesized a 3D Fe–Co-LDH/Ti_3C_2-based MXene composite as a modifying agent for the GCE platform for the sensitive detection of As^{3+}.[167] LDHs are 2D inorganic nanomaterials with good activity and a larger specific surface area. Out of various bimetallic components of LDHs, Fe–Co was used as an excellent electrode material due to its variable
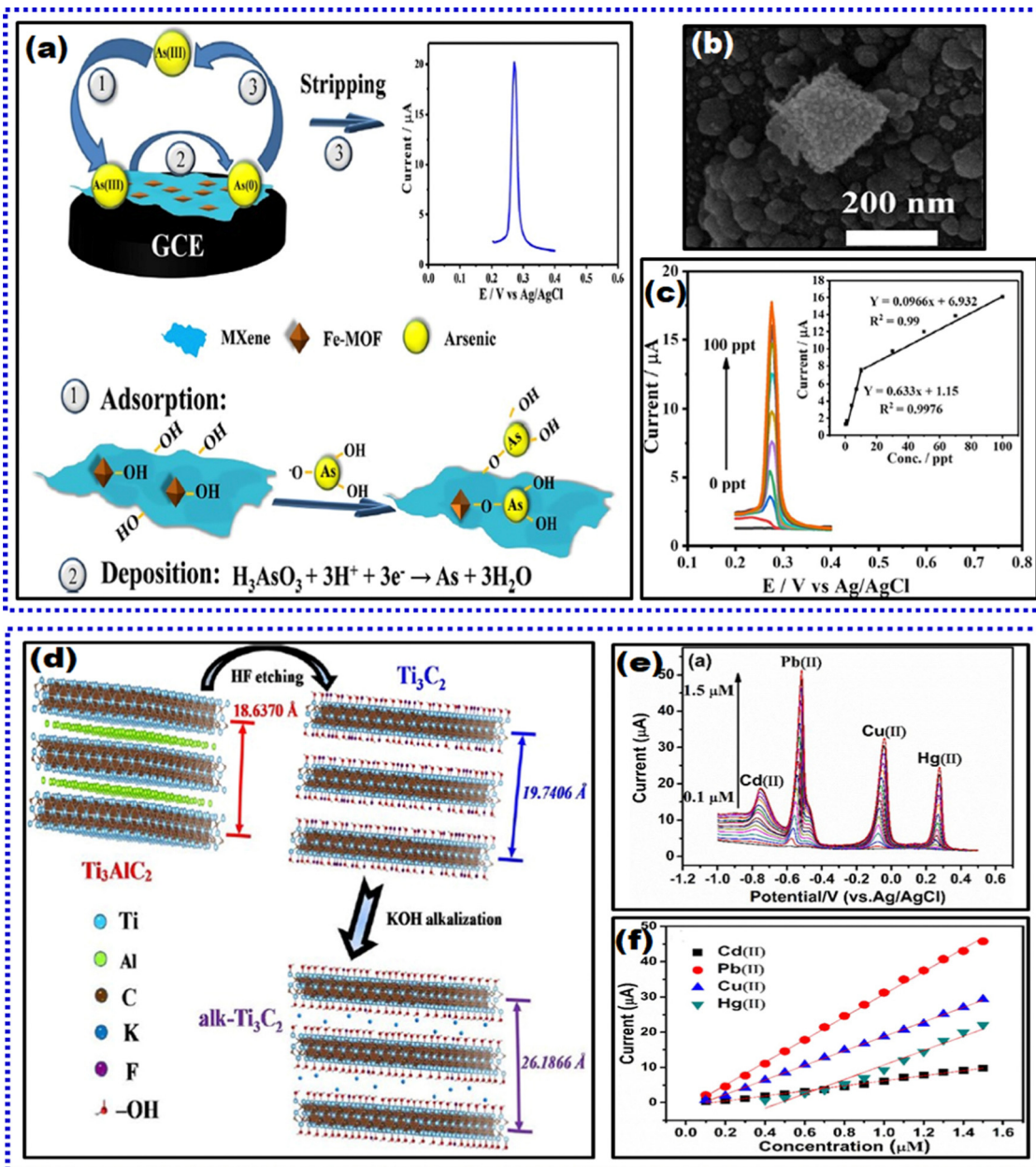
Fig. 8 (a) Schematic representation of adsorption-assisted As^{3+} determination on Fe-MOF/MXene/GCE employing SWASV, (b) SEM image of Fe-MOF/MXene, and (c) SWASV plots of various concentrations of As^{3+} at Fe-MOF/MXene/GCE, inset: calibration curve.[166] (d) Graphical representation of the parental Ti$_3$AlC$_2$ MAX phase and post-etching MXene pre- and post-alkalization treatment, (e) SWASV simultaneous responses of Pb^{2+}, Hg^{2+}, Cd^{2+}, and Cu^{2+} HMIs, and (f) corresponding calibration plots of HMIs.[168] Reproduced with permission from ref. 166 and 168. Copyright Elsevier (2022), and Elsevier (2017).

valences. The synergy between the Fe–Co bimetallic center and the layered structure of LDH significantly contributed to an accelerated charge transfer rate *via* a shorter ion transport path, leading to an amplified EC sensing response. To prepare the modifying agent, initially, MXene was synthesized employing the LiF etching method. Next, the solution composed of Co(NO$_3$)$_2$·7H$_2$O and FeSO$_4$·7H$_2$O in DI water, NH$_4$F, urea, and the as-prepared MXene was introduced with vigorous stirring. This mixture was later transferred into a tetrafluoroethylene-lined autoclave for a hydrothermal reaction to obtain Fe–Co-

LDH/MXene. This nanocomposite was suspended in DI water and drop-cast coated on the pre-cleaned GCE surface, dried at RT, and used for further analysis. The sensor was soaked in a phosphate buffer solution (PBS, pH 5.0) containing a known concentration of As^{3+}. After the preconcentration step, a SWASV scan was performed to get stripping signals for As^{3+}. Strong stripping signals were obtained due to (a) MXene's well-charged transfer kinetics and conductivity, (b) abundant OH groups in both MXene and Fe–Co-LDH that facilitate the exchange of arsenite oxoanions, improving analyte adsorption, and

(c) the Fe–Co-LDH surface featuring ample Fe atom centers, forming strong Fe–O–As bonds. Furthermore, the mechanism of solid binding of the sensing electrode with As^{3+} was investigated using an XPS scan, similar to the abovementioned research on As^{3+} detection. The results suggested that the exchange reaction between hydroxyl groups and arsenite oxygen anions occurs on the surface of Fe–Co-LDH/MXene, and the hydroxyl groups are exchanged *via* arsenite, thus improving the adsorption capacity of As^{3+}. The sensor depicted good sensitivity with an LOD of 0.9 ppt and selectivity even in Cu^{2+} forming intermetallic compounds. This strong anti-interference ability was mainly due to the specific interaction of As^{3+} with Fe–Co-LDH/MXene, as verified through XPS investigations. In addition, the presence of 10 ppb Fe^{3+}, Hg^{2+}, Cd^{2+}, and Pb^{2+} did not affect the stripping signals for As^{3+}. Fe–Co-LDH/MXene depicted good recoveries of As^{3+} from spiked tap, lake, and river water samples, verifying its feasibility for As^{3+} determination in aqua systems.

These are numerous reports on individual detection of HMI based on MXene-modified electrochemical sensors. Furthermore, real-time and onsite analysis is a significant challenge because mutual interference is observed due to the formation of intermediate alloys and electroactive sites undergoing competitive adsorption. Hence, several researchers have developed MXene-based EC sensors to determine HMI simultaneously. Zhu *et al.* reported the first simultaneous detection of Pb^{2+}, Cd^{2+}, Hg^{2+}, and Cu^{2+}.[168] In their work, the MXene surfaces were modulated through alkaline intercalation between the nanosheets, which improved the adsorption capability of heavy metals. This phenomenon can be attributed to the exfoliation and alkalization process of MXenes, which significantly enhances its binding energies and adsorption capabilities. A pictorial representation of the parental Ti_3AlC_2 MAX phase and the post-etching MXene before and after alkalization treatment is depicted in Fig. 8(d). It represents the process of alkalization that magnified the c lattice parameter of $Ti_3C_2T_x$ from 19.741 Å to 26.187 Å, with unique morphology and modification in surface chemistry. The sensor was fabricated on the GCE substrate by drop casting the alkalization intercalated Ti_3C_2 (Alk-Ti_3C_2) homogenous suspension on its surface. Compared to the pristine Ti_3C_2-sensor surface, the Alk-Ti_3C_2 exhibited a greater peak current with a well-defined peak shape, indicating that the latter surface possessed distinct surface chemical properties and morphology. They demonstrated well-resolved voltammetric peak potentials for each HMI without significant mutual interference (even with increased metal ion concentrations) through SWASV. Electrostatic interactions amplified the charge transfer to the negatively charged Ti_3C_2 from cationic heavy metals. Hence, the sensor acted as a reliable platform for sensing Cu^{2+}, Hg^{2+}, Cd^{2+}, and Pb^{2+}, and the individual LODs were 0.032 μM, 0.130 μM, 0.098 μM, and 0.041 μM, respectively. This study observed intermetallic interference for synchronously determining the co-existing Cu^{2+}, Hg^{2+}, Cd^{2+}, and Pb^{2+} metal ions. The correlation coefficients, LOD, and sensitivities shifted from the determination response of individual metal ions, and the stripping signals were amplified during co-existence.

It was observed that when metal ions co-existed with metal, the response signal of the other component was amplified. More interestingly, as illustrated in Fig. 8(e) and (f), all four species displayed well-resolved peaks. This determination promotes the presence of one metal over the other, and hence, when they co-exist in real samples, the exact concentrations are difficult to determine. The sensor's reproducibility was assessed for the simultaneous determination of Cu^{2+}, Hg^{2+}, Cd^{2+}, and Pb^{2+} metal ions, and their corresponding RSD values are 2.16%, 4.05%, 6.57%, and 0.80% respectively. Furthermore, the sensor's storage stability for 3 weeks produced satisfactory RSD values of 96.3%, 93.8%, 90.5%, and 94.3% for Cu^{2+}, Hg^{2+}, Cd^{2+}, and Pb^{2+}, respectively.

In the subsequent years, Zhu and collaborators attempted to reduce the cost of sensor fabrication and micromachining with good precision computer numerical control (CNC) as a promising substitute.[169] The as-synthesized nanomaterial was micro-milled into a microgrid structure and integrated into a microelectrode assembly. Researchers synthesized Bi@d-Ti_3C_2 by initially dispersing Ti_3C_2 in ethanol *via* sonication and subsequent addition of $NaBH_4$. Later, a $Bi(NO_3)_3$ solution prepared in ethylene glycol was introduced dropwise into the d-Ti_3C_2 solution and stirred for 2 h to obtain the required product. This nanocomposite Bi@d-Ti_3C_2 was incorporated into graphite inks and NMP solvent through blending in an agate mortar to achieve a homogenous paste. The paste was then pressed onto the polyethylene terephthalate (PET) substrate. After that, the microgrid electrode was constructed by curing the prepared substrate at 150 °C to eliminate NMP, followed by engraving to the designed pattern utilizing a CNC milling machine. d-Ti_3C_2 nanosheets exhibit good EC characteristics with a huge contact area at the interface and rapid charge and ion transport kinetics. Also, bismuth nanostructures prevented the d-Ti_3C_2 nanosheets from restacking and facilitated abundant active sites to form alloys with target HMIs. Moreover, compared to conventional carbon/bismuth composites, the preparation method employed in this work did not require thermochemical reduction reactions, thus decreasing the energy expenditure. Comprehensive characterization studies verified the electrostatically induced self-assembly between negatively charged d-Ti_3C_2 nanosheets and positively charged Bi cations. As depicted in Fig. 9(a), the microgrid structure remarkably improved the diffusion of the target analyte through hemispherical diffusion in preference to conventional planar diffusion, thus facilitating the accumulation of HMIs during the cathodic reduction process. Under optimized conditions, Bi@d-Ti_3C_2/MSA was utilized to determine Pb^{2+}, Cd^{2+}, and Zn^{2+} *via* SWASV simultaneously, and their LODs were 0.2, 0.4, and 0.5 μg L^{-1}, respectively. The inherent high current density and small IR drop characteristics of the microelectrode structure magnified the signal-to-noise ratio. A 100-fold excess of Na^+, K^+, Mg^{2+}, Ca^{2+}, Fe^{2+}, and Ni^{2+}, and a 50-fold excess of Cu^{2+} were added to the 0.1 M HAc–NaAc solution containing Cd^{2+}, Pb^{2+}, and Zn^{2+}. The results demonstrated the high resistance of Bi@d-Ti_3C_2/MSA to the added interferences. The sensor demonstrated suitable long-term stability (after 2 weeks of storage) with RSD values of 96.67%, 97.53%, and 96.30% for Cd^{2+}, Pb^{2+}, and Zn^{2+},
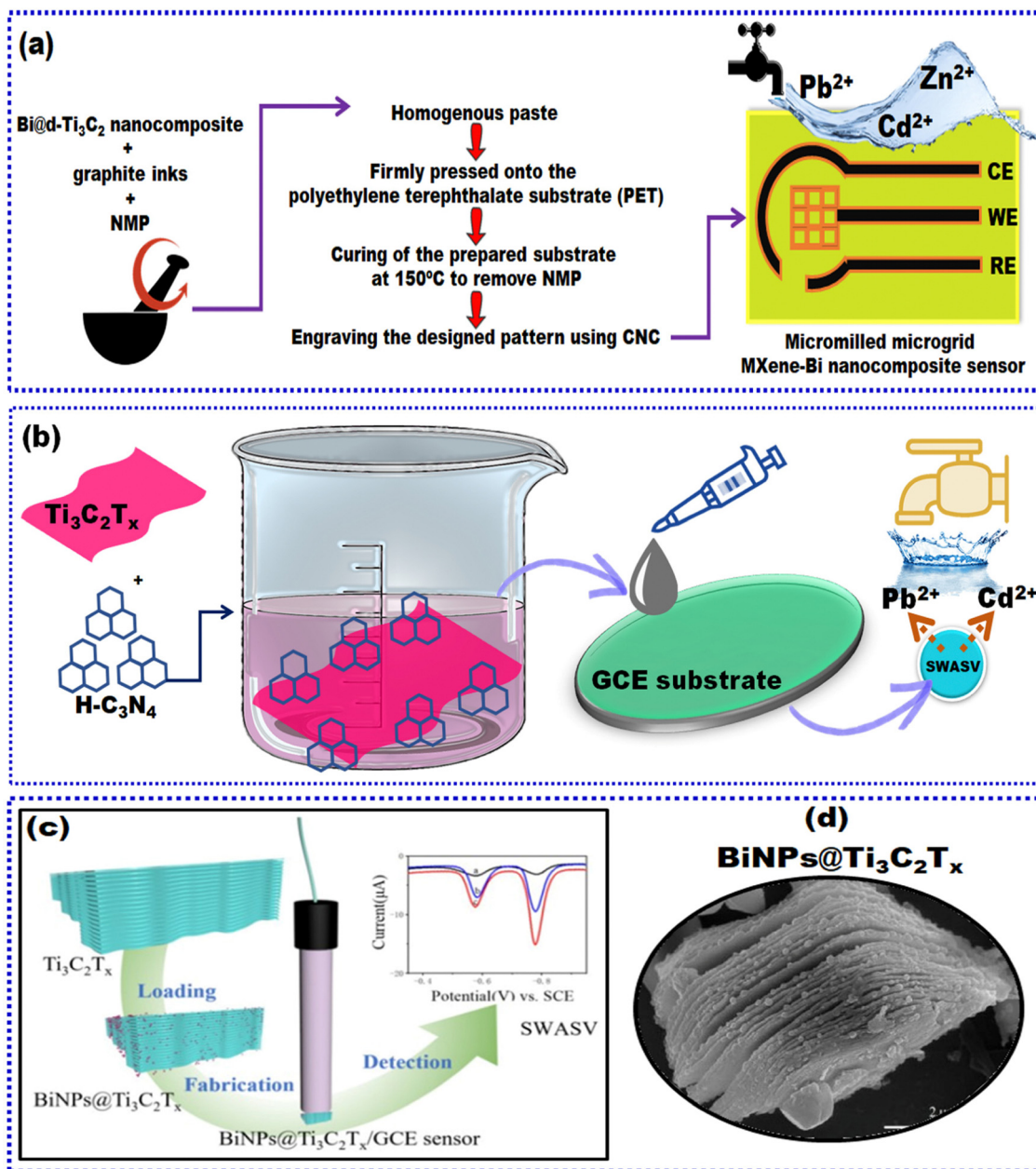
Fig. 9 (a) Construction scheme for Bi@d-Ti$_3$C$_2$/MSA and (b) schematic representation of H-C$_3$N$_4$/Ti$_3$C$_2$T$_x$ synthesis, and fabrication of C$_3$N$_4$/Ti$_3$C$_2$T$_x$/GCE. (c) Graphical illustration of BiNPs@Ti$_3$C$_2$T$_x$/GCE sensor construction and (d) TEM image of BiNPs@Ti$_3$C$_2$T$_x$.[171] Reproduced with permission from ref. 171. Open access MDPI (2020).

respectively. The reproducibility of SWASV (RSD: ±2.5%) and three different electrodes (RSD: 7.55%, 8.01%, 8.34% for Cd^{2+}, Pb^{2+}, and Zn^{2+}) depicted satisfactory RSD values. Finally, the sensor was validated for trace concentration and simultaneous determination of Cd^{2+}, Pb^{2+}, and Zn^{2+} from the spiked tap and drinking water samples with acceptable recoveries ranging from 86.0% to 112.0%. Theoretically, 112.0 recovery % is unacceptable for validating the sensor's good sensitivity. However, the work demonstrates the attempt to construct an integrated miniaturized system for sensitive, portable, and affordable EC monitoring of heavy metal contaminants from aqueous solutions. The strategy

employed to synthesize the nanocomposite is the accretion of Bi^{3+} via electrostatic interaction on the surface delaminated Ti$_3$C$_2$ nanosheets followed via in situ growth of bismuth nanorods.

Lv and the team reported the synthesis of Ti$_3$C$_2$T$_x$ with protonated carbon nitride, namely, H-C$_3$N$_4$/Ti$_3$C$_2$T$_x$.[170] Due to enhanced electrostatic interactions, a large amount of H-C$_3$N$_4$ was distributed on the Ti$_3$C$_2$T$_x$ surface. The advantages of this synthesis process were: (i) excellent conductivity derived from the synergistic interaction between H-C$_3$N$_4$ and Ti$_3$C$_2$T$_x$ with abundant electroactive deposition sites for the HMIs and (ii) good stability of the nanocomposite attributed to the

protective $H-C_3N_4$ coating. The nanomaterial was prepared by taking an appropriate amount of $Ti_3C_2T_x$ dispersed in 100 ml of deionized water assisted by 1 h sonication in an argon atmosphere. Subsequently, $H-C_3N_4$ was added and ultrasonicated for about an hour, followed by stirring for 24 h. Finally, the suspension was suction-filtered and lyophilized to obtain the desired product. A schematic illustration of the synthesis and structures is depicted in Fig. 9(b). Furthermore, to modify the electrode surface, a suspension of the nanomaterial mentioned above was prepared in 5 mL of DI water and drop-cast coated on a pre-cleaned GCE. SWASV aided in detecting Pb^{2+} and Cd^{2+} taken in 0.1 M acetate buffer solution (HAc–NaAc) of pH 6.0. Initially, the preconcentration step was carried out by applying a negative voltage of 1.2 V with continuous stirring to achieve the deposition of HMIs. The proposed $H-C_3N_4/Ti_3C_2T_x$ sensor depicted remarkable sensitivity for the simultaneous determination of Pb^{2+} and Cd^{2+}. Here, the homogeneous dispersion of $H-C_3N_4$ on the $Ti_3C_2T_x$ surface amplified the stability of $Ti_3C_2T_x$ and provided active sites for the ions under investigation. At the same time, $Ti_3C_2T_x$ served as an efficient support, reinforcing the conductivity and charge transfer. Therefore, the $H-C_3N_4/Ti_3C_2T_x/GCE$ displayed better sensitivity during simultaneous detection than individual detection of Pb^{2+} and Cd^{2+}. Furthermore, the addition of a 100-fold excess of interferent ions and organic molecules did not affect the peak currents of Pb^{2+} and Cd^{2+}, while the reproducibility and stability (for 15 days) RSD values were 0.45%, 1.79%, and 1.42%, 1.52% for Pb^{2+} and Cd^{2+}, respectively. The fabricated sensor was examined in a real tap water sample with acceptable recoveries of 98.0–97.8% and 101.0–102.0% for Cd^{2+} and Pb^{2+}, respectively. In conclusion, the formation of intermetallic compounds improved the peak current response at low concentrations, while competitive deposition partially offset the affinity at higher concentrations. This work provided a facile method to enhance the stability of the MXene composite and demonstrated the good functionality of the EC sensor for the determination of HMIs.

Furthermore, He *et al.* prepared $BiNPs@Ti_3C_2T_x$ nanocomposites by admixing $Ti_3C_2T_x$ nanosheets with Bi sequentially for Pb^{2+} and Cd^{2+} detection from the tap and lake water.[171] Initially, $Ti_3C_2T_x$ was dispersed in ethylene glycol *via* ultrasonication, followed by the addition of $C_6H_5Na_3O_7$. Subsequently, $Bi(NO_3)_3·5H_2O$ was added to the mixture and stirred for 12 h. Next, $NaBH_4$ was introduced *via* shaking, and the solid products were precipitated using centrifugation, followed by washing and drying for further application. Furthermore, the sensor was constructed by drop cast coating the $BiNPs@Ti_3C_2T_x$ nanocomposite dispersed in a 0.2% chitosan solution onto the GCE surface and allowed to air-dry. A schematic representation of sensor fabrication is presented in Fig. 9(c). Fig. 9(d) depicts the TEM image of $BiNPs@Ti_3C_2T_x$, wherein the Bi nanoparticles are dispersed on the surface or interlayer of $Ti_3C_2T_x$ nanosheets. The constructed sensor was investigated for the mutual interface between the two target analytes, and the SWASV responses demonstrated the good anti-interference trait of the sensor. However, in the presence of interfering Cu^{2+}, the response signals decreased, attributed to the formation of

intermetallic compounds. The authors then added ferrocyanide to eliminate interference from Cu^{2+}. Furthermore, the reproducibility RSD values were 4.0% Pb^{2+} and 4.6% Cd^{2+}, and the 6-day storage stability RSDs were 95.2% and 94.5%. The good stability achieved was attributed to the binding strength and structural stability of the $BiNPs@Ti_3C_2T_x$ modified GCE. Finally, the sensor was validated successfully in tap and lake water samples *via* the standard addition method, with the recovery % in the range of 98.3–106.3. Considering the effective surface area and good conductivity of $BiNPs@Ti_3C_2T_x$, the nanocomposite is depicted as a good sensor material.

Wen *et al.* harnessed the presence of oxygen vacancies and surface defects in metal oxides to develop a sensor for Pb^{2+} and Cd^{2+}.[172] These defects absorb O_2 molecules, and the oxides furnish electrons to combine O_2 to form $O_2^{•-}$, thereby offering active sites for the adsorption and charge transfer of HMIs. However, these metal-oxides with abundant oxygen vacancies are commonly poor conductors. Hence, this work combines CuO nanoparticles with 3D MXenes, typically prepared by hybridizing MXenes with other nanomaterials (like GO). Initially, $Ti_3C_2T_x$ and graphene-oxide (GO) were combined *via* sonication, and later, ethylenediamine (EDA) was added. This mixture was then transferred into a Teflon reactor to assemble the MXene aerogel. Next, CuO nanoparticles were formed by dissolving $Cu(NO_3)_2·3H_2O$ and $C_6H_3(COOH)_3$ in DMF, and this precipitant was heated in a tubular furnace for 5 h. The two precursors were mixed with a precleaned flexible carbon cloth (CC) for 0.5 h at 500 rpm. The obtained MXA-CuO/CC was sliced into 0.5 cm × 0.8 cm MXA-CuO/CC WE. Fig. 10(a) illustrates the fabrication steps of the MXA-CuO/CC sensor, and Fig. 10(b) shows the SEM image. The proposed sensor's feasibility was tested for the detection of individual Cd^{2+} and Pb^{2+} *via* a series of differential pulse anodic stripping voltammetry (DPASV) measurements in an acetate buffer solution (ABS) (Fig. 10(c) and Fig. 10(d)). In this work, bismuth ions were combined to form alloys with Cd^{2+} and Pb^{2+}, indirectly improving their adsorption. Hence, the DPASV signals depicted a good linear relationship for Cd^{2+} and Pb^{2+}, and the calculated LODs were 0.5 μg L^{-1} and 1.0 μg L^{-1}, respectively. Furthermore, the sensor was investigated for its ability to detect Cd^{2+} and Pb^{2+}, and the attained LODs were 0.3 μg L^{-1} and 0.2 μg L^{-1}, respectively (Fig. 10(e)). The observed results were attributed to (a) the huge specific surface area of MXene, (b) the introduction of Bi^{3+} that served as a stable binding site, and (c) abundant oxygen vacancies offered by CuO to capture electrons and its string affinity for metal ions enhanced the reduction of metal cations on the surface of the electrode to elemental metals. MXA-CuO/CC was examined for selectivity with various metal ions, namely, H_2PO^-, SO_4, Fe^{3+}, Cr^{3+}, NH^{4+}, Mg^{2+}, Zn^{2+}, Hg^{2+}, K^+, and Ca^{2+}, and also for mutual interference. The results depicted excellent anti-interference characteristics of the sensor. The reproducibility and intra-day stability RSDs were 5.25% and 3.82% (Cd^{2+} and Pb^{2+}) and 1.6% and 1.64% (Cd^{2+} and Pb^{2+}), respectively. MXA-CuO/CC sensor's practical applicability was evaluated in grain (94.5% to 107.4% (Cd^{2+}) and 96.8% to 110.2% for (Pb^{2+})) and water (94.5% to 107.4% (Cd^{2+}) and 96.4% to 111.5% for
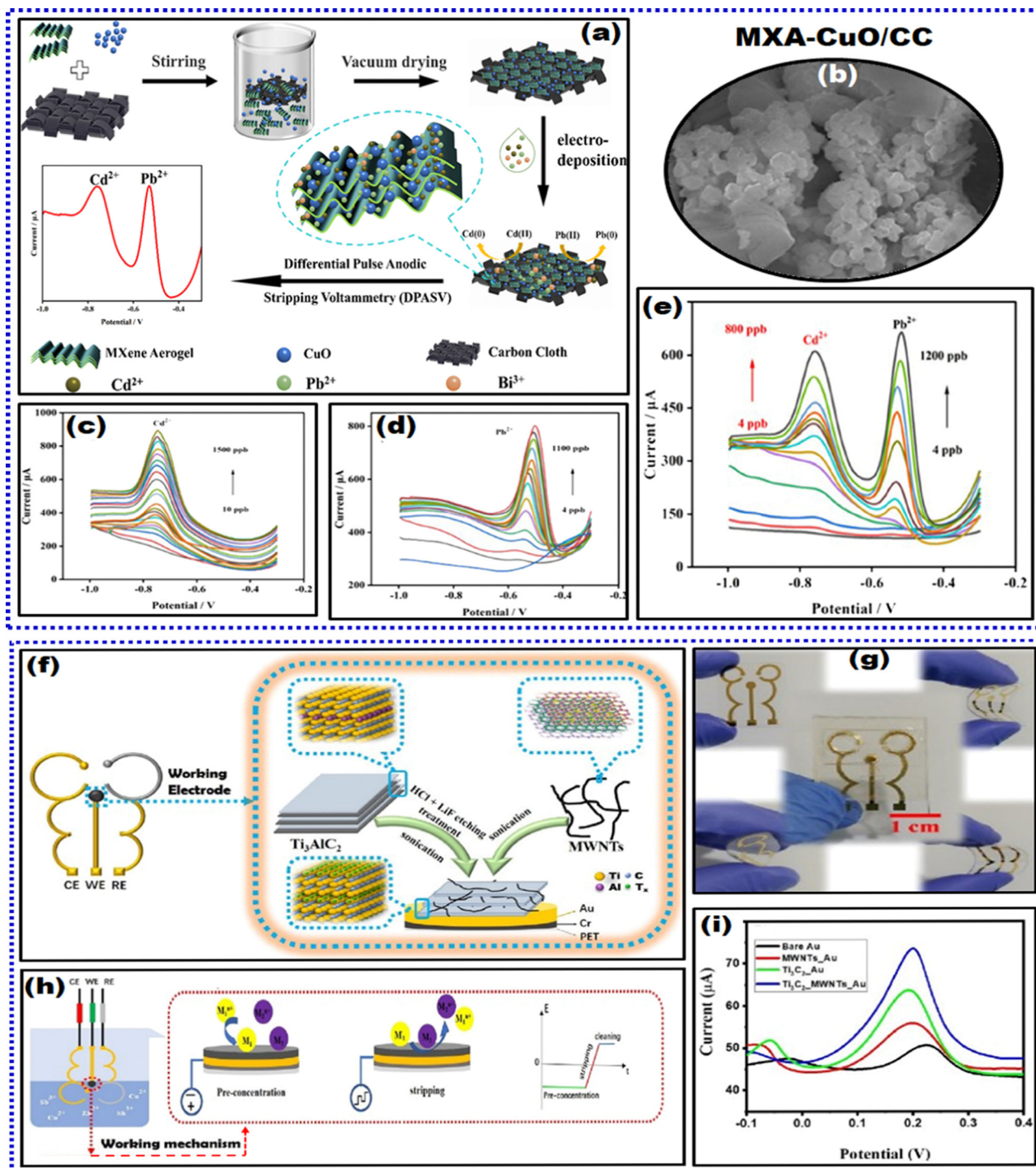
Fig. 10   (a) Fabrication steps of the MXA–CuO/CC sensor and schematics of the simultaneous detection of Pb²⁺ and Cd²⁺, (b) SEM image of MXA–CuO/CC and DPASV response curves for (c) individual Cd²⁺ and (d) individual Pb²⁺, and (e) simultaneously Pb²⁺ and Cd²⁺.[172] (f) Construction sequences of the Ti₃C₂Tₓ/MWCNT/Au/PET sensor, (g) photographs depicting the flexibility of the proposed sensor, (h) working mechanism for HMI determination, and (i) SWASV responses of Cu²⁺ at the developed electrode and the comparative electrodes.[173] Reproduced with permission from ref. 172 and 173. Copyright Elsevier (2022) and American Chemical Society (2020).

(Pb²⁺)) samples with satisfactory recovery %. However, the authors have not justified the reason for some of the above acceptable range recovery % values and lack of long-term stability. In conclusion, the authors have reported for the first time the

detection of Cd²⁺ and Pb²⁺ through DPASV and, more importantly, synergistic adsorption of oxygen vacancies and Bi³⁺.

Hui and group have proposed a layer-by-layer Ti₃C₂Tₓ/MWCNT nanocomposites modified gold/polyethylene terephthalate

($Ti_3C_2T_x$/MWCNTs/Au/PET) electrode to detect zinc and copper ions (Fig. 10(f)).[173] The two modifying agents were prepared by first etching $Ti_3C_2T_x$ from its MAX phase. Next, $Ti_3C_2T_x$ and MWCNTs were dissolved separately in the DMF dispersant. Then, the two mixtures were sonicated for 90 minutes. Next, the three-electrode configuration was patterned through photolithography, as illustrated in Fig. 10(g). The sensor was fabricated on a PET platform, coated with two metal layers of Cr and Au sequentially *via* electron beam evaporation. Finally, MWCNT dispersion was homogenously coated on the WE surface, and upon drying, $Ti_3C_2T_x$ was drop-coated for further applications. The SWASV measurements were performed *via* simultaneous *in situ* accumulation of Sb films, and target metal ions were taken in an ABS with a pH of 4.6. The working mechanism comprises three steps schematically represented in Fig. 10(h). An optimum concentration of Sb^{3+} added to the analyte facilitated an inflated response signal attributed to the formation of alloys or intermetallic compounds. Fig. 10(i) presents the SWASV responses of Cu^{2+} at the developed and comparative electrodes. The sensor depicted a good detection range of 350.0–830.0 ppb and 10.0–600.0 ppb for Zn^{2+} and Cu^{2+}, respectively. At the same time, the estimated detection limits were 1.5 ppb and 0.1 ppb, respectively. MWCNTs, with good conductive and electrical properties along with a greater specific surface area were introduced as anti-pile layers and spacers, which mitigated the aggregation of $Ti_3C_2T_x$ layers as MWCNTs filled the empty surface area that was not covered by $Ti_3C_2T_x$, further improving the effective surface area of the electrode and facilitating facile charge transfer. Additionally, the repeatability test exhibited an RSD value of 1.71%, while the 10-day stability was satisfactory, demonstrating the sensor's accuracy. Zn^{2+} and Cu^{2+} were successfully quantified from spiked biological fluids. Thus, incorporating MWCNTs exposed MXene's larger surface area and active sites effectively, favorably enhancing the EC performance *via* synergistic interactions. *In situ*, Sb^{3+} electrodeposition was performed to amplify the sensitive performance *via* alloy formation. In conclusion, a flexible device was constructed to determine Cu^{2+} and Zn^{2+} contents in biological fluids, which can be further applied for on-site analysis.

Lead (Pb) is commonly utilized in diverse anthropogenic activities and industrial processes. Pb^{2+} ions are known to cause severe biological toxicity and environmental hazards due to their high accumulation at contaminated sites. Hence, to individually detect Pb^{2+}, Rasheed *et al.* fabricated an $Nb_4C_3T_x$-modified GCE sensor. $Nb_4C_3T_x$ is another member of the MXene family synthesized *via* HF etching Al from the Nb_4AlC_3 MAX phase.[174] $Nb_4C_3T_x$ comprises niobium (Nb) as the transition metal and carbon (C) as the carbide component. Like $Ti_3C_2T_x$, it is also terminated with functional groups (T_x) on the surface. Rasheed *et al.* compared the sensing performance of $Nb_2C_3T_x$ and $Nb_4C_3T_x$ on GCE. Initially, the etched multilayered-$Nb_2C_3T_x$ (ML-$Nb_2C_3T_x$) and ML-$Nb_4C_3T_x$ MXenes in DI water were probe sonicated to obtain delaminated-$Nb_2C_3T_x$ (DL-$Nb_2C_3T_x$) and DL-$Nb_4C_3T_x$. The device was fabricated as shown in Fig. 11(a) by drop-cast coating of the

nanomaterials on the GCE substrate for stripping analysis of Pb^{2+}. The SWASV response for $Nb_4C_3T_x$ was higher than that for $Nb_2C_3T_x$, attributed to the larger interlayer spacing and high c lattice parameter value than those of the latter. Moreover, the EIS R_{ct} value for $Nb_4C_3T_x$ was lower compared to $Nb_2C_3T_x$. Furthermore, quantification with $Nb_4C_3T_x$/GCE generated a linear relationship in the concentration range from 0.025 μM to 0.5 μM with a LOD of 12.0 nM (Fig. 11(b)). The sensor depicted no significant impact of interfering metal ions such as Cd^{2+} and Cu^{2+} when concurrently determining Pb^{2+}. Next, the stability assessment of the proposed sensor involved five repetitive measurements with the same electrode, resulting in an RSD of 2.34%, while the 7-day stability RSD was 3.15%. Finally, the practicality of the sensor was validated in spiked bottled drinking water and tap water with good recovery % (Fig. 11(c)). The analytical performance of $Nb_4C_3T_x$ was compared with that of previously discussed modified $Ti_3C_2T_x$ and alkaline intercalated $Ti_3C_2T_x$.[165–173] In conclusion, the high conductivity, greater interlayer spacing, and large c lattice parameter of $Nb_4C_3T_x$ allowed for the accommodation of Pb^{2+} ions without annihilating the layered electrode structure. Thus, the potential application of the $Nb_4C_3T_x$ type of MXene for EC sensing was demonstrated for the first time. Table 1 summarizes the developed MXene sensors for HMIs and their significant results. Adsorption is considered the most effective approach to remove HMIs, as we can note from the table that HMIs are detected using adsorptive stripping voltammetry. Due to the presence of MXene's abundant active sites on their surface, HMIs can absorb metal ions through electrostatic and chemical interactions. This review shows us that MXene and its composites are good adsorbents for HMI electrochemical detection.

6.2. MXene electrochemical sensors for phenolic moiety-containing environmental samples

The phenolic molecules targeted for this review article are the bisphenol family, phenol, chlorophenol, nonylphenol, paraben, triclosan, naphthol, resorcinol (RES), bisphenol (BP), nitrophenol (NP), catechol (CAT), and hydroquinone (HQ).

A variety of phenolic compounds persist in our environment as widespread organic pollutants, introduced through agricultural irrigation, application of pesticides, industrial sewage draining, and others. US-EPA and the EU have classified these as priority pollutants that must be regulated.[175] This enlistment is due to the pieces of evidence that these chemicals are toxic and possess severe short- and long-term effects on the ecosystem. Therefore, the occurrence of phenolic compounds in the ecosystem is not only objectionable and undesired but also poses hazardous effects. Consequently, numerous techniques have been developed for their detection and management. However, some of these techniques are not feasible for field investigations. Hence, EC sensors play a pivotal role in that aspect, with the advantages they possess as described in the first and sixth sections of the manuscript. Several articles and reviews have been published in this regard; however, they have not prioritized MXene-based sensors.[176–181] Thereby, the only MXene-based biosensor reported in the literature was designed
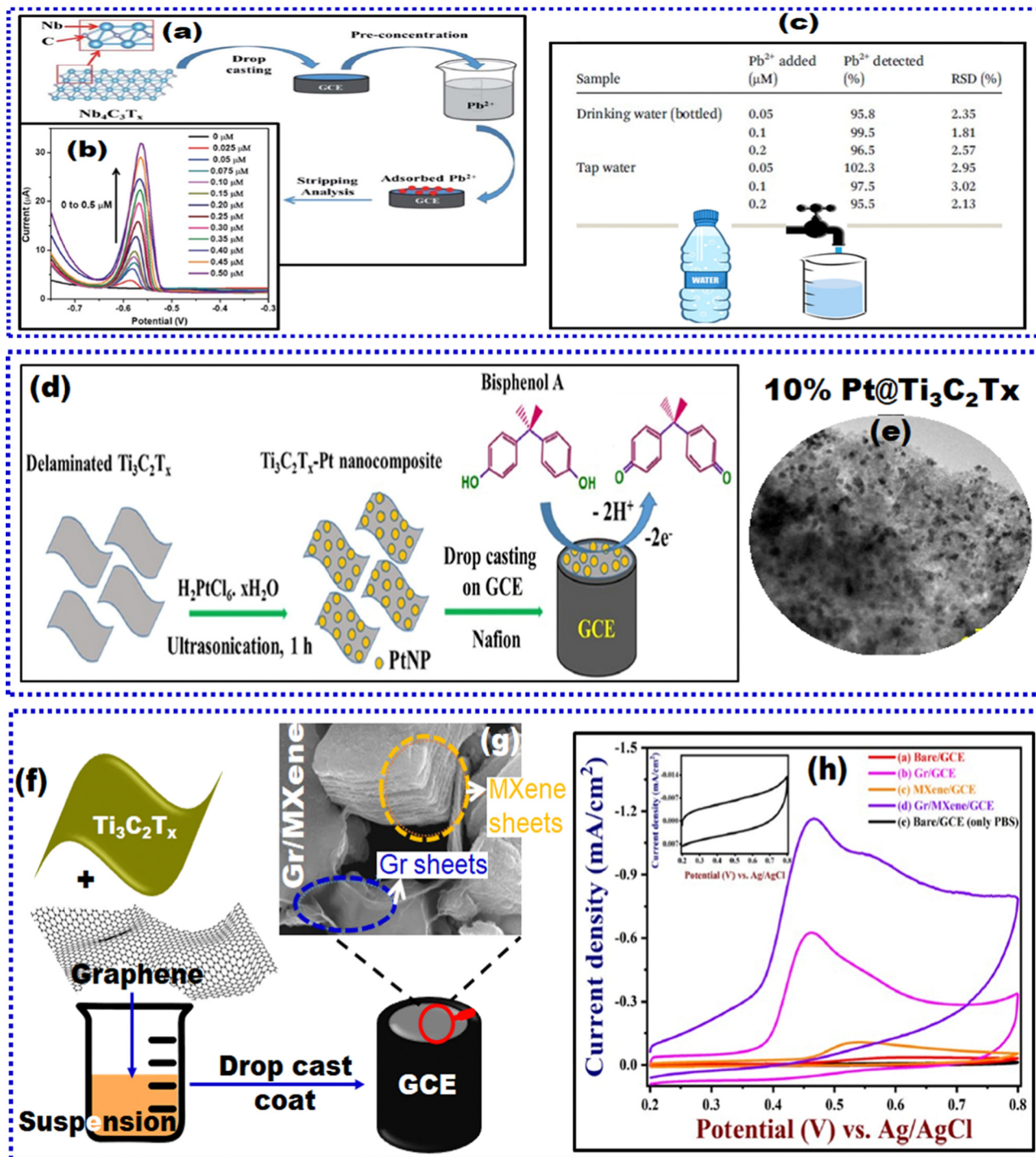
Fig. 11 (a) Fabrication schematics of the $Nb_4C_3T_x$ sensor, (b) SWASV signals for Pb^{2+} at $Nb_4C_3T_x$/GCE, and (c) recovery percentages of Pb^{2+} from drinking water at $Nb_4C_3T_x$/GCE.[174] (d) Schematic illustrations of the BPA sensing mechanism at the proposed $Pt@Ti_3C_2T_x$/GCE. (e) TEM image of 10%$Pt@Ti_3C_2T_x$.[185] (f) Fabrication schematics of Gr/MXene/GCE, (g) HR-SEM image of Gr/MXene composite, and (h) CV response of BPA at various comparative electrodes.[186] Reproduced with permission from ref. 174, 185, and 186. Open access RSC Advances (2020), Copyright Elsevier (2021), and Elsevier (2022).

by Wu *et al.*, wherein an MXene-based tyrosinase biosensor was used for the sensitive detection of phenol.[182] MXene's graphene-like 2D nanostructure was exploited to immobilize tyrosinase, a mediator-free biosensor with excellent analytical performances with high sensitivity, rapid response, and lower

LODs for phenol quantification. A large group of phenolic compounds have been proven to have wide industrial applications and persist as organic pollutants in our ecosystem.[13,24,27]

6.2.1. Bisphenol A. Bisphenol A (BPA) is a well-documented endocrine-disrupting chemical widely employed for synthesizing

Table 1 Developed MXene-based EC sensors for HMIs and their significant results

MXene-type	Buffer, pH value	EC method employed	LDR	LOD	Interferent	Real sample	Ref.
PANI-Ti$_3$C$_2$/GCE	0.005 M H$_2$SO$_4$	ASV	0.1–20.0 μg L^{-1}	Hg^{2+}: 0.017 μg L^{-1}	10-fold excess: Fe^{3+}, Co^{2+}, Ni^{2+}, Cu^{2+}, Pb^{2+}, K$^+$, Na$^+$	Tap, lake water	165
Fe-MOF/MXene-1.5/GCE	0.1 M PBS, 5.0	SWASV	1–10 ng L^{-1}, 10.0–100.0 ng L^{-1}	As^{3+}: 0.58 ng L^{-1}	100-folds: Cu^{2+}, Pb^{2+}, Mn^{2+}, Cd^{2+}, Hg^{2+}, Fe^{3+}, Cl$^-$, NO$_3^-$	Tap, river, lake water	166
Fe-Co-LDH/MXene/GCE	0.1 M PBS, 5.0	SWASV	1.0–10.0 ppt	As^{3+}: 0.9 ppt	10-ppb: Fe^{3+}, Hg^{2+}, Cd^{2+}, Pb^{2+}, Cu^{2+}	Tap, river, lake water	167
Alk-Ti$_3$C$_2$/GCE	HAcNaAc, 5.0	SWASV	For all: 0.1–1.5 μM	Cd^{2+}: 0.098 μM, Pb^{2+}: 0.041 μM, Cu^{2+}: 0.032 μM, Hg^{2+}: 0.130 μM	Intermetallic	—	168
Bi@d-Ti$_3$C$_2$/MSA	0.1 M HAcNaAc, 4.5	SWASV	Cd^{2+}: 0.84 μA L μ g^{-1}, Pb^{2+}: 0.98.0 μA L μ g^{-1}, Zn^{2+}: 0.60 μA L μ g^{-1}	Cd^{2+}: 0.4, Pb^{2+}: 0.2, Zn^{2+}: 0.5 μg L^{-1}	100-fold excess: Na$^+$, K$^+$, Mg^{2+}, Ca^{2+}, Fe^{2+}, Ni^{2+} 50-fold Cu^{2+}	Tap, drinking water	169
H-C$_3$N$_4$/Ti$_3$C$_2$T$_x$/GCE	HAcNaAc, 6.0	SWASV	Cd^{2+}: 0.5–1.5 μM, Pb^{2+}: 0.5–1.5 μM	Cd^{2+}: 0.001.0 μM, Pb^{2+}: 0.0006 μM	100-fold excess: Na$^+$, K$^+$, Ca^{2+}, Cr^{2+}, Hg^{2+}, Cu^{2+}, PO$_4^-$, NO$_3^-$, Cl$^-$, ascorbic acid, uric acid, acetaminophen, glucose, nicotinamide	Tap water	170
BiNPs@Ti$_3$C$_2$T$_x$/GCE	HAcNaAc, 5.0	SWASV	Pb^{2+}: 0.06–0.6 μM, Cd^{2+}: 0.08–0.8 μM	Pb^{2+}: 10.8 nM, Cd^{2+}: 12.4 nM	10 μM: Mg^{2+}, Fe^{3+}, Co^{2+}, Ni^{2+}, Mn^{2+}, Zn^{2+}, Al^{3+}, Cu^{2+}	Tap, lake water	171
MXA-CuO/CC	ABS, 5.0	DPASV	Cd^{2+}: 4.0–800.0 μg L^{-1}, Pb^{2+}: 4.0–1200.0 μg L^{-1}	Cd^{2+}: 0.3 μg L^{-1}, Pb^{2+}: 0.2 μg L^{-1}	H$_2$PO$^-$, SO$_4^{2-}$, Fe^{3+}, Cr^{3+}, NH$_4^+$, Mg^{2+}, Zn^{2+}, Hg^{2+}, K$^+$, Ca^{2+}	Grain, water	172
Ti$_3$C$_2$T$_x$/MWCNTs/Au/PET	ABS, 4.6	SWASV	Zn^{2+}: 350.0–830.0 ppb, Cu^{2+}: 10.0–600.0 ppb	Zn^{2+}: 1.5 ppb, Cu^{2+}: 0.1 ppb	—	Body fluid	173
Nb$_4$C$_3$T$_x$/GCE	HAcNaAc, 5.0	SWASV	0.025–0.5 μM	Pb^{2+}: 12.0 nM	5-Fold excess: Cd^{2+}, Cu^{2+}	Drinking bottled and tap water	174

standard epoxy resins, plastic products, and many others. BPA leaches into food and drinking water, increasing the risk of cancer, heart disease, and diabetes.[24,183] These findings necessitate the regulation of BPA.[184] Therefore, detecting them by applying facile and sensitive methods is crucial. Researchers Rasheed et al. constructed an MXene-based nanocomposite by reducing Pt salt into Pt nanoparticles Pt-NPs on the MXene nanosheet surface through self-reduction.[185] This is the first report on MXene-based sensors for BPA determination. The delaminated Ti$_3$C$_2$T$_x$ was initially synthesized via acid etching of the Ti$_3$AlC$_3$ MAX phase with subsequent sonication. Next, into the Ti$_3$C$_2$T$_x$ aqueous solution, different Pt loadings and specific volumes of chloroplatinic acid hydrate were added dropwise under constant stirring. This was followed by bath sonication of the reaction mixture for 1 h, which was later purified by centrifugation. Various Pt loadings were examined during the nanocomposite synthesis, and the EC potential was analyzed. Among them, 10% Pt/Ti$_3$C$_2$T$_x$ depicted the highest EC activity; this nanocomposite was drop-cast coated onto the GCE surface to detect and quantify BPA, a known environmental pollutant. CV illustrated an irreversible electron transfer for BPA as shown in Fig. 11(d), while Fig. 11(e) presents the TEM image of 10%Pt@Ti$_3$C$_2$T$_x$. The sensor displayed a LOD of 32.0 nM and a wide linear range under DPV-optimized conditions. This sensor was triumphantly employed for evaluating BPA from water and milk samples. Due to the electrical conductivity and sheet-like structure of MXene, the presence of PtNPs improved the surface-to-volume ratio which, in turn, amplified the sensor response. The 10%Pt@Ti$_3$C$_2$T$_x$/GCE electrode produced an RSD value of 2.1%, verifying its good reproducibility, while the stability response was examined for 7 days with an RSD of 3.2%.

Rajendran et al. have fabricated a 2D hybrid graphene/Ti$_3$C$_2$T$_x$ (Gr/MXene) electrode for BPA.[186] The nanohybrid was synthesized via a top-down method. The authors initially prepared the MAX phases and etched them with HF solution. An EC exfoliation method was employed to prepare graphene dispersion by applying +7 V between the graphite electrodes dipped in buffer (PBS 7.4) for 40 minutes. During the exfoliation process, the graphene sheets were peeled and settled in PBS. This reaction solution was thoroughly rinsed with water through vacuum filtration, ultrasonicated in DI water for 60 mins, and centrifuged to obtain the top supernatant as the graphene sheet dispersion. Finally, a known amount of graphene dispersion was combined with MXene dispersion, which was probe-sonicated for 30 minutes and continuously stirred at RT for 24 h. Next, 6 μL of this homogeneous dispersion was drop-coated onto the precleaned GCE and used as the sensor (Fig. 11(f)). Before coating the nanomaterial onto the WE surface, graphene/Ti$_3$C$_2$T$_x$ was characterized via HR-SEM (Fig. 11(g)), demonstrating the incorporation of MXene with graphene. It is evident from the voltammograms shown in (Fig. 11(h)) that the proposed sensor exhibited an electrocatalytic effect compared to other comparative electrodes. The authors have validated their sensor by two methods, DPV and AMP, and the LODs were 0.35 μM and 4.08 nM, respectively. Furthermore, BPA anodic currents observed upon adding interfering molecules/compounds were plotted to establish the

selectivity change, indicating a negligible change of only 3%. The repeatability RSD value for the sensor was 0.8%, while, even after 20 days, it retained its stability up to 74.3%. Although the stability is not exceptional, their reproducibility was satisfactory.

6.2.2. 4-Nitrophenol. Aromatic molecules anchored with nitro moieties are widely utilized in pharmaceuticals, industries, dyes, pesticides, and others. Typically, aromatic molecules with nitro derivatives are more carcinogenic to the biosphere. Among nitrated phenol derivatives (namely, 2-nitrophenol, 3-nitrophenol, and 4-nitrophenol (4-NP)), 4-NP is the most toxic phenolic derivative and a significant chemical intermediate with vast applications in producing textiles, plasticizers, paints, dyes, pesticides, and explosives.[187] However, due to its negative impact on the biosphere, 4-NP is considered the primary toxic pollutant by the US Environmental Protection Agency (EPA).[188] Hence, the quantitative determination of 4-NP is the need of the hour for monitoring the environment and, in particular, water quality.

Krishnamoorty and co-workers[189] have emphasized the significance of controlled $Ti_3C_2T_x$-MXene, devoid of external surface treatment, to boost the EC and catalytic traits, invoking efficient sensitivity and LOD of the target analyte, 4-NP. Layered 2D MXene was synthesized from 3D ceramic MAX in the presence of etchant HF. After etching for 36 h, the exfoliated MXene was extracted *via* continuous water wash through centrifugation, and the final cake-like wet MXene was vacuum-dried. The MXene powder was used for EC experiments without further modification *via* drop-cast coating onto the GCE surface. The electrode depicted a sensing mechanism of the 4-NP reduction process as presented in the following equations: (a) $Ti_3C_2T_x + 4e^- \rightarrow (Ti_3C_2T_x)^{4-}$ and (b) $(Ti_3C_2T_x)^{4-} + 4\text{-NP} + 4H^+ \rightarrow Ti_3C_2T_x + 4\text{-HAP} + H_2O$. To substantiate, during the electrode reaction, MXene was initially EC reduced, and subsequently, 4-NP was chemically reduced to 4-hydroxylaminophenol (4-HAP) without intermediate formation (Fig. 12(a) and Fig. 12(b)). The proposed sensor depicted excellent EC performance for the catalytic reduction of 4-NP with a DPV sensitivity of 16.35 μA μM^{-1} cm^2 and the detection range of 0.5–100.0 μM L^{-1} along with a LOD of 42.0 nM L^{-1}. The excellent performance is attributed to (i) surface-exposed titanium integrated with the robust carbon elemental composition of $Ti_3C_2T_x$ that generated conducting channels for charge transfer, (ii) the presence of abundant surface functional groups with a negative surface charge of MXene that favored the detection of positively charged molecules, and (iii) stacked layers of bulk MXene exfoliated from MAX possess large active surface sites. Furthermore, the selectivity investigation depicted in Fig. 12(c–h) exhibited minor changes in the reduction peak current for 4-NP, validating the sensor's anti-interference properties. The selective trait is ascribed to the presence of the nitro group in 4-NP at the para position to the OH group, which feasibly underwent an electrophilic substitution by the –OH group. This electrophilic substitution reaction occurred only in 4-NP and not among other phenolic derivatives. Furthermore, the sensor could detect 4-NP in spiked tap water samples with good recoveries in the 95.09–99.15% range. The work does not present a report on the reproducibility and stability of RSD. In conclusion, the application of stacked $Ti_3C_2T_x$ layers through a controlled exfoliation procedure with good sensitivity, selectivity, and detection limit was demonstrated. The key parameters were optimally controlled chemical etching conditions for producing bulk-stacked 2D MXene with functional moieties. The sensor was validated for the determination of 4-NP from the low pH soil–water system.

Chen and workers have reported the reduction studies of 4-NP to 4-aminophenol (4-AP) on carbon quantum dots@MXene.[187] Here, MXene acted as an ideal support to reduce the accumulation of nanocomposites during the catalysis process as observed in UV-vis absorption studies. Thus, the only other EC reductive detection of 4-NP based on MXene sensing was reported by Wang and researchers who prepared the $Ti_3C_2T_x$-MXene/graphene composite.[190] The restacking of 2D layered materials (like MXene and graphene) leads to spontaneous aggregation triggered by interlayer interactions. This phenomenon may also lead to a decline in active surface area and electrical conductivity, further restraining its EC performance. Thus, the MXene/GR composite was synthesized through self-assembly to reduce the restacking of MXene and graphene, as MXene or graphene were considered interlayer spacers for one another. Initially, the delaminated MXene was synthesized by the optimized MILD method, followed by the self-assembly method to form D-$Ti_3C_2T_x$/graphene composites (D-$Ti_3C_2T_x$/GR). Here, the optimized etching route involved LiF/HCl, with Li$^+$ serving as an intercalant, and no sonication was employed for the delamination process. Later, post drying, D-$Ti_3C_2T_x$ was added into graphene solution in DMF and sonicated until a homogenous suspension was achieved. This suspension was coated onto the GCE surface as an EC sensor, as illustrated schematically in Fig. 12(i). D-$Ti_3C_2T_x$/GR depicted an excellent 4-NP reduction detection limit *via* a sensitive DPV technique with an LOD of 0.16 μM. Furthermore, the anti-interference performance was evaluated by adding a 100-fold excess of Na_2SO_4, KNO_3, $CaCl_2$, and a 10-fold concentration of 2,4-DCP, *p*-CP. The results unveiled that the introduction of the aforementioned high concentration of inorganic ions and chlorinated phenolic molecules did not significantly influence the 4-NP response signal. Finally, the practicality of the constructed sensor was demonstrated through spiked tap and seawater samples, exhibiting excellent recoveries. The reproducibility of the sensing device was examined for five parallel detectors, and the RSD value was 1.98%. The storage stability for 10 days was satisfactory (89.28% of the initial current). The sensor depicted good sensitivity; however, further investigation is essential concerning stability and restacking issues concerning MXene and GR.

Furthermore, the hydrothermally assisted exfoliated multi-layer oxidized $Ti_3C_2T_x$ MXene for simultaneous detection of 4-chlorophenol (4-CP) and 4-NP from water samples has been demonstrated with good sensitivity and LOD by Lei and team.[191] The report presents, for the first time, the utilization of NaF/HCl solution for hydrothermal exfoliation of MAX into multilayered $Ti_3C_2T_x$ nanosheets, which were coated onto the
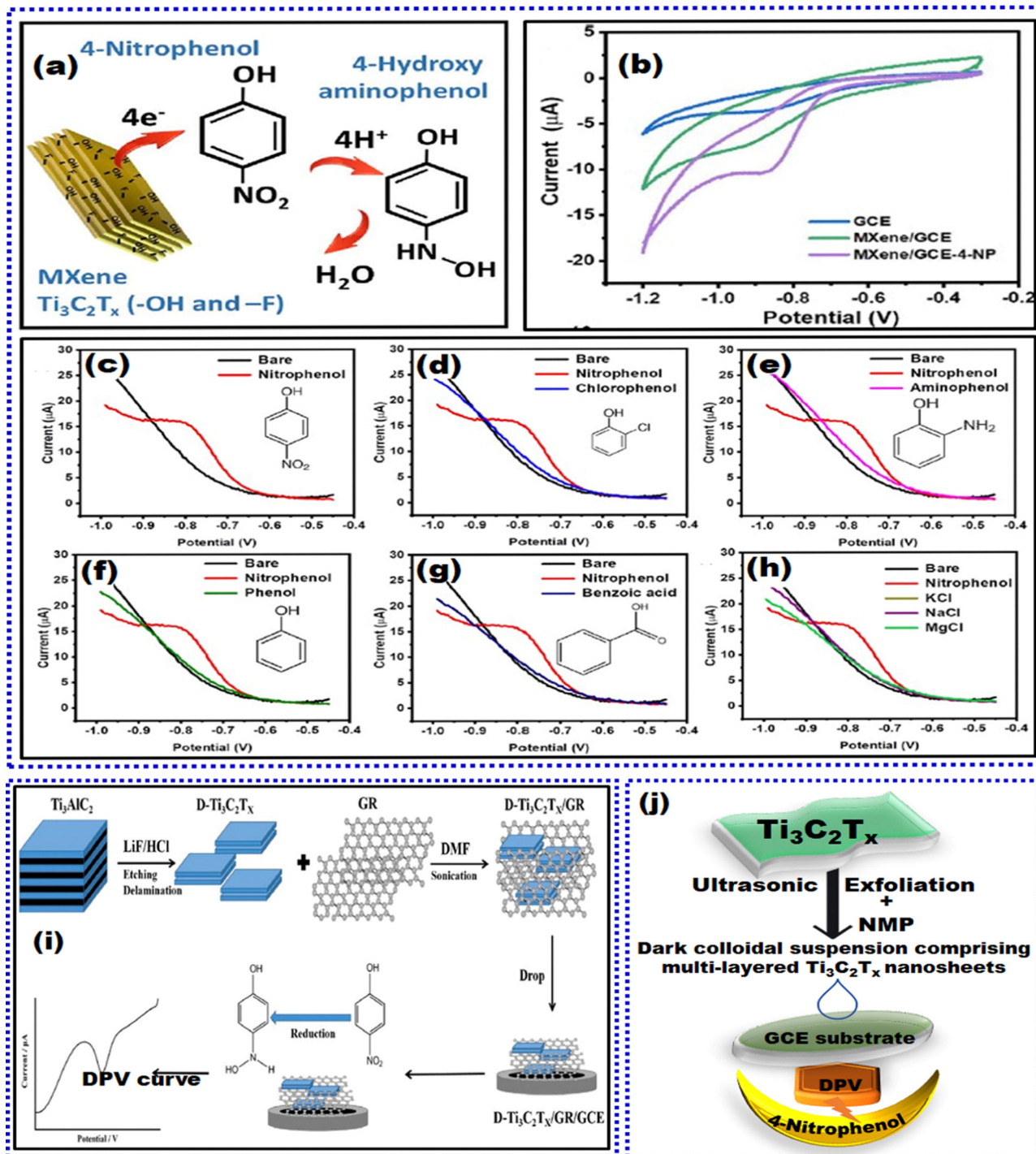
Fig. 12 (a) Schematic representation of electrochemical 4-NP reduction at MXene, (b) cyclic voltammograms of 4-NP at bare and MXene modified electrodes, and differential pulse voltammograms for 4-NP in the presence of interferers: (c) 4-NP, (d) chlorophenol, (e) aminophenol, (f) phenol, (g) benzoic acid, and (h) inorganic ions.[189] (i) Schematic representation of the D-Ti$_3$C$_2$T$_x$/GR/GCE sensor fabrication process for detecting 4-NP.[190] (j) Fabrication process of Ti$_3$C$_2$T$_x$ nanosheets coated onto the GCE platform as a sensor. Reproduced with permission from ref. 189, and 190. Open access ACS Omega (2022), Copyright Elsevier (2022).

GCE platform (Fig. 12(j)). The as-prepared sensor was employed in the simultaneous detection of 4-CP and 4-NP using DPV, wherein the oxidation peak currents depicted linearity with the increase in concentration. The evaluated LODs were 0.062 µM and 0.11 µM for 4-CP and 4-NP, respectively. Likewise, the repeatability test indicated a good RSD value of 4.50% and 4.58%, respectively. Furthermore, the introduction of potential interferents such as H$_2$O$_2$, Cd^{2+}, Pb^{2+}, CAT, trinitrophenol, and

phenol into the 4-NP solution did not affect its current response value. Finally, the sensor was attested for its practicality from 4-NP fortified wastewater samples.

6.2.3. Catechol. The International Agency for Research on Cancer (IARC) categorizes CAT as a carcinogen. Even concentrations ranging from 5–25 ppm are considered toxic to aquatic organisms. Hence, detecting and regulating CAT from the effluents before discharge is crucial. Although there are several reports of its detection employing enzymes, they suffer from shortcomings like rate inhibition by reaction products, low stability, in some cases, the necessity of a third component like H_2O_2 for catalytic function completion, and difficulties in direct immobilizing enzymes on electrodes.[192] Hence, surface-modified EC sensors are more feasible and reliable. This section will discuss the reported MXene-based sensors in the literature for CAT. The two positional isomers of a dihydroxy-benzene moiety, namely, CAT and HQ, are extensively employed in dyes, cosmetics, pharmaceuticals, pesticides, plasticizers industries, and oil refineries. Both CAT and HQ do not degrade quickly and have been found to be severely hazardous to the biosphere and are listed as human carcinogens by the International Agency for Research on Cancer; the US EPA and the European Union (EU) have considered these isomers a threat to environmental safety.[193] Additionally, they usually co-exist due to their structural and property resemblance. Hence, the factors mentioned above necessitate the fabrication of a straightforward and efficient qualitative and quantitative sensing device for the two phenolic isomers.[194]

The hybridization of 1D–2D-based nanocomposites impedes inter-nanosheet aggregation and leads to stabilized active sites, which are eminently desirable for sensor devices. The designing of ultrathin 2D materials coupled with a 1D network exhibits distinct characteristics (like anisotropic electron transport and high specific surface area). These characteristics promote them as a potential transducer for EC sensing with structural and EC stability. Therefore, Huang et al. introduced MWCNTs as interlayer spacers, an effective strategy to prevent MXene from aggregation.[195] Here, the constructed sensor was employed in the selective detection of CAT. They synthesized Ti_3C_2/MWCNTs via dispersing Ti_3C_2 and MWCNTs in ultrapure water and sonication. This suspension was drop-cast coated on the glazed GCE surface for sensing CAT and H_2O_2, as illustrated in Fig. 13(a), while the TEM image of Ti_3C_2-MWCNT is presented in Fig. 13(b). The DPV simultaneous quantification depicted a LOD of 6.6 nM and 3.9 nM for HQ and CAT, respectively (Fig. 13(c) and Fig. 13(d)). The well-designed structure of 1D-MWCNTs and hierarchical 2D-MXenes significantly amplified the sensor response, particularly during selectivity studies in the presence of inorganic ions (Na^+, K^+, Ca^{2+}, Cu^{2+}, Mg^{2+}, Zn^{2+}, NO_3^-, and Cl^-) and organic molecules (ascorbic acid (AA), glucose (Glu), 4-NP, BPA, and RES). The sensor's reproducibility, stability, and repeatability were evaluated using DPV, and the RSD values were good. The standard addition method was employed to practically apply the constructed sensor with reliable recoveries (96.9% to 104.7% and 93.1% to 109.9% for HQ and CAT, respectively) from industrial wastewater. The nanocomposite, intercalated with MWCNTs,

enlarged the spacing between MXene-sheets, enhancing the surface area and providing greater channels for charge transfer.

In the same year, researcher Huang again, with other group members, reported the alkalization-intercalated Ti_3C_2 with the N-PC/GCE (alk-Ti_3C_2/N-PC/GCE) sensor for CAT and H_2O_2.[196] First, the exfoliated Ti_3C_2 was alkalized using KOH, and the obtained product was alk-Ti_3C_2. Next, nitrogen-doped porous carbon was prepared by carbonizing MOF-5-NH_2. Finally, the two were dispersed in ultrapure water via ultrasonication for 30 minutes. This suspension was dropped on the GCE surface to construct the EC sensor, as represented in Fig. 13(e). Thus, the alk-Ti_3C_2/N-PC/GCE was assessed for the sensitive determination of CAT and HQ. The estimated LODs during the simultaneous detection of CAT and HQ were 3.1 nM and 4.8 nM, respectively. In the MXene/MOF heterostructure, alkalized Ti_3C_2 with expanded interlayer spacing exhibited good conductivity and ample –OH functional groups. The alkalized Ti_3C_2 captured CAT and HQ based on the H-bond and interactions of –OH on its surface and the –OH in the CAT and HQ. Moreover, MOF-5-NH_2-derived N-PC possessed a unique C–N bond that could attract the –OH of CAT and HQ. Hence, adding N-PC as an intercalator into the Ti_3C_2 sheets yielded a double effect on detecting CAT and HQ (Fig. 13(f)). Also, the decoration of alk-Ti_3C_2 with N-PC (with a porous structure and large surface area) led to the exposure of numerous active sites, further improving the surface area and hastening the charge transport rate. The results also illustrated reduced charge transfer resistance and enhanced EC response concerning current. Additionally, the sensor depicted good anti-interference properties in the presence of 100 mM inorganic ions (Na^+, K^+, Ca^{2+}, Cu^{2+}, Mg^{2+}, Zn^{2+}, NO_3^-, and Cl^-) and 0.1 mM organic molecules (RES, BPA, Glu, AA, 4-AP, 4-NP, tetracycline (TC), and chloramphenicol (CAP)). The reproducibility, repeatability, and stability of RSD values were acceptable. Finally, the sensor was attested for practicality in quantifying CAT and HQ from industrial wastewater samples with good recovery percentages in the range of 98.2–106.4% for CAT and 97.7–106.8% for HQ. Thus, to a greater extent, the coordination between K^+–Ti_3C_2 and the H-bonding between alk-Ti_3C_2–N-PC were the driving forces that enabled the utilization of the material for EC sensing.

Ranjit et al. have recently constructed a hybridized 1D–2D $MnMoO_4$ nanocomposite as a high-performing EC sensing platform for quantifying the dehydrobenzene isomers.[197] They experimented with the hybrid heterostructure with surface-functional advantages to augment the selectivity and sensitivity of the sensing electrode. Designing defect-rich X-MoO nanostructures has fostered higher surface-active EC sites than numerous bimetallic nanostructures, satisfying the EC requirements. Ultra-thin Ti_3C_2F-MXene was prepared via HF etching followed by sonication in tetrabutylammonium. Fig. 14(a) shows the synthesis and delamination procedure of a few layered Ti_3C_2F-MXene. Subsequently, $MnMoO_4$ was synthesized via the electrospun method. To prepare the hybrid composite of the two, delaminated MXene was functionalized with a definite amount of 3-mercaptopropionic acid (MPA), followed by its treatment with $MnMoO_4$ in ethanol solution and hydrothermal
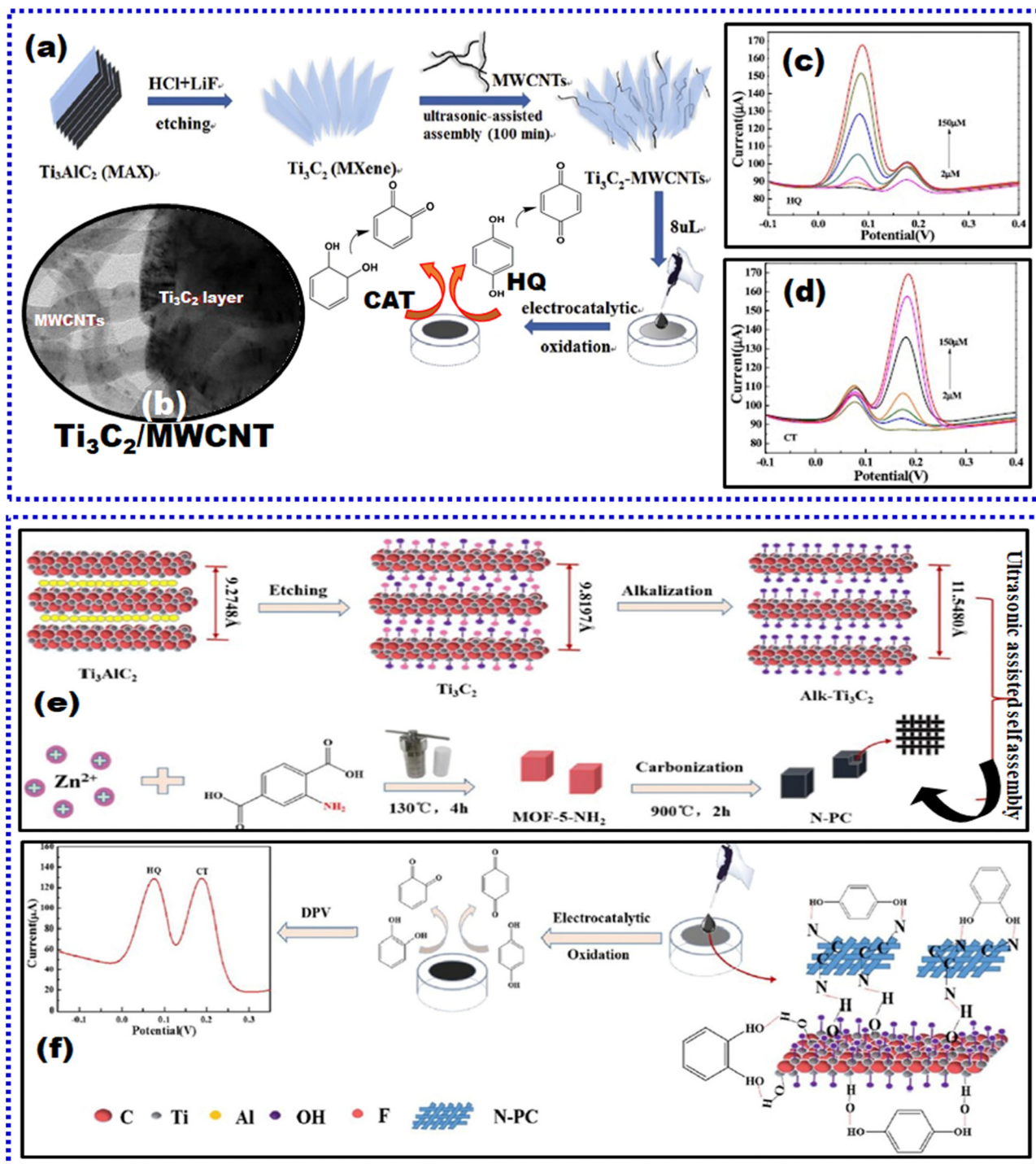
Fig. 13 (a) Schematics of Ti₃C₂-MWCNT synthesis and fabrication of the EC sensor for CAT and HQ oxidative quantification. (b) TEM image of Ti₃C₂-MWCNTs and DPV signal for (c) HQ and (d) CAT at various concentrations.[195] (e) Schematic of Alk-Ti₃C₂/N-PC composite synthesis. (f) Graphical representation of alk-Ti₃C₂/N-PC/GCE sensor fabrication and the response of CAT and HQ oxidation process.[196] Reproduced with permission from ref. 195, and 196. Copyright Elsevier (2019), and Elsevier (2020).

stirring for 6 h to obtain the desired product. MoO/MXene and MnO₂/MXene hybrids were also synthesized *via* the procedure mentioned above for comparative inspections (Fig. 14(b)–(d)). A schematic of the synthesis and fabrication of the sensor is depicted in Fig. 14(e). The catalytic sensing of CAT and HQ

protracted the best response at MnMoO₄/MXene/GCE compared to MoO/MXene/GCE, MnO/MXene/GCE, MnMoO₄/GCE, MXene/GCE as shown in Fig. 14(f). These results can be correlated to EIS R_ct values, as depicted in Fig. 14(g), wherein the MnMoO₄/MXene/GCE explicitly exhibits a fast charge
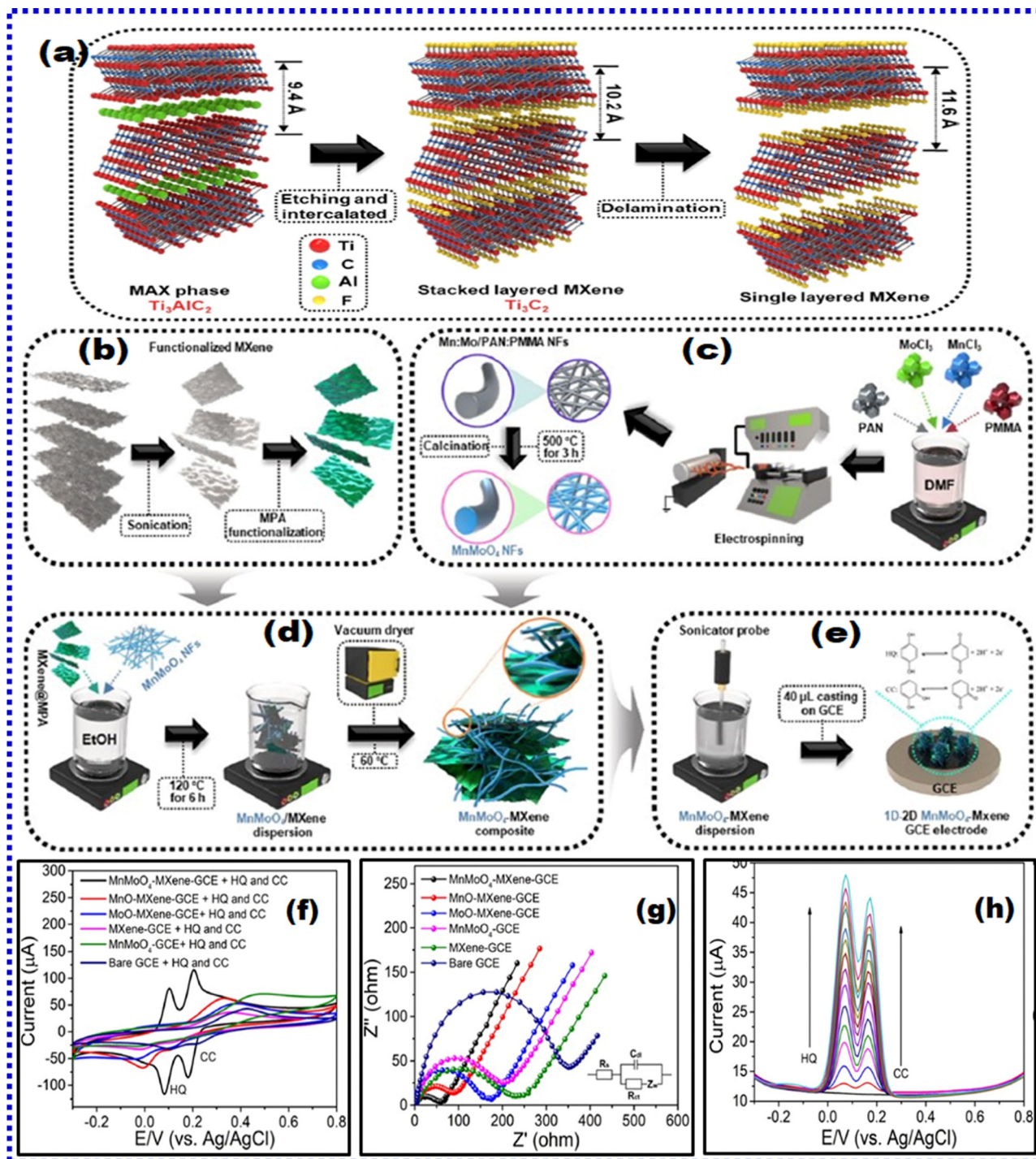
Fig. 14 (a) Schematic representation of layered Ti_3C_2F-MXene synthesis, (b) graphical illustration of the construction process of the $MnMoO_4$-MXene hybrid composite sensor for CAT and HQ determination: (b) functionalization of MXene, (c) synthesis of $MnMoO_4$, (d) synthesis of $MnMoO_4$-MXene, (e) fabrication of the sensor, and (f) EIS data of the proposed sensor against the comparative electrodes – inset: equivalent circuit. (g) Cyclic voltammetric response of CAT and HQ at $MnMoO_4$/GCE and other comparative electrodes. (h) DPV curves for the simultaneous determination of CAT and HQ.[197] Reproduced with permission from ref. 197. Copyright Elsevier (2022).

transfer rate with good conductivity, attributed to the ample active sites with hybridized architecture that promoted the catalytic effect. Moreover, the MXene's surface functionality facilitated the tagging of the $MnMoO_4$ nanofibers, thus forming

a heterostructure with high electrical mobility. Furthermore, the DPV simultaneous quantification of CAT and HQ depicted good sensitivity with LODs of 0.30 nM and 0.26 nM, respectively. The simultaneous quantification of CAT and HQ voltammograms

is illustrated in Fig. 14(h). Moreover, the detection sensitivities were 6.471 μA nM^{-1} and 7.437 μA nM^{-1} for CAT and HQ, respectively. The fluffy 3D network structure of 1D–2D MnMoO$_4$/MXene/GCE facilitated numerous surface-active sites for the adsorption and oxidation of the target analytes. Furthermore, it exhibited better resistance to surface fouling and as a favorable nanomaterial for sensitive and selective detection of CAT and HQ during individual selectivity over the simultaneous determination. Furthermore, the practical applicability was verified in river and seawater samples with appreciable and significant recoveries. The results indicated the high suitability of the proposed sensor for the simultaneous detection of CAT and HQ. The proposed sensor depicted good reproducibility (RSD: 3.18%), repeatability (RSD: CAT-3.12%, HQ-1.84%), catalytic stability (RSD: CAT-94%, HQ: 92), strong adsorption interaction between the nanocomposite interface and toxic pollutants under aqueous conditions. MnMoO$_4$-MXene nanocomposite suspension was then drop-coated onto the GCE substrate as the working electrode. In conclusion, the electron-spun MnMoO$_4$ nanofibers were combined with the delaminated single-layered MXene nanosheets, forming the hybrid 1D–2D MnMoO$_4$-MXene nanocomposites/GCE that diminished the overpotential and improved the oxidation response current for CAT and HQ. Table 2 presents the comprehensive collection of the MXene-based sensor performances for BPA, 4-NP, CAT, and HQ.

The literature unveils several other nanomaterials which have been employed in modifying the sensing substrate and demonstrated good sensing attributes.[198–202] However, MXene is an emerging 2D material. Through this review, we have drawn out the potentialities of MXene and its composites that depict captivating applications in advancing the electrochemical sensing technology, particularly in detecting HMIs and phenolic moiety-containing molecules.

In summary, we came across various mechanisms (Fig. 15(a)) for sensing a few of the target HMIs, which include ion exchange electrostatic interactions and the formation of intermetallic compounds. Deposition potential and deposition time are crucial factors regulating the electrochemical detection mechanism. We noticed that composites of other nanomaterials with MXenes depicted synergistic effects, along with electroactive sites for the deposition of HMIs in them that resulted in the formation of a conducting electron network. The most common method of sensing HMIs was the formation of intermetallic compounds. Foreseeably, during the simultaneous detection of two HMIs, the response signals are greater compared to the signal strength for a single metal ion. This phenomenon is attributed to the synergistic effect produced in ensuing two HMIs. Such HMIs amplified the SWASV response signal. Meanwhile, the MXene-based sensors for BPA, 4-NP, CAT, and HQ depicted adsorptive, oxidative, and reductive mechanisms of EC detection. To summarize, the developed sensors for HMI and toxic phenolic moiety-containing molecules utilized pristine, delaminated, and aerogel MXenes (Fig. 15(b)). Furthermore, MXene nanocomposites were prepared to employ graphene, MWCNTs, MOF, p-C$_3$N$_4$, nanofibers, metal nanorods, polymers, and LDH, enhancing the sensor performance.

Table 2 A comparative table representing the MXene-based EC sensors' results for BPA, 4-NP, CAT, and HQ

| MXene-type	Buffer, pH value	EC method employed	LDR	LOD	Interferent	Real sample	Ref.
10%Pt@Ti$_3$C$_2$T$_x$/GCE	0.1 M PBS, 7.4	DPV	BPA: 50.0 nM–5.0 μM	BPA: 32.0 nM	10-fold excess: phenol, NP, uric acid, hydrazine, citric acid, Glu	Drinking water, fresh milk	185
Gr/MXene/GCE	0.1 M PBS, 7.4	DPV	BPA: DPV: 1.0–10.0 μM, AMP: 10.0–180.0 nM	BPA: DPV: 0.35 μM, AMP: 4.08 nM	Na$_2$SO$_4$, NaCl, CH$_3$OH, CdCl$_2$, Cu(C$_2$H$_3$O$_2$)$_2$, FeCl$_2$, KCl, Pb(C$_2$H$_3$O$_2$)$_2$	Plastic products	186
MXene/GCE	0.1 M PBS, 3.0	DPV	4-NP: 0.5–100.0 μM L^{-1}	4-NP: 42.0 nM L^{-1}	Phenol, chlorophenol, aminophenol, benzoic acid, K$^+$, Na$^+$, Mg^{2+}	Tap water	189
D-Ti$_3$C$_2$T$_x$/GR/GCE	0.1 M PBS, pH 7.0	DPV	4-NP: 1.0–175.0 μL	4-NP: 0.16 μL	100-fold excess: Na$_2$SO$_4$, KNO$_3$, CaCl$_2$, 10-fold: p-CP, 2,4-DCP	Tap, seawater	190
MXene/GCE	0.1 M PBS, 7.0	DPV	4-NP: 0.5–25.0 μM; 4-CP: 0.1–20.0 μM	4-NP: 0.11 μM; 4-CP: 0.062 μM	H$_2$O$_2$, Cd^{2+}, Pb^{2+}, CAT, trinitrophenol, phenol	Wastewater	191
Ti$_3$C$_2$/MWCNTs/GCE	0.1 M PBS, pH 6.5	DPV	HQ: 2.0–150.0 μM, CAT: 2.0–150.0 μM	HQ: 6.6 nM, CAT: 3.9 nM	Na$^+$, K$^+$, Ca^{2+}, Cu^{2+}, Mg^{2+}, Zn^{2+}, NO$_3^-$, Cl$^-$, AA, Glu, 4-NP, BPA, RES	Industrial wastewater	195
Alk-Ti$_3$C$_2$/N-PC/GCE	0.1 M PBS, pH 7.0	DPV	CAT: 0.5–150.0 μM, HQ: 0.5–150.0 μM	CAT: 3.1 nM HQ: 4.8 nM	Na$^+$, K$^+$, Ca^{2+}, Cu^{2+}, Mg^{2+}, Zn^{2+}, NO$_3^-$, Cl$^-$, RES, BPA, Glu, AA, 4-AP, 4-NP, TC, CAP	Industrial wastewater	196
MnMoO$_4$-MXene/GCE	0.05 M PBS, 7.0	DPV	CAT: 5.0–65.0 μM, HQ: 5.0–65.0 μM	CAT: 0.30 μM, HQ: 0.26 μM	CAT, HQ	River, seawater	197
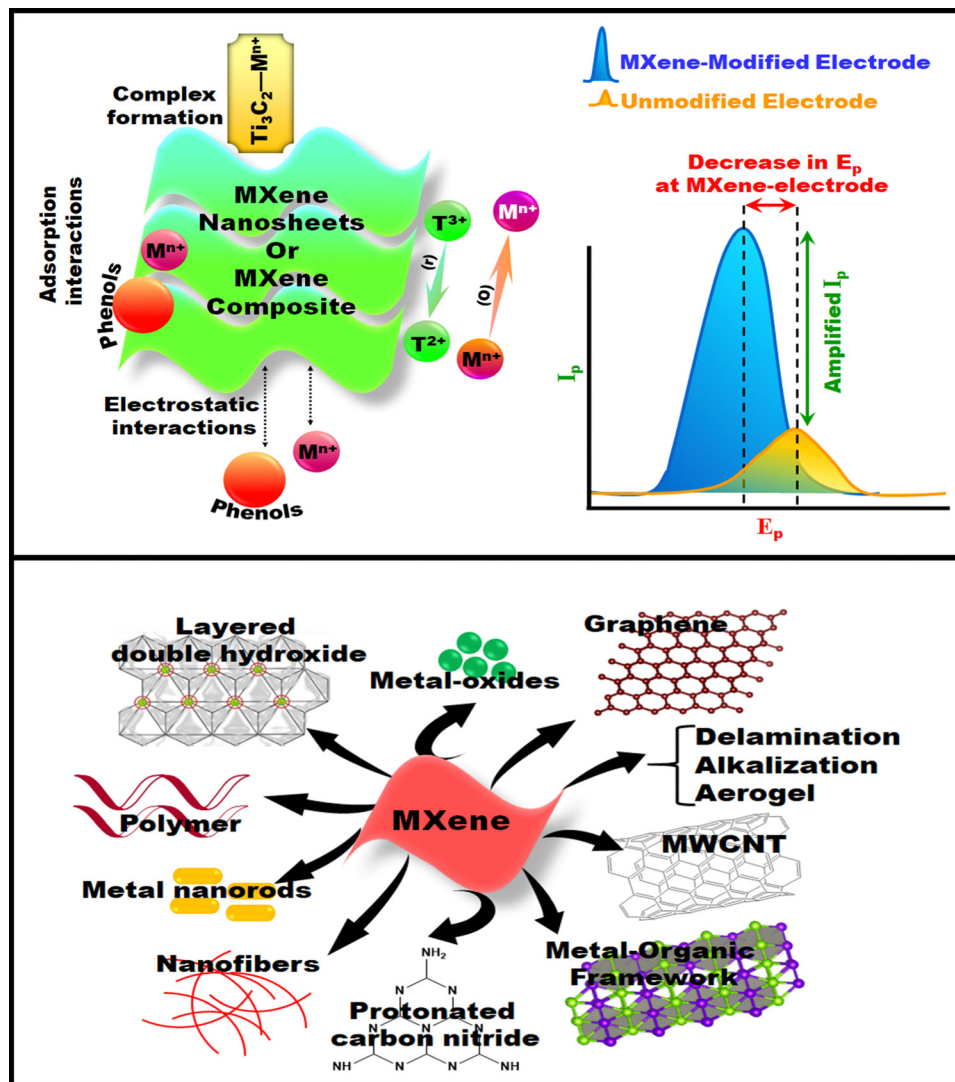
Fig. 15 (a) Detection mechanisms of the targeted HMI and phenolic molecules at various MXene–based EC sensors. (b) Summary of MXene EC sensors for determining HMIs and phenolic moiety containing industrial chemicals.

7. Conclusion and future prospectives

Electrochemical techniques have been classified as enzymatic and non-enzymatic methods. The demerits of enzymatic-based sensors, like enzyme instability, degradation, and reliability issues, have led to the creation of new and alternative sensing materials for sensing applications based on non-enzymatic techniques.[203] Moreover, the relationship between the enzyme's conformation and catalytic activity requires further research, potentially leading to significant research in the enzymatic biosensor field.[204] Thus, as an alternative to enzymatic sensors, non-enzymatic sensors are emerging as an effective technique to detect phenolic residues.[205] Non-enzymatic sensors enable the direct redox process of the target analyte for its detection, unlike the enzymatic ones. However, non-enzymatic sensors also have drawbacks concerning the poor simultaneous detection of two or more phenolic species in a complex system. Thus, further research is essential in the realm of non-enzymatic sensors for

simultaneous and specific detection of several analytes at one single sensing electrode.

The 2D material field has matured since the discovery of graphene, with fast-growing research in material science, nanotechnology, chemistry, and physics. The engineering of 2D layered materials is ambitious as their applications are propitious. MXenes are graphene-like 2D materials with excellent physical and chemical properties. Conventionally, MXenes are prepared by selecting a suitable etchant to curb the weak binding force between the 'A' and the M–X layers to denude the 'A' layers from the MAX phase. Hence, the surface of $Ti_3C_2T_x$ possesses various functional groups. The etching of MAX phases unavoidably includes hazardous chemicals and complex procedures. The procedure for preparing MXenes typically employs F-containing environmentally hazardous reagents. Hence, there is a demand for key methods to prepare MXenes without the application of HF. The rapid advancement in 2D/MXene applications is undeniable and valuable. MXenes

are optimized extrinsically and intrinsically through structure engineering, among the vistas of nanostructure synthesis, metal-atom doping, terminal modification, and hybridization. MXenes and their composites have been demonstrated as suitable electrocatalysts for EC sensors.

EC sensing devices constitute an acceptable solution to detect analytes of interest with adequate accuracy for variable samples. For instance, EC sensors excel in the analytical chemistry of chemicals and species that could be directly detected with other techniques or with high-end equipment like HPLC. Hence, the EC sensors are the epitome of decentralized testing and screening with miniaturized instrumentation. An ideal sensor exhibits superior sensitivity with low detection limits, which is imparted by the modifying agents used in the process of sensor preparation. The construction of MXene-based EC sensors has been gaining popularization among researchers owing to their remarkable traits. As a potentially promising electrode material, MXenes manifest characteristics such as (i) high surface areas, hydrophilicity, electrical conductivity, electrocatalysis, and (ii) environmental friendliness. Through this review, we marked all the current MXene-EC sensors for HMIs and toxic phenolic moiety-containing molecules. Thus, priority was given to evaluating MXene's total capacity and potential for transferring their propitious qualities to EC sensors to achieve excellent performance in terms of sensitivity and LOD.

This review article assessed the trending research on MXene EC sensing devices for the aforementioned target analytes by describing the approaches utilized to construct the sensor and tailoring material properties. We have understood that MXene sensors are being researched for EC sensors, attributed to their extraordinary characteristics. Due to their substantial specific surface area and controlled surface-mediated features, 2D MXenes can be utilized to their fullest potential for sensing. These features magnify the sensitivity and selectivity of the sensing device toward target analytes. Another significant feature is modifying the MXene's surface without forgoing the good electrical conductivity innate to pure MXenes. Their structure engineering has provided numerous possibilities to develop novel EC sensors with desired properties. Further progress in facile methods of MXene synthesis and hybrid formations is anticipated to result in practical and economical applications.

After examining the literature for the progress in EC sensors employing MXene materials, the critical figures of merit of MXenes are: (i) MXenes are highly conductive, attributed to their hydrophilicity and open-end morphology, (ii) the combination of edge-terminated transition metal and metallic active MXenes accounts for the excellent electroactivity, (iii) high aspect ratio, electroconductivity, and enriched surface chemistry of MXenes are appealing properties for sensor construction. The constructed sensors, reviewed in this article, incorporating MXene heterostructures, including nanoparticles (0D), CNTs (1D), graphene (2D), polymers, MOFs, and others, have demonstrated an efficient strategy to enhance the RT EC sensing performance of the device. We have provided evidence of the reported EC sensors exhibiting reliable performance towards

HMIs and other miscellaneous molecules in natural complex water systems that can be applied in environmental pollutant management applications. This review has offered broad insights into the development of MXene-EC sensors, along with perspective on the future generation of cost-effective, multi-modal sensors and high-performance applications.

Future prospectives

Presently, applying MXenes for sensors demands an in-depth understanding of their surface-related EC behavior. Although integrating MXenes in EC sensors has amplified the response signal sensitivity and LODs for several analytes, the contribution of MXenes in most cases is limited to enhanced conductivity. A profound understanding of the structure–property relationship of MXene will favor establishing the sensing mechanisms. Foreseeably, the MXene substrates and analytes that achieve sensor selectivity are not yet distinctly understood. Instead, reports provide a general and plausible interaction between the MXene surface and analyte that are amenable to the sensor's selection. Thus, future research works must consider the characterization of the MXene surface's zeta potential to understand the charge on the sensing substrate that will support and substantiate the interaction mechanism between the electrode and analyte. Furthermore, the *in situ* Raman spectroscopy technique can be applied to understand the changes occurring at the MXene's surface when a potential is applied during electrochemical analysis. XRD characterizations can also be considered for a more detailed reactant (analyte) mechanism, possibly *in situ*.

Furthermore, thorough investigations are needed into the fundamental properties of these materials, including variations between multilayer/monolayer 2D materials, heterojunction traits, interfacial characteristics, and surface modification effects, namely, hybridization, doping, and defect engineering. These extensive investigations will lead to the discovery of new materials with improved characteristics, a boon to industries and society.

In general, MXenes are reported to be terminated with functional moieties. Hence, preparing MXenes devoid of functional moieties is intriguing, particularly for EC sensing applications. Consequently, an immediate requirement exists to probe efficient procedures like the bottom-up routes that allow fine control over the size of layers, morphology, and surface terminal group distributions. Hence, the complex surface chemistry of MXene is crucial for tailoring several sensing applications. Much investigation and understanding are required regarding how the surface chemistry of MXene impacts the sensor device application. Understanding the limiting factors of the scalable synthesis of MXenes is crucial. In addition, we are testing new, less hazardous etching methods for cost-efficient production with greater yield. Additionally, a thorough examination of the impact of chemical stability on the repeatability, error, selectivity, and other ambiguous characteristics of the MXene-based sensor equipment helps extend the shelf life of the sensors and realize their broad range of applications. Finally, the MXene-based EC sensors should be biased toward enhancing the

oxidation resistance of materials, extending the applicable scenarios of the nanomaterials in variable environments, and amending their cost-effectiveness for practical applications by designing simple structures with good performance and diverse functions.

To amplify the application prospects of MXenes, facile and quick protocols need to be conceived for the synthesis of MXene hybrid nanocomposites with various functionalities, namely, MXene-nanostructures and MXene-polymer materials. Noble metal nanoclusters/nanoparticles can also be decorated on the MXene surface for improved catalytic performance. Therefore, extensive efforts are vital for synthesizing MXenes with superior nanoarchitecture surface chemistry and heterostructures, making them promising electrode modification agents. Most MXenes have various functional groups, while the development of MXene with a single type of surface termination group is recommended for governing the surface characteristics of the MXene, such as affinity towards specific chemical species (selectivity). Furthermore, DFT investigations have evidenced that the synthesis of MXenes with no surface functional groups can change the chemical characteristics of MXene substantially, which can be of greater interest for developing chemical sensors.[206]

Next are the real-world applications where workability and durability must be verified. Flexible MXenes can be engineered. Unlike variant 2D materials, MXenes are hardly stretchable; thus, polymers can be included to enhance their mechanical robustness. The hybridization of MXenes with polymers can improve the selectivity and conductivity during sensor development. This can be done by optimizing the MXene concentration and appropriate selection of polymers. Furthermore, considering the distinct compositions of MAX phases, an array of MXenes is anticipated to subsist with unprecedented characteristics, thus catering to a broad scope in the sensing field.

Nonetheless, the MXene EC sensor research is still in its infancy, and commercialization necessitates solutions to the issues experienced by the researchers. This is because the EC sensor's performance standards and other prerequisites for commercialization are yet to be systematically established; for example, the crucial factors are its multifunctionality,

reproducibility, and stability. Another critical factor is productivity, which is the lack of good yield from the method used for MXene synthesis. Hence, this issue must be addressed in the future as it will favor the development of reliable and scalable fabrication procedures for mass production. The key challenges that need to be addressed for this 2D material to attain market value include: (i) we have come across the literature showing that MXenes are synthesized through diverse techniques with 'on-demand' tuning of structural and electronic properties; however, they are not yet wholly accomplished. 2D material-based devices (i) reproducible and reliable synthesis procedures, (ii) high-volume manufacturing (mass-production of MXene is tedious, and MAX phase production is not cost-effective), and (iii) 2D materials with heterostructure configurations pave the way for broader applications. Besides, the most widely utilized procedure for sensor fabrication is a manual drop-cast coating, which can only be produced on the laboratory-scale. This lack of a pathway toward large-scale production is one significant roadblock in bringing more EC sensing devices from the laboratory to market. Therefore, exploring other methods that offer repeatability in electrode construction and improved reproducibility in sensing measurements is one approach towards large-scale manufacturing of EC sensors. Fig. 16 illustrates the summary and the prospects of MXene's application in fabricating EC sensors.

Although several challenges need to be addressed, a tremendous understanding of the structural fundamentals is expected shortly based on the promising results from the current research. Addressing these challenges will further propel the fabrication of MXene EC sensors. These sensors are anticipated to be applied in environmental, human, and robotics monitoring. Uncharted fields like food engineering will benefit from MXene-based sensors. Surmounting these shortcomings will open infinite applications. This review addressed factors concerning process-structured-sensor property relationships among the emerging MXene sensors. We hope that our readers have gained an understanding of the current scenario of MXene-based sensors, which have not received significant scientific attention.
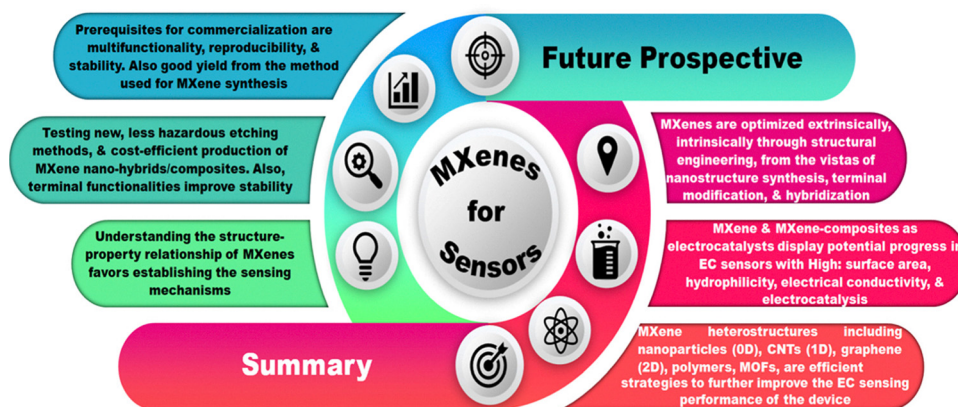

Fig. 16 Concluding remarks and future perspectives of MXene-based EC sensors.

Author contributions

Manasa: conceptualization, data curation, formal analysis, investigation, visualization, and writing – original draft. CS Rout: conceptualization, project administration, supervision, validation, and writing – review and editing.

Conflicts of interest

The authors declare no conflict of interest.

Acknowledgements

References

1 J. Wu, H. Liu, B. Ma and H. Ju, Device integration of electrochemical biosensors, *Nat. Rev. Bioeng.*, 2023, **1**, 346–360, DOI: 10.1038/s44222-023-00032-w.

2 G. Manasa, R. J. Mascarenhas, A. K. Satpati, O. J. D'Souza and A. Dhason, Facile preparation of polymethylene blue modified carbon paste electrode for the detection and quantification of catechin, *Mater. Sci. Eng., C*, 2017, **73**, 552–561.

3 L. M. Castle, D. A. Schuh, E. E. Reynolds and A. L. Furst, Electrochemical sensors to detect bacterial foodborne pathogens, *ACS Sens.*, 2021, **6**, 1717–1730.

4 H. S. Magar, R. Y. A. Hassan and M. N. Abbas, Non–enzymatic disposable electrochemical sensors based on CuO/Co$_3$O$_4$@MWCNTs nanocomposite modified screen–printed electrode for the direct determination of urea, *Sci. Rep.*, 2023, **13**, 2034.

5 F. Silveri, F. della Pelle, A. Scroccarello, Q. U. A. Bukhari, M. del Carlo and D. Compagnone, Modular graphene mediator film-based electrochemical pocket device for chlorpyrifos determination, *Talanta*, 2022, **240**, 123212.

6 G. Manasa, R. J. Mascarenhas, A. K. Bhakta and Z. Mekhalif, MWCNT/Nileblue heterostructured composite electrode for flavanone naringenin quantification in fruit juices, *Electroanalysis*, 2020, **32**, 939–948.

7 G. Manasa, C. Raj, A. K. Satpati and R. J. Mascarenhas, SOMWCNT/modified carbon paste – A non-enzymatic amperometric sensor for direct determination of 6-mercaptopurine in biological fluids, *Electroanalysis*, 2020, **32**, 2431–2441.

8 G. Manasa, R. J. Mascarenhas, S. J. Malode and N. P. Shetti, Graphene-based electrochemical immunosensors for early detection of oncomarker carcinoembryonic antigen, *Biosens. Bioelectron.: X*, 2022, **11**, 100189.

9 G. Manasa, R. J. Mascarenhas, N. P. Shetti, S. J. Malode and T. M. Aminabhavi, Biomarkers for early diagnosis of ovarian carcinoma, *ACS Biomater. Sci. Eng.*, 2022, **8**, 2726–2746.

10 H. Shen, T. Liu, D. Qin, X. Bo, L. Wang, Q. Yuan, T. Wagberg, G. Hu and M. Zhou, in *Micro and nano technologies*, ed. H. Peng, Q. Li, T. Chen, Elsevier, ch. 7, 2017, pp. 179–199.

11 M. Wang, Y. Yang, J. Min, Y. Song, J. Tu, D. Mukasa, C. Ye, C. Xu, N. Heflin, J. S. McCune, T. K. Hsiai, Z. Li and W. Gao, A wearable electrochemical biosensor for the monitoring of metabolites and nutrients, *Nat. Biomed. Eng.*, 2022, **6**, 1225–1235.

12 H. Teymourian, M. Parrilla, J. R. Sempionatto, N. F. Montiel, A. Barfidokht, R. V. Echelpoel, K. De Wael and J. Wang, Wearable electrochemical sensors for the monitoring and screening of drugs, *ACS Sens.*, 2020, **5**, 2679–2700.

13 G. Manasa, A. K. Bhakta, Z. Mekhalif and R. J. Mascarenhas, Voltammetric study and rapid quantification of resorcinol in hair dye and biological samples using ultrasensitive maghemite/MWCNT modified carbon paste electrode, *Electroanalysis*, 2019, **31**, 1363–1372.

14 J. Z. Hassan, A. Raza, Z. U. D. Babar, U. Qumar, N. T. Kaner and A. Cassinese, 2D materials-based sensing devices: an update, *J. Mater. Chem. A*, 2023, **11**, 6016–6063.

15 L. Wang, M. Zhang, B. Yang, J. Tan, X. Ding and W. Li, Recent advances in multidimensional 1D, 2D, and 3D composite sensors derived from MXene: Synthesis, structure, application, and perspective, *Small Methods*, 2021, **5**, 2100409.

16 H. Riazi, G. Taghizadeh and M. Soroush, MXene-based nanocomposite sensors, *ACS Omega*, 2021, **6**, 11103–11112.

17 R. A. Soomro, S. Jawaid, Q. Zhu, Z. Abbas and B. Xu, A mini-review on MXenes as versatile substrate for advanced sensors, *Chin. Chem. Lett.*, 2020, **31**, 922–930.

18 G. Manasa, N. P. Shetti, R. J. Mascarenhas and K. R. Reddy, in *Smart nanodevices for point-of-care applications*, ed. S. Kanchi, R. Chokkareddy, M. Rezakazemi, CRC Press, 1st edn, 2022, ch. 10, pp. 1–12.

19 T. O. Varol, in *Drug targets in cellular processes of cancer: from nonclinical to preclinical models*, ed. H. S. Tuli, Springer, 1st edn, 2020, ch. 2.

20 R. Shiwaku, H. Matsui, K. Nagamine, M. Uematsu, T. Mano, Y. Maruyama, A. Nomura, K. Tsuchiya, K. Hayasaka, Y. Takeda, T. Fukuda, D. Kumaki and S. Tokito, A printed organic circuit system for wearable amperometric electrochemical sensors, *Sci. Rep.*, 2018, **8**, 6368.

21 D. Grieshaber, R. MacKenzie, J. Voros and E. Reimhult, Electrochemical sensors - Sensor principles and architecture, *Sensors*, 2008, **8**, 1400–1458.

22 M. S. Artiles, C. S. Rout and T. S. Fisher, Graphene-based hybrid materials and devices for biosensing, *Adv. Drug Delivery Rev.*, 2011, **63**, 1352–1360.

23 M. Mathew, S. Radhakrishnan, A. Vaidyanathan, B. Chakraborty and C. S. Rout, Flexible and wearable electrochemical biosensors based on two-dimensional materials:

recent developments, *Anal. Bioanal. Chem.*, 2021, **413**, 727–762.

24 G. Manasa, R. J. Mascarenhas, A. K. Satpati, B. M. Basavaraja and S. Kumar, An electrochemical bisphenol F sensor based on ZnO/G nanocomposite and CTAB surface modified carbon paste electrode architecture, *Colloids Surf., B*, 2018, **170**, 144–151.

25 R. Ponnusamy, R. Venkatesan, M. Kandasamy, B. Chakraborty and C. S. Rout, MnO_2 polymorph selection for non-enzymatic glucose detection: An integrated experimental and density functional theory investigation, *Appl. Surf. Sci.*, 2019, **487**, 1033–1042.

26 C. S. Rout, S. H. Krishna, S. R. C. Vivekchand, A. Govindaraj and C. N. R. Rao, Hydrogen and ethanol sensors based on ZnO nanorods, nanowires and nanotubes, *Chem. Phys. Lett.*, 2006, **418**, 586–590.

27 G. Manasa, R. J. Mascarenhas and B. M. Basavaraja, Sensitively-selective determination of propyl paraben preservative based on synergistic effects of polyaniline-zinc-oxide nano-composite incorporated into graphite paste electrode, *Colloids Surf., B*, 2019, **184**, 110529.

28 G. Manasa, R. J. Mascarenhas, A. K. Bhakta and Z. Mekhalif, Nano-graphene-platelet/Brilliant-green composite coated carbon paste electrode interface for electro-catalytic oxidation of flavanone Hesperidin, *Microchem. J.*, 2021, **160**, 105768.

29 G. Manasa, R. J. Mascarenhas, N. P. Shetti, S. J. Malode, A. Mishra, S. Basu and T. M. Aminabhavi, Skin patchable sensor surveillance for continuous glucose monitoring, *ACS Appl. Bio. Mater.*, 2022, **5**, 945–970.

30 G. Manasa, A. K. Bhakta, J. Bafna, R. J. Mascarenhas, S. J. Malode and N. P. Shetti, An amperometric sensor composed of carbon hybrid-structure for the degradation of aminotriazole herbicide, *Environ. Res.*, 2022, **212**, 113541.

31 R. Ponnusamy, A. Gangan, B. Chakraborty, D. J. Late and C. S. Rout, Improved nonenzymatic glucose sensing properties of Pd/MnO_2 nanosheets: Synthesis by facile microwave-assisted route and theoretical insight from quantum simulations, *J. Phys. Chem. B*, 2018, **122**, 7636–7646.

32 S. Lakshmy, S. Santhosh, N. Kalarikkal, C. S. Rout and B. Chakraborthy, A review of electrochemical glucose sensing based on transition metal phosphides, *J. Appl. Phys.*, 2023, **133**, 070702.

33 M. V. Sulleiro, A. D. Alfaro, N. Alegret, A. Silvestri and I. J. Gomez, 2D materials towards sensing technology: From fundamentals to applications, *Sens. Bio-Sens. Res.*, 2022, **38**, 100540.

34 S. Su, J. Chao, D. Pan, L. Wang and C. Fan, Electrochemical sensors using two-dimensional layered nanomaterials, *Electroanalysis*, 2015, **27**, 1062–1072.

35 R. Khan, A. Radoi, S. Rashid, A. Hayat, A. Vasilescu and S. Andreescu, Two-Dimensional nanostructures for electrochemical biosensor, *Sensors*, 2021, **21**, 3369.

36 C. S. Rout, *2D materials-based electrochemical sensors*, Elsevier, 1st edn, 2023.

37 V. Shanmugam, R. A. Mensah, K. Babu, S. Gawusu, A. Chanda, Y. Tu, R. E. Neisiany, M. Forsth, G. Sas and O. Das, A review of the synthesis, properties, and applications of 2D materials, *Part. Part. Syst. Charact.*, 2022, **39**, 2200031.

38 A. J. Mannix, B. Kiraly, M. C. Hersam and N. P. Guisinger, Synthesis and chemistry of elemental 2D materials, *Nat. Rev. Chem.*, 2017, **1**, 0014.

39 S. V. S. Prasad, R. K. Mishra, S. Gupta, S. B. Prasad and S. Singh, in *Advanced applications of 2D nanostructures*, ed. S. Singh, K. Verma, C. Prakash, Springer, 2021, ch. 1, pp. 1–10.

40 *Fundamentals and sensing applications of 2D materials*, ed. C. S. Rout, D. J. Late, H. Morgan, Elsevier Science, 1st edn, 2019.

41 P. V. Shinde, A. Tripathi, R. Thapa and C. S. Rout, Nano-ribbons of 2D materials: A review on emerging trends, recent developments and future perspectives, *Coord. Chem. Rev.*, 2022, **453**, 214335.

42 M. Xu, T. Liang, M. Shi and H. Chen, Graphene-like two-dimensional materials, *Chem. Rev.*, 2013, **113**, 3766–3798.

43 X. Zhang and A. Beyer, Mechanics of free-standing inorganic and molecular 2D materials, *Nanoscale*, 2021, **13**, 1443–1484.

44 C. Mackin, A. Fasoli, M. Xue, Y. Lin, A. Adebiyi, L. Bozano and T. Palacios, Chemical sensor systems based on 2D and thin films materials, *2D Mater.*, 2020, **7**, 022002.

45 S. N. Faisal and F. Iacopi, Thin-film electrodes based on two-dimensional nanomaterials for neural interfaces, *ACS Appl. Nano Mater.*, 2022, **5**, 10137–10150.

46 J. Kudr, L. Richtera, L. Nejdl, K. Xhaxhiu, P. Vitek, B. R. Nedecky, D. Hyek, P. Kopel, V. Adam and R. Kizek, Improved electrochemical detection of zinc ions using electrode modified with electrochemically reduced graphene oxide, *Materials*, 2016, **9**, 31.

47 P. Wang, C. Y. Han, F. Y. Zhou, J. S. Lu, X. G. Han and Z. W. Wang, Electrochemical determination of tert-butyl-hydroquinone and butylated hydroxyanisole at choline functionalized film supported graphene interface, *Sens. Actuators, B*, 2016, **224**, 885–891.

48 M. Mishra, S. K. Behura, M. Beidaghi, K. Verma and S. Singh, in *Advanced applications of 2D nanostructures*, ed. S. Singh, K. Verma, C. Prakash, Springer, 2021, ch. 6, pp. 73–98.

49 B. Xu and Y. Gogotsi, MXenes: from discovery to applications, *Adv. Funct. Mater.*, 2020, **30**, 2007011.

50 F. Shahzad, S. A. Zaidi and R. A. Naqvi, 2D transition metal carbides MXene for electrochemical sensing: A review, *Crit. Rev. Anal. Chem.*, 2022, **52**, 848–864.

51 D. Kim, T. Y. Ko, H. Kim, G. H. Lee, S. Cho and C. M. Koo, Nonpolar organic dispersion of 2D Ti_3C_2Tx MXene flakes via simultaneous interfacial chemical grafting and phase transfer method, *ACS Nano*, 2019, **13**, 13818.

52 J. M. George, A. Antony and B. Mathew, Metal oxide nanoparticles in electrochemical sensing and biosensing: A review, *Microchim. Acta*, 2018, **185**, 358.

53 A. Pandikumar and P. Rameshkumar, *Metal oxides in nanocomposites-based electrochemical; sensors for toxic chemicals*, Elsevier, 2021.

54 G. B. Subbaiah, K. V. Ratnam, S. Janardhan, K. Shiprath, H. Manjunath, M. Ramesha, N. V. K. Prasad, S. Ramesh and T. A. Babu, Metal and metal oxide based advanced ceramics for electrochemical biosensors-A short review, *Front. Mater.*, 2021, **8**, 682025.

55 D. H. Ho, Y. Y. Choi, S. B. Jo, J.-M. Myoung and J. H. Cho, Sensing with MXenes: Progress and prospects, *Adv. Mater.*, 2021, **33**, 2005846.

56 S. Radhakrishnan, P. Mane, K. A. S. Raj, B. Chakraborty and C. S. Rout, In-situ construction of hierarchical 2D MoS$_2$/1D Te hybrid for supercapacitor applications, *J. Energy Storage*, 2023, **60**, 106703.

57 N. H. A. Junaidi, W. Y. Wong, K. S. Loh, S. Rahman and W. R. W. Daud, A comprehensive review of MXenes as catalyst supports for the oxygen reduction reaction in fuel cells, *Int. J. Energy Res.*, 2021, **45**, 15760–15782.

58 M. Mathew, P. V. Shinde, R. Samal and C. S. Rout, A review on mechanisms and recent developments in pn heterojunctions of 2D materials for gas sensing applications, *J. Mater. Sci.*, 2021, **56**, 9575–9604.

59 F. Dixit, K. Zimmermann, R. Dutta, N. J. Prakash, B. Barbeau, M. Mohseni and B. Kandasubramanian, Application of MXene for water treatment and energy-efficient desalination: A review, *J. Hazard. Mater.*, 2022, **423**, 127050.

60 S. Zhou, X. Yang, W. Pei, N. Liu and J. Zhao, Heterostructures of MXenes and N-doped graphene as highly active bifunctional electrocatalyst, *Nanoscale*, 2018, **10**, 10876–10883.

61 L. Wu, X. Lu Dhanjai, Z. S. Wu, Y. Dong, X. Wang, S. Zheng and J. Chen, 2D transition metal carbide MXene as a robust biosensing platform for enzyme immobilization and ultrasensitive detection of phenol, *Biosens. Bioelectron.*, 2018, **107**, 69–75.

62 L. Lorencova, T. Bertok, J. Filip, M. Jerigova, D. Velic, P. Kasak, K. A. Mahmoud and J. Tkac, Highly stable Ti$_3$C$_2$T$_x$ MXene/Pt nanoparticles-modified glassy carbon electrode for H$_2$O$_2$ and small molecules sensing applications, *Sens. Actuators, B*, 2018, **263**, 360–368.

63 F. Wang, C. Yang, M. Duan, Y. Tang and J. F. Zhu, TiO$_2$ nanoparticle modified organ-like Ti$_3$C$_2$ MXene nanocomposite encapsulating hemoglobin for a mediator-free biosensor with excellent performances, *Biosens. Bioelectron.*, 2015, **74**, 1022–1028.

64 S. K. Kailasa, D. J. Joshi, J. R. Koduru and N. I. Malek, Review on MXenes-based nanomaterials for sustainable opportunities in energy storage, sensing and electrocatalytic reactions, *J. Mol. Liq.*, 2021, **342**, 117524.

65 Q. Wang, N. Han, Z. Shen, X. Li, Z. Chen, Y. Cao, W. Si, F. Wang, B.-J. Ni and V. K. Thakur, MXene-based electrochemical (bio) sensors for sustainable applications: roadmap for future advanced materials, *Nano Mater. Sci.*, 2023, **5**, 39–52.

66 F. Shahzad, S. A. Zaidi and R. A. Naqvi, 2D transition metal carbides MXene for electrochemical sensing: A review, *Crit. Rev. Anal. Chem.*, 2022, **52**, 848–864.

67 A. Sinha Dhanjai, H. Zhao, Y. Huang, X. Lu, J. Chen and R. Jain, MXene: An emerging material for sensing and biosensing, *TrAC, Trends Anal. Chem.*, 2018, **105**, 424–435.

68 B. Xu, C. Zhi and P. Shi, Latest advances in MXene biosensors, *J. Phys.: Mater.*, 2020, **3**, 031001.

69 X. Wu, P. Ma, Y. Sun, F. Du, D. Song and G. Xu, Application of MXene in electrochemical sensors: A review, *Electroanalysis*, 2021, **33**, 1827–1851.

70 M. R. Ali, M. S. Bacchu, M. R. Al-Mamun, M. I. Hossain, A. Khaleque, A. Khatun, D. D. Ridoy, M. A. S. Aly and M. Z. H. Khan, Recent advanced in MXene research toward biosensor development, *Crit. Rev. Anal. Chem.*, 2022, **6**, 1–18, DOI: 10.1080/10408347.2022.2115286.

71 A. A. P. R. Perera, K. A. U. Madhushani, B. T. Punchihewa, A. Kumar and R. K. Gupta, MXene-based nanomaterials for multifunctional applications, *Materials*, 2023, **16**, 1138.

72 K. Grabowski, S. Srivatsa, A. Vashisth, L. Mishnaevsky Jr. and T. Uhl, Recent advances in MXene-based sensors for structural health monitoring applications: A review, *Measurement*, 2022, **189**, 110575.

73 G. J. Soufi, P. Iravani, A. Hekmatnia, E. Mostafavi, M. Khatami and S. Iravani, MXenes and MXene-based materials with cancer diagnostics applications: Challenges and opportunities, *Comments Inorg. Chem.*, 2022, **42**, 174–207.

74 R. Rajeev, D. A. Thadathil and A. Varghese, New horizons in surface topography modulation of MXenes for electrochemical sensing towards potential biomarkers of chronic disorders, *Crit. Rev. Sol. Stat. Mater. Sci.*, 2022, **48**, 580–622, DOI: 10.1080/10408436.2022.2078789.

75 I. Patra, K. M. Kammoud, Z. H. Al-qaim, I. I. Mamadoliev, M. A. Jawad, A. T. Hammid, Y. S. Karim and G. Yasin, Perspective and trends in advanced MXenes-based optical biosensors for the recognition of food contaminants, *Crit. Rev. Anal. Chem.*, 2022, **24**, 1–20, DOI: 10.1080/10408347. 2022.2091921.

76 M. Khatami and S. Iravani, MXenes and MXene-based materials for the removal of water pollutants: Challenges and opportunities, *Comments Inorg. Chem.*, 2021, **41**, 213–248.

77 C. Zhang, Y. Ma, X. Zhang, S. Abdolhosseinzadeh, H. Sheng, W. Lan, A. Pakdel, J. Heier and F. Nuesch, Two-dimensional transition metal carbides and nitrides MXenes: Synthesis, properties, and electrochemical energy storage applications, *Energy Environ. Mater.*, 2020, **3**, 29–55.

78 J. Zhu, E. Ha, G. Zhao, Y. Zhou, D. Huang, G. Yue, L. Hu, N. Sun, Y. Wang, L. Y. S. Lee, C. Xu, K.-Y. Wong, D. Astruc and P. Zhao, Recent advance in MXenes: A promising 2D material for catalysis, sensor and chemical adsorption, *Coord. Chem. Rev.*, 2017, **352**, 306–327.

79 M. Naguib, O. Mashtalir, J. Carle, V. Presser, J. Lu, L. Hultman, Y. Gogotsi and M. W. Barsoum, Two-dimensional transition metal carbides, *ACS Nano*, 2012, **6**, 1322–1331.

80 J. Zhu, E. Ha, G. Zhao, Y. Zhou, D. Huang, G. Yue, L. Hu, N. Sun, Y. Wang, L. Y. S. Lee, C. Xu, K.-Y. Wong, D. Astruc

and P. Zhao, Recent advances in MXenes: A promising 2D material for catalysis, sensor and chemical adsorption, *Coord. Chem. Rev.*, 2017, **352**, 306–327.

81 S. K. Hwang, S.-M. Kang, M. Rethinasabapathy, C. Roh and Y. S. Huh, MXene: An emerging two-dimensional layered material for removal of radioactive pollutants, *Chem. Eng. J.*, 2020, **397**, 125428.

82 M. Naguib, M. Kurtoglu, V. Presser, J. Lu, J. Niu, M. Heon, L. Hultman, Y. Gogotsi and M. W. Barsoum, Two-dimensional nanocrystals produced by exfoliation of Ti_3AlC_2, *Adv. Mater.*, 2011, **23**, 4248–4253.

83 C. Tan, X. Cao, X. J. Wu, Q. He, J. Yang, X. Zhang, J. Chen., W. Zhao, S. Han, G. H. Nam, M. Sindoro and H. Zhang, Recent advances in ultrathin two-dimensional nanomaterials, *Chem. Rev.*, 2017, **117**, 6225–6331.

84 M. M. Hasan, M. Milon Hossain and H. K. Chowdhury, Two-dimensional MXene-based flexible nanostructures for functional nanodevices: a review, *J. Mater. Chem.*, 2021, **9**, 3231–3269.

85 F. Shahzad, A. Iqbal, H. Kim and C. M. Koo, 2D transition metal carbides MXenes: Applications as an electrically conducting material, *Adv. Mater.*, 2020, **32**, 2002159.

86 M. R. Farani, B. N. Khiarak, R. Tao, Z. Wang, S. Ahmadi, M. Hassanpour, M. Rabiee, M. R. Saeb, E. C. Lima and N. Rabiee, 2D MXene nanocomposites: electrochemical and biomedical applications, *Environ. Sci.: Nano*, 2022, **9**, 4038.

87 M. Mathew and C. S. Rout, Electrochemical biosensors based on Ti_3C_2Tx MXene: future perspectives for on-site analysis, *Curr. Opin. Electrochem.*, 2021, **30**, 100782.

88 C. Sun, P. Zuo, W. Sun, R. Xia, Z. Dong, L. Zhu, J. Lv, G. Deng, L. Tan and Y. Dai, Self-assembly of alternating stacked 2d/2d Ti_3C_2Tx MXene/ZnMnNi LDH van der Waals heterostructures with ultrahigh supercapacitance performance, *ACS Appl. Energy Mater.*, 2020, **3**, 10242–10254.

89 M. M. Hasan, M. M. Hossain and H. K. Chowdhury, Two-dimensional MXene-based flexible nanostructures for functional nanodevices: A review, *J. Mater. Chem. A*, 2021, **9**, 3231–3269.

90 J. Xu, T. Peng, Q. Zhang, H. Zheng, H. Yu and S. Shi, Intercalation effects on the electrochemical properties of $Ti_3C_2T_x$ MXene nanosheets for high-performnace supercapacitors, *ACS Appl. Nano Mater.*, 2022, **5**, 8794–8803.

91 L. Lorencova, K. K. Sadasivuni, P. Kasak and J. Tkac, in Ti3C2 MXene-based nanobiosensors for detection of cancer biomarkers, *Novel nanomaterials*, ed. K. Krishnamoorty, inTechOpen, 2021.

92 V. M. H. Ng, H. Huang, K. Zhou, P. S. Lee, W. Que, J. Z. Xu and L. B. Kong, Recent progress in layered transition metal carbides and/or nitrides MXenes and their composites: synthesis and applications, *J. Mater. Chem. A*, 2017, 5, 3039–3068.

93 K. Deshmukh, T. Kovarik and S. K. K. Pasha, State of art recent progress in two dimensional MXenes based gas sensors and biosensors: A comprehensive review, *Coord. Chem. Rev.*, 2020, **424**, 213514.

94 O. Mashtalir, M. Naguib, V. N. Mochalin, Y. Dall'Agnese, P. Rozier, P. L. Taberna, M. Naguib, P. Simon, M. W. Barsoum and Y. Gogotsi, Cation intercalation and high volumetric capacitance of two-dimensional titanium carbide, *Science*, 2013, **341**, 1716.

95 J. Peng, X. Chen, W. J. Ong, X. Zhao and N. Li, Surface and heterointerface engineering of 2D MXenes and their nanocomposites: Insights into electro-and photocatalysis, *Chem. Press Rev.*, 2019, **5**, 18–50.

96 L. Wu, X. Lu Dhanjai, Z. S. Wu, Y. Dong and X. Wang, 2D transition metal carbide MXene as a robust biosensing platform for enzyme immobilization and ultrasensitive detection of phenol, *Biosens. Bioelectron.*, 2018, **107**, 69–75.

97 M. Alhabeb, K. Maleski, B. Anasori, P. Lelyukh, L. Clark, S. Sin and Y. Gogotsi, Guidelines for synthesis and processing of two-dimensional titanium carbide Ti_3C_2Tx MXene, *Chem. Mater.*, 2017, **29**, 7633–7644.

98 X. Huang and P. Wu, A facile, high-yield, and freeze-and-thaw-assisted approach to fabricate MXene with plentiful wrinkles and its application in on-chip micro-supercapacitors, *Adv. Funct. Mater.*, 2020, **30**, 1910048.

99 X. Zang, J. Wang, Y. Qin, T. Wang, C. He, Q. Shao, H. Zhu and N. Cao, Enhancing capacitance performance of Ti_3C_2Tx MXene as electrode materials of supercapacitors: from controlled preparation to composite structure construction, *Nano-Micro Lett.*, 2022, **12**, 77.

100 K. Huang, Z. Li, J. Lin, G. Han and P. Hunag, Two-dimensional transition metal carbides and nitrides MXenes for biomedical applications, *Chem. Soc. Rev.*, 2018, **74**, 5109–5124.

101 C. J. Zhang, L. Mckeon, M. P. Kremer, S.-H. Park, O. Ronan, A. S. Ascaso, S. Barwich, C. O. Coileain, N. McEvoy and H. C. Nerl, Additive-free MXene inks and direct printing of micro-supercapacitors, *Nat. Commun.*, 2019, **10**, 1–9.

102 L. Verger, V. Natu, M. Carey and M. W. Barsoum, MXenes: An introduction of their synthesis, select properties, and applications, *Trends Chem.*, 2019, **1**, 656–669.

103 L. Verger, C. Xu, V. Natu, H.-M. Cheng, W. Ren and M. W. Barsoum, Overview of the synthesis of MXenes and other ultrathin 2D transition metal carbides and nitrides, *Curr. Opin. Solid State Mater. Sci.*, 2019, **23**, 149–163.

104 T. Haneef, K. Rasool, J. Iqbal, R. Nawab, M. R. Ul Mustafa, K. A. Mahmoud, T. Sarkar and A. Shahzad, Recent progress in two dimensional MXenes for photocatalysis: A critical review, *2D Mater.*, 2023, **10**, 012001.

105 A. Lipatov, M. Alhabeb, M. R. Lukatskaya, A. Boson, Y. Gogotsi and A. Sinitskii, Effect of synthesis on quality, electronic properties and environmental stability of individual monolayer Ti_3C_2 MXene flakes, *Adv. Electron. Mater.*, 2016, **2**, 1600255.

106 B. Anasori, C. Shi, E. J. Moon, Y. Xie, C. A. Voigt, P. R. C. Kent, S. J. May, S. J. L. Billinge, M. W. Barsoum and Y. Gogotsi, Control of electronic properties of 2D carbides MXenes by manipulating their transition metal layers, *Nanoscale Horiz.*, 2016, **1**, 227–234.

107 M. Khazaei, M. Arai, T. Sasaki, C.-Y. Chung, N. S. Venkataramanan, M. Estili, Y. Sakka and Y. Kawazoe, Novel electronic and magnetic properties of two-dimensional transition metal carbides and nitrides, *Adv. Funct. Mater.*, 2013, **23**, 2185–2192.

108 Q. Tang, Z. Zhou and P. Shen, Are MXenes promising anode materials for Li ion batteries? Computational studies on electronic properties and Li storage capacity of Ti_3C_2 and $Ti_3C_2X_2$ X= F, OH monolayer, *J. Am. Chem. Soc.*, 2012, **134**, 16909–16916.

109 L. Shen, X. Zhou, X. Zhang, Y. Zhang, Y. Liu, W. Wang, W. Si and X. Dong, Carbon-intercalated Ti_3C_2Tx MXene for high performance electrochemical energy storage, *J. Mater. Chem. A*, 2018, **6**, 23513–23520.

110 S. A. Zahra and S. Rizwan, MWCNT-modified MXene as cost–effective efficient bifunctional catalyst for overall water splitting, *RSC Adv.*, 2022, **12**, 8405–8413.

111 D. Zhao, M. Clites, G. Ying, S. Kota, J. Wang, V. Natu, X. Wang, E. Pomerantseva, M. Cao and M. W. Barsoum, Alkali-induced crumpling of Ti_3C_2Tx MXene to form 3D porous networks for sodium ion storage, *Chem. Commun.*, 2018, **54**, 4533–4536.

112 Y. Dong, Z. S. Wu, S. Zheng, X. Wang, J. Qin, S. Wang, X. Shi and X. Bao, Ti_3C_2 MXene-derived sodium/potassium titanate nanoribbons for high performance sodium/potassium ion batteries with enhanced capacities, *ACS Nano*, 2017, **11**, 4792–4800.

113 P. Lian, Y. Dong, Z.-S. Wu, S. Zheng, X. Wang, S. Wang, C. Sun, J. Qin, X. Shi and X. Bao, Alkalized Ti_3C_2 MXene nanoribbons with expanded interlayer spacing for high-capacity sodium and potassium ion batteries, *Nano Energy*, 2017, **40**, 1–8.

114 S. S. Shankar, R. M. Shereema and R. B. Rakhi, Electro-chemical determination of adrenaline using MXene/graphite composite paste electrodes, *ACS Appl. Mater. Interfaces*, 2018, **10**, 43343–43351.

115 C. Karaman, O. Karaman, N. Atar and M. L. Yola, Electrochemical immunosensor development based on core-shell high-crystalline graphitic carbon nitride@carbon dots and Cd0.5Zn0.5S/d-Ti3C2Tx MXene composite for heart-type fatty acid-binding protein detection, *Mikrochim. Acta*, 2021, **188**, 182.

116 A. VahidMohammadi, J. Rosen and Y. Gogotsi, The world of two-dimensional carbides and nitrides MXenes, *Science*, 2021, **372**, 10242–10254.

117 M. Khazaei, M. Arai, T. Sasaki, C.-Y. Chung, N. S. Venkataramanan, M. Estili, Y. Sakka and Y. Kawazoe, Novel electronic and magnetic properties of two-dimensional transition metal carbide and nitride, *Adv. Funct. Mater.*, 2013, **23**, 2185–2192.

118 C. Ling, L. Shi, Y. Ouyang, Q. Chen and J. Wang, Transition metal-promoted V_2CO_2 MXenes: A new and highly active catalyst for hydrogen evolution reaction, *Adv. Sci.*, 2016, **3**, 1600180.

119 A. N. Enyashin and A. L. Ivanovskii, Structural and electronic properties and stability of MXenes Ti_2C and Ti_3C_2 functionalized by methoxy groups, *J. Phys. Chem. C*, 2013, **117**, 13637–13643.

120 M. Tang, J. Li, Y. Wang, W. Han, S. Xu, M. Lu, W. Zhang and H. Li, Surface terminations of MXene: Synthesis, characterization, and properties, *Symmetry*, 2022, **14**, 2232.

121 S. Ramki, R. Sukanya, S.-M. Chen, M. Sakthivel and Y.-T. Ye, Electrochemical detection of toxic anti-scaled agent diphenylamine using oxidized carbon nanofiber encapsulated titanium carbide electrocatalyst, *J. Hazard. Mater.*, 2019, **368**, 760–770.

122 S. Li, P. Tuo, X. Zhang, J. Xu, J. Bao, B. Pan and Y. Xie, Ultrathin MXene nanosheets with rich fluorine termination groups realizing efficient electrocatalytic hydrogen evolution, *Nano Energy*, 2018, **47**, 512–518.

123 M. Xin, J. Li, Z. Ma, L. Pan and Y. Shi, MXenes and their applications in wearable sensors, *Front. Chem.*, 2020, **8**, 297.

124 G. Samal, S. P. Kaur, C. S. Rout and B. Chakraborty, Defect-engineering of 2D dichalcogenides VSe_2 to enhance ammonia sensing: Acumens from DFT calculations, *Biosensors*, 2023, **13**, 257.

125 L. Feng, X.-H. Zha, K. Luo, Q. Huang, J. He, Y. Liu, W. Deng and S. Du, Structures and mechanical and electronic properties of the Ti_2CO_2 MXene incorporated with neighbouring elements Sc, V, B and N, *J. Electron. Mater.*, 2017, **46**, 2460–2466.

126 X. H. Zha, K. Luo, Q. Li, Q. Huang, J. He, X. Wen and S. Du, Role of the surface effect on the structural, electronic and mechanical properties of the carbide MXenes, *Europhys. Lett.*, 2015, **111**, 26007.

127 R. Kumar and L. Singh, Ti_3C_2Tx MXene as electrocatalyst for designing robust glucose biosensors, *Adv. Mater. Technol.*, 2022, **7**, 2200151.

128 H. Riazi, G. Taghizadeh and M. Soroush, MXene-based nanocomposites sensors, *ACS Omega*, 2021, **6**, 11103–11112.

129 W. Huang, L. Hu, Y. Tang, Z. Xie and H. Zhang, Recent advances in functional 2D MXene-based nanostructures for next-generation devices, *Adv. Funct. Mater.*, 2020, **30**, 2005223.

130 L. Wang, M. Zhang, B. Yang, J. Tan, X. Ding and W. Li, Recent advances in multidimensional 1D, 2D, 3D composite sensors derived from MXene: synthesis, structure, application, and perspective, *Small Methods*, 2021, **5**, 2100409.

131 T. Najam, S. S. A. Shah, L. Peng, M. S. Javed, M. Imran, M.-Q. Zhao and P. Tsiakaras, Synthesis and nano-engineering of MXenes for energy conversion and storage applications: Recent advances and perspectives, *Coord. Chem. Rev.*, 2022, **454**, 214339.

132 H. Medetalibeyoglu, M. Beytur, O. Akyildirim, N. Atar and M. L. Yola, Validated electrochemical immunosensor for ultra-sensitive procalcitonin detection: carbon electrode modified with gold nanoparticles functionalized sulfur doped MXene as sensor platform and carboxylated graphitic carbon nitride as signal amplification, *Sens. Actuators, B*, 2020, **319**, 128195.

133 H. Medetalibeyoglu, G. Kotan, N. Atar and M. L. Yola, A novel and ultrasensitive sandwich-type electrochemical immunosensor based on delaminated MXene@AuNPs as signal amplification for prostate specific antigen PSA detection and immunosensor validation, *Talanta*, 2020, **220**, 121403.

134 W. Zhong, F. Gao, J. Zou, S. Liu, M. Li, Y. Gao, Y. Yu, X. Wang and L. Lu, MXene@Ag based ratiometric electrochemical sensing strategy for effective detection of carbendazim in vegetable samples, *Food Chem.*, 2021, **360**, 130006.

135 X. Tu, F. Gao, X. Ma, J. Zou, Y. Yu, M. Li, F. Qu, X. Huang and L. Lu, MXene/carbon nanohorn/β-cyclodextrin-metal-organic frameworks as high-performance electrochemical sensing platform for sensitive detection of carbendazim pesticide, *J. Hazard. Mater.*, 2020, **396**, 122776.

136 X. Liu, J. Yang, J. Cheng, Y. Xu, W. Chen and Y. Li, Facile preparation of four-in-one nanozyme catalytic platform and the application in selective detection of catechol and hydroquinone, *Sens. Actuators, B*, 2021, **337**, 129763.

137 S. Abdolhosseinzadeh, X. Jiang, H. Zhang, J. Qiu and C. J. Zhang, Perspective on solution processing of two-dimensional MXenes, *Mater. Today*, 2021, **48**, 214–240.

138 L. Ding, D. Xiao, Z. Lu, J. Deng, Y. Wei, J. Caro and H. Wang, Oppositely charged Ti$_3$C$_2$Tx MXene membranes with 2D nanofluidic channels for osmotic energy harvesting, *Angew. Chem.*, 2020, **59**, 8720–8726.

139 M. Carey and M. W. Barsoum, MXene polymer nanocomposites: a review, *Mater. Today Adv.*, 2021, **9**, 100120.

140 H. Riazi, S. K. Nemani, M. C. Grady, B. Anasori and M. Soroush, Ti$_3$C$_2$ MXene-polymer nanocomposite and their applications, *J. Mater. Chem. A*, 2021, **9**, 8051–8098.

141 K. Maleski, V. N. Mochalin and Y. Gogotsi, Dispersion of two-dimensional titanium carbide MXene in organic solvents, *Chem. Mater.*, 2017, **29**, 1632–1640.

142 Y. Lu, X. Liang, C. Niyungeko, J. Zhou, J. Xu and G. Tian, A review of identification and detection of heavy metal ions in the environment by voltammetry, *Talanta*, 2018, **178**, 324–338.

143 A. K. S. Kumar, Y. Zhang, D. Li and R. G. Compton, A mini-review: How reliable is the drop casting technique?, *Electrochem. Commun.*, 2020, **121**, 106867.

144 H. An, T. Habib, S. Shah, H. Gad, M. Radovic, M. J. Green and J. L. Lutkenhaus, Surface-agnostic highly stretchable and bendable conductive MXene multilayers, *Mater. Adv.*, 2018, **4**, aaq0118.

145 K. Hantanasirisakul, M.-Q. Zhao, P. Urbankowski, J. Halim, B. Anasori, S. Kota, C. E. Ren, M. W. Baroum and Y. Gogotsi, Fabrication of Ti$_3$C$_2$Tx transparent thin films with tuneable optoelectronic properties, *Adv. Mater.*, 2016, **2**, 1600050.

146 Z. Wang, H. Kim and H. N. Alshareef, Oxide thin-film electronics using all-MXene electrical contacts, *Adv. Mater.*, 2018, **30**, 1706656.

147 Y. Dong, S. S. K. Mallineni, K. Maleski, H. Behlow, V. Mochalin, A. M. Rao, Y. Gogotsi and R. Podila, Metallic MXenes: A new family of materials for flexible triboelectric nanogenerators, *Nano Energy*, 2018, **44**, 103.

148 Y. Lei, Y. Cui, Q. Huang, J. Dou, D. Gan, F. Deng, M. Liu, X. Li, X. Zhang and Y. Wei, Facile preparation of sulfonic groups functionalized MXenes for removal of methylene blue, *Ceram. Int.*, 2019, **45**, 17653–17661.

149 S. Abdolhosseinzadeh, R. Schneider, A. Verma, J. Heier, F. Nuesch and C. Zhang, Turning trash into treasure: additive free MXene sediment inks for screen-printed micro-supercapacitors, *Adv. Mater.*, 2020, **32**, 2000716.

150 B. K. Bansod, T. Kumar, R. Thakur, S. Rana and I. Singh, A review on various electrochemical techniques for heavy metal ions detection with different sensing platform, *Biosens. Bioelectron.*, 2017, **94**, 443–455.

151 N. Panigrahy, A. Priyadarshini, M. M. Sahoo, A. K. Verma, A. Daverey and N. K. Sahoo, A comprehensive review on eco-toxicity and biodegradation of phenolics: Recent progress and future outlook, *Environ. Techbol. Innov.*, 2022, **27**, 102423.

152 A. Dhillon, N. Singh, M. Nair and D. Kumar, Analytical methods to determine and sense heavy metal pollutants using MXene and MXene-based composites: Mechanistic prophecy into sensing properties, *Chemosphere*, 2022, **303**, 135166.

153 J. Briffa, E. Sinagra and R. Blundell, Heavy metal pollution in the environment and their toxicological effects on humans, *Heliyon*, 2020, **6**, e04691.

154 J. Liu, L. Zhang, G. Lu, R. Jiang, Z. Yan and Y. Li, Occurrence, toxicity and ecological risk of bisphenol A analogues in aquatic environment – A review, *Ecotoxi. Environ. Safety*, 2021, **208**, 111481.

155 E. Ahmad, K. Nagaoka, M. Fayez, M. M. A. Daim, H. Samir and G. Watanabe, Suppressive effects of long-term exposure to p-nitrophenol on gonadal development. Hormonal profile with disruption of tissue integrity, and activation of caspase-3 in male Japanese quail *Conturnix japonica*, *Environ. Sci. Pollut. Res.*, 2015, **22**, 10930.

156 S. Suresh, V. C. Srivastava and I. M. Mishra, Adsorption of Catechol, resorcinol, hydroquinone, and their derivatives: a review, *Int. J. Eng. Environ. Eng.*, 2012, **3**, 32.

157 Y. Wang, L. Wang, W. Huang, T. Zhang, X. Hu, J. A. Perman and S. Ma, Metal–organic framework and conducting polymer based electrochemical sensor for high performance cadmium ions detection, *J. Mater. Chem. A*, 2017, **5**, 8385–8393.

158 S. Tajik, H. Beitollahi, F. G. Nejad, I. Sheikhshoaie, A. S. Nugraha, H. W. Jang, Y. Yamauchi and M. Shokouhimehr, Performance of metal-organic frameworks in the electrochemical sensing of environmental pollutants, *J. Mater. Chem. A*, 2021, **9**, 8195–8220.

159 M. Berkani, Y. Vasseghian, V. T. Le, E.-N. Dragoi and K. A. Mousavi, The Fenton-like reaction for arsenic removal from groundwater: health risk assessment, *Environ. Res.*, 2021, **202**, 111698.

160 Y. Vasseghian, S. S. Rad, J. A. V. Boas and A. Khataee, A global systematic review, meta-analysis, and risk assessment of the concentration of vanadium in drinking water resources, *Chemosphere*, 2021, **267**, 128904.

161 M. Moradi, Y. Vasseghian, H. Arabzade and K. A. Mousavi, Various wastewaters treatment by sono-electrocoagulation process: a comprehensive review of operational parameters and future outlook, *Chemosphere*, 2021, **263**, 128314.

162 M. B. Gumpu, S. Sethuraman, U. M. Krishnan and J. B. B. Rayappan, A review on detection of heavy metal ions in water – An electrochemical approach, *Sens. Actuators, B*, 2015, **213**, 515–533.

163 W. Liu, Y. Liu, Z. Yuan and C. Lu, Recent advances in the detection and removal of heavy metal ions using functionalized layered double hydroxides: A review, *Ind. Chem. Mater.*, 2023, **1**, 79–92.

164 C. Liu, X. Chen, B. Zong and S. Mao, Recent advances in sensitive and rapid mercury determination with graphene–based sensors, *J. Mater. Chem. A*, 2019, **7**, 6616–6630.

165 H. Cheng and J. Yang, Preparation of Ti_3C_2-PANI composite as sensor for electrochemical determination of mercury ions in water, *Int. J. Electrochem. Sci.*, 2020, **15**, 2295–2306.

166 P. Xiao, G. Zhu, X. Shang, B. Hu, B. Zhang, Z. Tnag, J. Ynag and J. Liu, An Fe-MOF/MXene-based ultra-sensitive electrochemical sensor for arsenic III measurement, *J. Electroanal. Chem.*, 2022, **916**, 116382.

167 L. Chen, P. Xiao, B. Hu, Y. Wang, J. Yang and J. Liu, Preparation of Fe-Co-LDH/MXene modified electrode for sensitive determination of arsenic III in aquatic system, *Electroanalysis*, 2023, e202200521.

168 X. Zhu, B. Liu, H. Hou, Z. Huang, K. M. Zeinu, L. Huang, X. Yuan, D. Guo, J. Hu and J. Yang, Alkaline intercalation of Ti_3C_2 MXene for simultaneous electrochemical detection of CdII, PbII, CuII and HgII, *Electrochim. Acta*, 2017, **248**, 46–57.

169 X. Zhu, B. Liu, L. Li, L. Wu, S. Chen, L. Huang, J. Yang, S. Liang, K. Xiao, J. Hu and H. Hou, A micromilled microgrid sensor with delaminated MXene-bismuth nanocomposite assembly for simultaneous electrochemical detection of lead(II), cadmium(II) and zinc(II), *Microchim. Acta*, 2019, **186**, 776.

170 X. Lv, F. Pei, S. Feng, Y. Wu, S.-M. Chen, Q. Hao and W. Li, Facile synthesis of protonated carbon nitride/Ti3C2Tx nanocomposite for simultaneous detection of Pb^{2+} and Cd^{2+}, *J. Electrochem. Soc.*, 2020, **167**, 067509.

171 Y. He, L. Ma, L. Zhou, G. Liu, Y. Jiang and J. Gao, Preparation and application of bismuth/MXene nano-composite as electrochemical sensor for heavy metal ions detection, *Nanomaterials*, 2020, **10**, 866.

172 L. Wen, J. Dong, H. Yang, J. Zhao, Z. Hu, H. Han, C. Hou, X. Luo and D. Huo, A novel electrochemical sensor for simultaneous detection of Cd2+ and Pb2+ by MXene aero-CuO/carbon cloth flexible electrode based on oxygen vacancy and bismuth film, *Sci. Total Environ.*, 2022, **851**, 158325.

173 X. Hui, Md Sharifuzzaman, S. Sharma, X. Xuan, S. Zhang, S. G. Ko, S. H. Yoon and J. Y. Park, High performance flexible electrochemical heavy metal sensor based on layer-by-layer assembly of Ti_3C_2Tx/MWCNTs nanocomposites for noninvasive detection of copper and zinc ions in

human biofluids, *ACS Appl. Mater. Interfaces*, 2020, **12**, 48928–48937.

174 P. A. Rasheed, R. P. Pandey, T. Gomez, M. Naguib and K. A. Mahmoud, Large interlayer spacing Nb4C3Tx MXene promotes the ultrasensitive electrochemical detection of Pb2+ on glassy carbon electrodes, *RSC Adv.*, 2020, **10**, 24697.

175 W. W. Anku, M. A. Mamo and P. P. Govender, in *Phenolic compounds – natural sources, importance and application*, ed. M. S. Hernandez, M. P. Tenango, R. G. Mateos, InTech, 1st edn, 2017, ch. 17, pp. 419–443.

176 H. S. Hashim, Y. W. Fen, N. A. S. Omar and N. I. M. Fauzi, Sensing methods for hazardous phenolic compounds based on graphene and conducting polymers-based materials, *Chemosensors*, 2021, **2**, 291.

177 T. Arfin, K. Sonawane and A. Tarannum, Review on detection of phenol in water, *Adv. Mater. Lett.*, 2019, **10**, 753–785.

178 H. S. Hashim, Y. W. Fen, N. A. S. Omar, N. I. M. Fauzi and W. M. E. M. M. Daniyal, Recent advances of priority phenolic compounds detection using phenol oxidases-based electrochemical and optical sensors, *Measurement*, 2021, **184**, 109855.

179 K. Mainali, M. H. Gagaa and S. H. Mood, Electroanalytical method for the detection of phenol: A brief, *Sci. J. Biol. Life Sci.*, 2022, **2**.

180 S. Sakthinathan, S. Palaniamy, S.-M. Chen, P.-S. Wu, L. Yao and B.-S. Lou, Electrochemical detection of phenol in industrial pollutant absorbed molecular sieves by electrochemically activated screen-printed carbon electrode, *Int. J. Electrochem. Sci.*, 2015, **10**, 3319–3328.

181 B. T. P. Quynh, L. G. Bach, B. J. Young and K. S. Hoon, Electrochemical detection of phenol in alkaline solution using nanoporous gold thin film electrode, *Mol. Cryst. Liq. Cryst.*, 2017, **645**, 139–144.

182 L. Wu Dhanjai, Z. S. Wu, Y. Dong, X. Wang, S. Zheng and J. Chen, 2D transition metal carbide MXene as a robust biosensing platform for enzyme immobilization and ultrasensitive detection of phenol, *Biosens. Bioelectron.*, 2018, **107**, 69–75.

183 M. F. Manzoor, T. Tariq, B. Fatima, A. Sahar, F. Tariq, S. Munir, S. Khan, M. M. A. N. Ranjha, A. Sameen, X.-A. Zeng and S. A. Ibrahim, An insight into bisphenol A, food exposure and its effects on health: A review, *Front. Nutr.*, 2022, **9**, 1047827.

184 U. Wazir and K. Mokbel, Bisphenol A: A concise review of literature and a discussion of health and regulatory implications, *In Vivo*, 2019, **33**, 1421–1423.

185 P. A. Rasheed, R. P. Pandey, K. A. Jabbar and K. A. Mahmoud, Platinum nanoparticles/Ti_3C_2Tx MXene composite for the effectual electrochemical sensing of bisphenol A in aqueous media, *J. Electroanal. Chem.*, 2021, **880**, 114934.

186 J. Rajendran, T. S. Kannan, L. S. Dhanasekaran, P. Murugan, R. Atchudan, Z. A. Alothaman, M. Ouladsmane and A. K. Sundramoorthy, Preparation of 2D graphene/MXene nanocomposite for the electrochemical determination

of hazardous bisphenol A in plastic products, *Chemosphere*, 2022, **287**, 132106.

187 Y. Chen, C. Yang, X. Huang, L. Li, N. Yu, H. Xie, Z. Zhu, Y. Yuan and L. Zhou, Two-dimensional MXene enabled carbon quantum dots@Ag with enhanced catalytic activity towards the reduction of p-nitrophenol, *RSC Adv.*, 2022, **12**, 4836.

188 B. R. Patel, M. Noroozifar and K. Kerman, Review-nano-composite-based sensors for voltammetric detection of hazardous phenolic pollutants in water, *J. Electrochem. Soc.*, 2020, **167**, 037568.

189 R. Krishnamoorthy, K. Muthumalai, T. Nagaraja, R. T. Rajendrakumar and S. R. Das, Chemically exfoliated titanium carbide MXene for highly sensitive electrochemical sensors for detection of 4-nitrophenols in drinking water, *ACS Omega*, 2022, **7**, 42644–42654.

190 X. Wang, M. Li, S. Yang, X. Bai and J. Shan, Self-assembled Ti$_3$C$_2$Tx MXene/graphene composite for the electrochemical reduction and detection of p-nitrophenol, *Microchem. J.*, 2022, **179**, 107473.

191 L. Lei, C. Li, W. Huang and K. Wu, Simultaneous detection of 4-chlorophenol and 4-nitrophenol using a Ti$_3$C$_2$Tx MXene based electrochemical sensor, *Analyst*, 2021, **146**, 7593–7600.

192 M. Chandran, E. Aswathy, I. Sharma, M. Vinoba, R. Kottappara and M. Bhagyalakshmi, Laccase immobilized on Au confined MXene based electrode for electrochemical detection of catechol, *Mater. Today: Proc.*, 2021, **46**, 3136–3143.

193 S. Suresh, V. C. Srivastava and I. M. Mishra, Adsorption of catechol, resorcinol, hydroquinone, and their derivatives: A review, *Int. J. Energy Environ. Eng.*, 2012, **3**, 32.

194 L. A. Alshahrani, X. Li, H. Luo, L. Yang, M. Wang, S. Yan, P. Liu, Y. Yang and Q. Li, The simultaneous electrochemical detection of catechol and hydroquinone with CuSal-β-Ala3,5-DMPz$_2$/SWCNTs/GCE, *Sensors Basel*, 2014, **14**, 22274–22284.

195 R. Huang, S. Chen, J. Yu and X. Jiang, Self-assembled Ti$_3$C$_2$/MWCNTs nanocomposites modified glassy carbon electrode for electrochemical simultaneous detection of hydroquinone and catechol, *Ecotoxicol. Environ. Safety*, 2019, **184**, 109619.

196 R. Huang, D. Liao, S. Chen, J. Yu and X. Jiang, A strategy for effective electrochemical detection of hydroquinone and catechol: decoration of alkalization-intercalated Ti$_3$C$_2$ with MOF-derived N-doped porous carbon, *Sens. Actuators*, 2020, **320**, 128386.

197 K. S. Ranjith, A. T. E. Vilian, S. M. Ghoreishian, R. Umapathi, S.-K. Hwang, C. W. Oh, Y. S. Huh and Y.-K. Han, Hybridized 1D-2D MnMoO$_4$ nanocomposites as high-performing electrochemical sensing platform for the sensitive detection of dehydrobenzene isomers in wastewater samples, *J. Hazard. Mater.*, 2022, **421**, 126775.

198 M. Baccarin, M. A. Ciciliati, O. N. Oliveira Jr., E. T. G. Cavalheiro and P. A. R. Pereira, Pen sensor made with silver nanoparticles decorating graphite-polyurethane electrodes to detect bisphenol-A in tap and river water samples, *Mater. Sci. Engi. C*, 2020, **114**, 110989.

199 N. O. Gomes, C. D. Mendonca, S. A. S. Machado, O. N. Oliveira Jr. and P. A. R. Pereira, Flexible and integrated dual carbon sensor for multiplexed detection of nonylphenol and paroxetine in tap water samples, *Microchim. Acta*, 2021, **188**, 359.

200 P. A. R. Pereira, A. M. Campos, T. M. Prado, L. N. Furini, N. V. Boas, M. L. Calegaro and S. A. S. Machado, Synergy between Printex nano-carbons and silver nanoparticles for sensitive estimation of antioxidant activity, *Anal. Chim. Acta*, 2016, **926**, 88–98.

201 A. M. de Campos, R. R. Silva, M. L. Calegaro and P. A. R. Pereira, Design and fabrication of flexible copper sensor decorated with bismuth micro/nanodentrites to detect lead and cadmium in noninvasive samples of sweat, *Chemosensors*, 2022, **10**, 446.

202 R. R. Silva, P. A. R. Pereira, A. M. Campos, D. Wilson, C. G. Otoni, H. S. Barud, C. A. R. Costa, R. R. Domeneguetti, D. T. Balogh, S. J. L. Ribeiro and O. N. Oliveira Jr., Microbial nanocellulose adherent to human skin used in electrochemical sensors to detect metal ions and biomarkers in sweat, *Talanta*, 2020, **218**, 121153.

203 T. S. Gopal, S. K. Jeong, T. A. Alrebdi, S. Pandiaraj, A. Alodhayb, M. Muthuramamoorthy and A. N. Grace, MXene-based composite electrodes for efficient electrochemical sensing of glucose by non-enzymatic method, *Mater. Today Chem.*, 2022, **24**, 100891.

204 M. H. Hassan, C. Vyas, B. Grieve and P. Bartolo, Recent Advances in enzymatic and non-enzymatic electrochemical glucose sensing, *Sensors*, 2021, **21**, 4672.

205 A. Rhouati, M. Berkani, Y. Vasseghian and N. Golzadeh, MXene-based electrochemical sensors for desstection of environmental pollutants: A comprehensive review, *Chemosphere*, 2022, **291**, 132921.

206 J. A. Junkaew and R. Arroyave, Enancemnet of the selectivity of MXenes (M$_2$C, M = Ti, V, Nb, Mo) *via* oxygen-functionalization: promising materials for gas-sensing and – separation, *Phys. Chem. Chem. Phys.*, 2018, **20**, 6073–6082.